ON INTERANNUAL VARIABILITY AND CLIMATE CHANGE IN THE NORTH PACIFIC

By

David Kurt Salmon

RECOMMENDED:

Chairman, Advisory Committee

Department Head

APPROVED:

Dean, School of Fisheries and Ocean Sciences

Dean of the Graduate School

5/1/92

Date

ON INTERANNUAL VARIABILITY AND CLIMATE CHANGE IN THE NORTH PACIFIC

A

THESIS

Presented to the Faculty

of the University of Alaska Fairbanks

in Partial Fulfillment of the Requirements

for the Degree of

DOCTOR OF PHILOSOPHY

By

David Kurt Salmon, B.A.

Fairbanks, Alaska

May 1992

Abstract

Long term changes in the atmospheric and oceanic environment of the North Pacific were investigated for the period 1946-1991. A climatology of North Pacific wind stress curl was developed because of the relevance of changes in wind stress curl to both oceanic and atmospheric variability. The dominant scales of spatial and temporal wind stress curl variability were determined and examined within the context of observed changes in North Pacific air temperature, sea surface temperature (SST), sea ice cover, oceanic mass transport and the occurrence of blocking anticyclones. Relationships between these variables and indices of tropical Pacific variability were also determined on interannual time scales.

During 1976-1988, phase relationships were very strong between long term mean anomalies of wind stress curl, SST, air temperature, sea ice cover, The Pacific North American index, the Southern Oscillation Index (SOI), and tropical Pacific SST. Long term mean anomalies of these parameters did not change sign during 1976-88. These strong phase relationships did not occur amongst these variables during any other period of the record. The 1976-1988 period is characterized by intensified storminess, the decreased occurrence of blocking anticyclones, and decreased sea ice cover in the subarctic North Pacific. Intensified atmospheric circulation also occurred in the western Pacific subtropical anticyclone. Anomalously low SST occurred across the central and western North Pacific during this period while anomalously high SST was present in the eastern North Pacific adjacent to North America. Changes

in the sign of the long term mean anomalies of wind stress curl, central North Pacific SST and the SOI suggest that this climate regime ended or relaxed after 1988.

After 1975, long term changes in anomalies of the Southern Oscillation Index, tropical Atlantic wind stress, Sahel rainfall, and Greenland Sea ice cover have characteristics similar to those observed in the North Pacific. It is suggested that the climate anomalies observed in the North Pacific during 1976-1988 occurred as part of a hemispheric or global scale climate regime.

Contents

List of Figures

List of Tables

Acknowledgments

I would like to take this opportunity to thank my advisor, Dr. Thomas C. Royer, for his support, encouragement, insight, and critical evaluation. Working with Dr. Royer for the past five years has been a pleasant and productive experience. I would also like to thank Dr. Thomas Weingartner and Dr. David Musgrave for taking an interest in this work. Their critical comments are greatly appreciated. Chirk Chu and Howard Maxwell provided valuable computer support work. I would also like to thank my colleagues Wiesiek Maslowski and Steven Okkonen for taking an active interest in this work. Finally, I would like to thank my partner in life Ms. Jayne Naze for her continual support, encouragement, and evaluation. This work has been supported under grants OCE 8608125 and OCE 9012866 as part of the Gulf of Alaska Recirculation Study.

Overview

Changes in weather and climate in the North Pacific are important to the populations living along the Pacific rim. They are directly important in the sense that weather and climate conditions constrain many human activities, both on land and at Sea. The spatially and temporally varying occurrences of droughts and floods produce life threatening shortages and excesses of water, which seriously impacts agricultural activity. On long time scales droughts and floods are manifestations of changing climatic conditions, in particular, changes in the conditions of the atmosphere and ocean and their interactions with the land masses. Winds and storm surges associated with typhoons and extratropical cyclones destroy life and property on land and at sea. The exploitation of the renewable and non-renewable natural resources of the oceans is rendered difficult and dangerous by severe storms that frequently occur over vast regions of the North Pacific. The weather serves as an indicator of changes in climatic conditions on regional and hemispheric to global scales.

Human induced changes to the global climate system, a presently popular topic, cannot be determined without first determining those changes caused by naturally occurring cycles and variations. At this point we do not fully understand the causal nature of recent observed trends in various environmental parameters. The natural variability in these parameters on decadal time scales is not fully understood, often due

to the short length of series of recorded observations. Changes in the global climate are the result of variations occurring in both the atmosphere and the ocean. Developing our understanding of the climate comes with a knowledge of how the separate components and the coupled system operate.

The purpose of this study is to further our understanding of the climate system of the atmosphere and the ocean in the North Pacific. In chapter 1 a climatology of wind stress curl is developed for the North Pacific for the period 1946-1991. Changes in wind stress curl are relevant to both oceanic and atmospheric variability. Therefore wind stress curl will prove to be a useful parameter in the study of interannual variability and climate change in the Pacific. Analysis of regional wind stress curl anomalies shows that the circulation in the Aleutian Low was anomalously weak during most of the period 1954-75 and anomalously strong during 1976-88. The strengthened circulation in the Aleutian Low during 1976-88 appears to be related to the reversal of a decreasing trend in East Asian cyclogenesis that occurred during 1950-77. These periods of weakened and intensified wind stress curl forcing are manifested more strongly over the Bering Sea than over the Gulf of Alaska. Interannual variations in Bering Sea wind stress curl are characterized by decadal scale changes while the Gulf of Alaska is dominated by higher frequency variations. Anomalies of wind stress curl in the anticyclones of the eastern and western subtropical Pacific suggest that long term changes in wind stress curl occur on the spatial scale of the North Pacific. Observed interannual variations of oceanic mass transports in the Gulf of Alaska

and the Oyashio current of the western subarctic are shown to fluctuate on the time scales of wind stress curl variations in the Gulf of Alaska and Bering Sea respectively, indicating that oceanographic variability responds to atmospheric fluctuations on time scales of years.

Chapter 2 establishes the dominant time scales of interannual variability of North Pacific air temperature, sea surface temperature (SST), and sea ice cover. Interannual variability of the Southern Oscillation Index, Pacific North American index, and tropical Pacific SST are also examined and provide links to the relationships between variations in the tropical Pacific and extratropical North and South Pacific. Interannual variability of North Pacific wind stress curl is examined in relation to changes in the above variables. Mechanisms of interaction between these variables are also investigated. The most striking aspect of interannual changes in the variables considered in this study is that their long term mean anomalies do not change sign during the period 1976-88, indicating the existence of a climate regime that is unique in both amplitude and duration. The correspondence between anomalies of the North Pacific variables and those in the tropical and South Pacific indicates that the observed climate regime has meridional scales that extend at least from the high latitude North Pacific into the subtropical South Pacific.

In chapter 3 climate change in the North Pacific is investigated from the perspective of changes in the frequency of occurrence of large scale blocking anticyclones over the high latitude North Pacific during 1946-91. Decadal scale variability in the fall and winter occurrence of

these features is most pronounced during 1976-88 relative to the previous three decades. These changes in blocking activity are consistent with long term variations in anomalies of central North Pacific SST and the strength of the subarctic atmospheric circulation.

Conclusions drawn from chapters 1 through 3 are presented in chapter 4. It is also shown that after 1975, anomalies of tropical Atlantic wind stress, Sahel (northwest Africa) rainfall, and Greenland Sea ice cover show patterns that are very similar to those observed in the Pacific. On the basis of these observations and physical links between them, it is suggested that the climate anomalies observed in the Pacific during 1976-88 occurred as part of a global scale climate regime.

Chapter One

A Climatology of North Pacific Wind Stress Curl

Introduction

The Role of Wind Stress Curl in Forcing Oceanic Variability

The large scale interactions of the wind field with the surface ocean are important processes by which the atmosphere drives oceanic motions. On time scales of more than a few days the curl of the wind stress is an important mechanism in causing variability in ocean circulation [Gill, 1982, Kutsuwada, 1988]. The importance of the wind stress curl over the ocean to the dynamics of the ocean is illustrated by the number of diverse oceanic processes that are influenced or controlled to some extent by the wind stress curl. These include the movements of the gyre scale horizontal currents [Munk, 1950], generation of mesoscale eddies [Muller and Frankignoul, 1979, Frankignoul and Muller, 1981, Dickson et al., 1982] , planetary wave motions [White and Saur, 1981, 1983, White, 1985, Reason et al., 1987, vertical and horizontal motions associated with wind induced upwelling and downwelling [Hickey, 1979, McCreary and Chao, 1985, Chao, 1985], and oceanic internal mixing processes [White et al., 1980].

The distribution of wind stress curl over the open ocean is responsible for driving the basin scale subtropical and subpolar gyres [Munk, 1950]. The wind driven upper ocean circulation is coupled to the interior ocean quasi-geostrophic circulation through the Ekman pumping mechanism. Cyclonic wind stress curl causes surface current divergences which results in upward displacements of the pycnocline and vortex tube stretching. Anticyclonic wind stress curl forcing causes surface convergences that depress the pycnocline and compress vortex tubes. It is through the stretching and compression of the large scale vortex tubes that the wind stress curl forcing at the ocean surface affects changes in the baroclinic structure of the interior ocean. The Sverdrup balance relates the meridional component of the interior ocean circulation to the curl of the wind stress. Therefore the wind stress curl has a central role in driving the large scale circulation. Cyclonic wind stress curl produces poleward motion in the interior ocean and anticyclonic wind stress curl produces equatorward motion according to the constraints imposed on the large scale circulation by the conservation of potential vorticity.

The wind stress curl also forces low frequency oceanic variability through the generation of planetary waves along eastern ocean boundaries and over the open ocean. White and Saur [1981] show that annual period baroclinic planetary waves are generated along a line source of high amplitude wind stress curl along the west coast of North America between 21°N-38°N and 115°W-125°W. The numerical model of Cummins et al. [1986] identify three distinct regions along the eastern boundary of the North Pacific (including that found by White and Saur), as

well as an open ocean region in the central North Pacific, where annual period planetary waves are generated by the curl of the wind stress. Reason et al. [1987] identify three source regions of annual period baroclinic planetary waves in the South Atlantic. These areas of generation are also regions of local maximum wind stress curl. Planetary waves with periods greater than one year are also generated by large scale wind stress curl variability. White and Saur [1981, 1983] and White [1985] show that planetary waves with periods greater than one year are generated by wind stress curl forcing in the eastern North Pacific. There are several mechanisms by which the wind stress curl forces planetary waves in the ocean. Over the open ocean, large amplitude localized wind stress curl forcing and resonance of the forcing function with freely propagating waves have been implicated as generating mechanisms [White and Saur, 1981, White, 1985], while in eastern boundary regions it is the variation of the wind stress curl near the boundary that appears to be important [White and Saur, 1983, Tabata, 1991b]. Based on observations between 20°N and 38°N, White and Saur [1983] propose that short term climatic variability of the wind stress curl over the Northeast Pacific is a forcing mechanism for the generation of oceanic interannual baroclinic planetary waves.

Away from boundary regions and intense boundary currents, the wind stress curl appears to be an important component in forcing seasonal variations in the mesoscale eddy field of the ocean. Muller and Frankignoul [1979] and Frankignoul and Muller [1981] suggest that the seasonal variation of wind stress curl is an important mechanism for

generating baroclinic eddies in the central Pacific Ocean. Dickson et al. [1982] suggest that this is also true in the North Atlantic.

The structure of the thermocline can be altered through internal mixing processes during periods of intensified synoptic storm activity [White et al., 1980]. Increases in cyclonic wind stress curl can be directly associated with increased synoptic storm activity [White et al. 1980], so that variability in the wind stress curl plays an indirect role in driving oceanic internal mixing processes.

The curl of the wind stress has also been implicated in driving poleward flows along eastern ocean boundaries. The coastal undercurrent off the coast of California appears to be primarily driven by the curl of the wind stress [Hickey, 1979, McCreary and Chao, 1985, Chao, 1985]. The dynamics of the coastal undercurrent appear to be different from Sverdrup dynamics since the undercurrent occurs in proximity to a coastal boundary while Sverdrup dynamics pertain to the interior ocean circulation.

The wind stress curl also appears to be indirectly involved in forcing variability in the intertropical convergence zone (ITCZ) of the Pacific. Upwelling of cold waters that decrease latent ocean-atmosphere heat fluxes in the ITCZ is hypothesized to be forced by variability in regional wind stress curl [Reiter, 1978]. These changes in the ITCZ and therefore in the Hadley circulation, are in turn related to ENSO events [Reiter, 1978], so that regional scale variability of the curl might be important in forcing hemispheric or global scale changes in the atmosphere and ocean.

The results stated above are derived both from observations and from numerical methods. They provide convincing evidence that the wind stress curl is extremely important in directly forcing low frequency variability in oceanic motions, and in indirectly altering the thermal structure of the upper ocean.

Previous Studies

Early studies of the large scale fields of wind stress were undertaken by Reid [1948] in the Pacific, and Munk [1950] in the Atlantic. Hidaka [1958], and Hellerman [1967] extended the study of the large scale wind fields to include those over the world ocean. Hellerman and Rosenstein [1983] note that those studies employed wind rose data, while more recent studies (e.g. Bunker [1976] in the North Atlantic, Wyrtki and Meyers [1976] in the tropical and subtropical Pacific, and Hastenrath and Lamb [1977] in the tropical Atlantic and Pacific) use ship observations.

Hellerman and Rosenstein [1983] use the "TDF-11" data set of the National Climatic Center to compute the climatological mean fields of wind stress, wind stress curl, and the wind driven oceanic mass transport stream function over the global ocean. The TDF-11 data consist of nearly 35 million ship observations for the period 1870 through 1976. Harrison [1989] computes wind stress, wind stress curl and Sverdrup transports over the global ocean using a reduced version of the TDF-11 data and a different formulation of the drag coefficient than that used by Hellerman and Rosenstein. Harrison uses data from 1850 through 1979 in the Indian

and Atlantic oceans while for the Pacific the analysis is limited to the period 1950 through 1979. Harrison notes that his stress values are often 20%-30% smaller than those of Hellerman and Rosenstein, especially those values of wind stress curl and Sverdrup transport found in the Gulf Stream and Kuroshio separation regions. Trenberth et al. [1989] have prepared a global ocean wind stress climatology using European Centre for Medium Range Weather Forecasts (ECMWF) data for the period 1980 through 1986. Large differences between the annual mean fields of wind stress curl of Hellerman and Rosenstein [1983] and Trenberth et al. [1989] occur across much of the Southern Ocean (>20.0 $*10^{-9}$ dynes/cm^3), and in the midlatitude North Pacific (10.0 $*10^{-9}$ dynes/cm^3, cf. figure 18, Trenberth et al. 1989). Over the North Pacific, these global analyses show a positive wind stress curl maximum over the Gulf of Alaska and a secondary maximum in the northwestern Pacific off Kamchatka. In contrast, maximum negative curl occurs in a broad region of the subtropical anticyclone near 30°N.

Climatological aspects of regional wind stress curl variability have been addressed to varying degrees and over different time periods in the Indian Ocean [Breidenbach, 1990], the North Atlantic [Barnier, 1986, Ehret and O'Brien, 1989], the Nordic seas [Jonsson, 1991], and the North Pacific [Kutsuwada, 1982, Rienecker and Ehret, 1988]. Kutsuwada [1982] uses ship report data from the Japan Meteorological Agency to examine seasonal variability in North Pacific wind stress curl between the equator and 50°N from 1961-1975. Kutsuwada finds that the maximum zonally averaged wind stress curl occurs in the subtropical anticyclone near 30°N

with a secondary maximum occurring in the westerlies near 50°N. Rienecker and Ehret [1988] examine the seasonal and interannual variability of North Pacific wind stress curl between 3°N and 55°N for the period 1960-1979 using the Comprehensive Ocean-Atmosphere Data Set (COADS). Rienecker and Ehret find that the dominant modes of wind stress curl variability on both seasonal and interannual time scales are associated with changes in the positions and intensities of the Aleutian Low and the North Pacific High. On seasonal time scales, a positive curl maximum occurs at about 50°N in the western basin [Rienecker and Ehret, 1988]. A secondary maximum appears to occur in the Gulf of Alaska, and a negative curl maximum between 20°N to 30°N occurs in the western basin [Rienecker and Ehret, 1988].

In this thesis a new wind stress curl climatology is developed for the North Pacific for the period 1946 to 1991. The purpose of developing this climatology is to update knowledge of the time scales of North Pacific wind stress curl variability and to evaluate changes in the wind field over time with observed changes in the ocean and atmosphere. The dominant modes of wind stress curl variability will be determined using empirical orthogonal functions. Seasonal and interannual variability of North Pacific Sverdrup transport will also be examined because of its direct link to wind stress curl. A set of regional time series of curl are constructed based on physical arguments. These series are used to determine relationships between regional curl fluctuations on seasonal to decadal time scales. Relationships between low frequency wind stress curl

variability and fluctuations in the subarctic gyres of the North Pacific Ocean are also examined.

This study also expands the areal coverage of earlier wind stress curl investigations through the inclusion of a new wind stress curl climatology of the Chukchi Sea and Bering Sea regions for the period 1981-90. The primary purpose of the analysis for the Chukchi and Bering regions is to determine the annual and interannual relationships between the fields of curl in the Aleutian Low and Arctic high pressure systems such as the Siberian High and the Beaufort anticyclone.

Data and Computations

Monthly mean sea level pressure (SLP) for the period January 1946 through July 1991 were obtained from Fleet Numerical Oceanographic Center (FNOC). The pressure data domain extends across the North Pacific basin between 18°N and 63°N. The grid consists of a 16 by 44 matrix spaced 3 degrees in both latitude and longitude. The surface geostrophic winds, wind stress and wind stress curl are computed on a 427 point subdomain of the SLP grid. The utility of the FNOC data lies in the fact that it provides a relatively long record for analysis of the pressure and derived wind data. The record will allow the determination and analysis of longer period trends and cycles in the wind field than was possible in previous studies, and the overlap of this record with those of earlier studies permits comparisons. SLP data on a 2.5 degree by 2.5 degree grid between 50°N and 80°N over the Bering and Chukchi seas for

the period January 1981 through December 1990 were also obtained from FNOC.

Geostrophic winds were calculated from the pressure fields using centered finite differences in spherical coordinates :

$$u_g = -\frac{1}{f\rho_a R}\frac{\partial P}{\partial \phi} \qquad v_g = \frac{1}{f\rho_a R\cos\phi}\frac{\partial P}{\partial \lambda} \tag{1.1}$$

where:

P is the sea level atmospheric pressure

u_g is the zonal component of the geostrophic wind

v_g is the meridional component of the geostrophic wind

λ is longitude

ϕ is latitude

Ω is the angular speed of the earth in radians per second

$f = 2\,\Omega \sin\phi$ is the Coriolis parameter

R is the mean radius of the earth, 6371 km

ρ_a is the mean density of the atmosphere

The geostrophic winds were rotated 15 degrees down the pressure gradient and reduced in magnitude to 0.7 of the computed value (after Bakun, 1973) in an attempt to include frictional effects in the atmospheric boundary layer. Meridional and zonal wind stresses and the curl of the wind stress were derived from the adjusted geostrophic component winds. The components of the wind stress were calculated using a standard quadratic bulk formula:

$$\tau=\rho_a C_D|\mathbf{v}|\mathbf{v} \qquad (1.2)$$

where:

$\tau=(\tau^x,\tau^y)$ is the vector wind stress of eastward and northward components respectively,

ρ_a =1.22 kg/m^3 is the density of the atmosphere,

C_D =0.0026 is the drag coefficient,

$\mathbf{v}$ = (u,v) is the velocity vector of the geostrophic wind,

and $|\mathbf{v}|$ is the magnitude of the velocity.

The vertical component of the horizontal wind stress curl was computed according to:

$$\vec{k}\cdot(\nabla\times\vec{\tau})=\frac{1}{R\cos\varphi}\left[\frac{\partial\tau_y}{\partial\lambda}-\frac{\partial(\tau_x\cos\varphi)}{\partial\varphi}\right] \qquad (1.3)$$

where:

φ is latitude

λ is longitude

Although the drag coefficient is a function of wind speed and atmospheric stability [Thompson et al.,1983, Hellerman and Rosenstein, 1983, Kutsuwada, 1988], a constant drag coefficient was used in this study. Willebrand [1978] notes that the use of a constant drag coefficient produces wind stress fields of comparable magnitude but with different spectral shape to those calculated using a variable (linear in the magnitude of the wind stress) drag coefficient. The use of a constant drag coefficient produces an underestimate of the wind stress [Thompson et al., 1983,

Rienecker and Ehret, 1988], and hence the curl of the wind stress as well. We will be concerned with relative variations in the wind field, so that our systematic underestimation of the winds due to the constant drag coefficient should not prove to be a serious difficulty.

In a similar approach to that used here, Breidenbach [1990] examines variability in the Indian Ocean wind field through the use of so called pseudo-stress vectors, which are defined as the magnitude of the wind multiplied by its components. Actual stresses are computed by multiplying by the product of the drag coefficient and air density. Since a constant air density was also used in this study, the wind stress and wind stress curl calculations produce results that differ only by a constant value from those using pseudo-stresses.

Analysis

Computed and Real Boundary Effects on Wind Stress Curl

A computational amplification of the wind stress curl occurs at some of the gridpoints adjacent to the coast due to the miscalculation of the geostrophic winds. The miscalculation results from an overestimation of the atmospheric pressure gradient. During winter, low pressure atmospheric circulation systems prevail over the Gulf of Alaska while high pressure systems occur inland of the coastal mountains. During summer, high pressure (East Pacific High) occurs over the eastern North Pacific off southern California while there is a low pressure feature

inland over the southwestern United States (U. S. thermal low) [Rienecker and Ehret, 1988]. In both cases the finite difference approximation of the geostrophic wind at the gridpoint adjacent to the coast uses a point from each side of a high mountain barrier. This results in an overestimation of the atmospheric pressure gradient at the offshore gridpoint that leads to an overestimate of the geostrophic wind and wind stress curl. In other words the horizontal atmospheric pressure gradient that is actually in equilibrium with the geostrophic wind is smaller than the computed gradient [Bakun, 1973]. Bakun [1973] found that upwelling indices based on Ekman transport calculations from Fleet Numerical Weather Center monthly mean pressure data were amplified during the summer off the coast of southern California near 30°N 119°W due to the presence of the high coastal mountain range, which effectively separates the oceanic East Pacific High pressure from the continental U. S. thermal low. This overestimation does not occur in this region during winter. Livingstone and Royer [1980] note that a similar effect could occur for the northern Gulf of Alaska, particularly in winter when the pressure difference between the oceanic and continental regions is greatest. This overestimation does not occur over the gulf region during the summer months when high pressure prevails over the ocean. Luick et al. [1987] find that the computed geostrophic winds significantly overestimate the measured winds over the coastal region of the northern Gulf of Alaska. Luick et al. [1987] determine that a 41% reduction in magnitude of the calculated winds is required to correct for frictional effects in the planetary boundary layer. The standard reduction used to account for

friction in the boundary layer for the calculated geostrophic winds is 30% [e.g. Bakun, 1973].

In order to assess the effects on the wind field introduced at the boundaries by the use of points over land in the finite difference approximations, the mean and variance fields of the curl were computed in two ways. The first method employed gridpoints over land in the finite difference approximation of the winds near the continental boundaries, while the second method did not utilize any points over land. The results of these computations did not change the fundamental spatial characteristics of the previously computed fields. The most pronounced effect produced by the computations that did not use continental gridpoints was a reduction in the amplitudes of the spatial maxima adjacent to coastlines, particularly over the northern Gulf of Alaska (along 60°N) during winter and off southern California (at 30°N 119°W) during summer. Another effect is that the removal of those gridpoints adjacent to the coast eliminates some of the points that represent the regional scale positive curl off the coast of California. Since the maxima do not disappear when the topographic effects are removed, this strongly suggests that these maxima are real. Therefore in contrast to the computational amplification of the calculated field of wind stress curl introduced near the mountainous boundaries of the domain by the coarse grid spacing, the Gulf of Alaska and eastern Pacific adjacent to the North American continent are regions where there is an actual physical amplification of the wind stress curl field due to the physical geography of

the area. This occurs principally as a result of the high coastal mountain ranges.

Mean Pressure Field

The annual mean SLP field over the extratropical North Pacific for the period 1946-1988 (figure 1.1) shows two basin scale elliptical features with the boundary between them lying roughly along the 1014 millibar (mb) isobar, which slopes northeastward from 35°N in the western basin to 50°N in the eastern basin. Poleward of the 1014 mb isobar, there is a basin wide low pressure feature with its principal axis slightly tilted southwest to northeast centered at about 55°N 175°E with a central pressure of 1006 mb. To the southeast of the low pressure system, there is a high pressure cell centered near 34°N 140°W with a central pressure of 1022 mb and principal axes aligned directly east to west. These patterns represent the average position and extent of the Aleutian Low and North (or East) Pacific High pressure systems. Pressures associated with the Indonesian Low system appear between 15°N-25°N and 130°E-165°E to the southwest of the 1014 mb isobar that slants southeastward from 25°N.

Angell and Korshover [1982] use monthly mean sea level pressure data on a grid spaced 5 degrees in latitude and longitude for the period 1899 to 1978 to calculate the average positions of the Aleutian Low and East Pacific High at 56°N 168°W and 35°N 143°W respectively. Angell and Korshover [1982] find the average central pressure of the Aleutian Low to

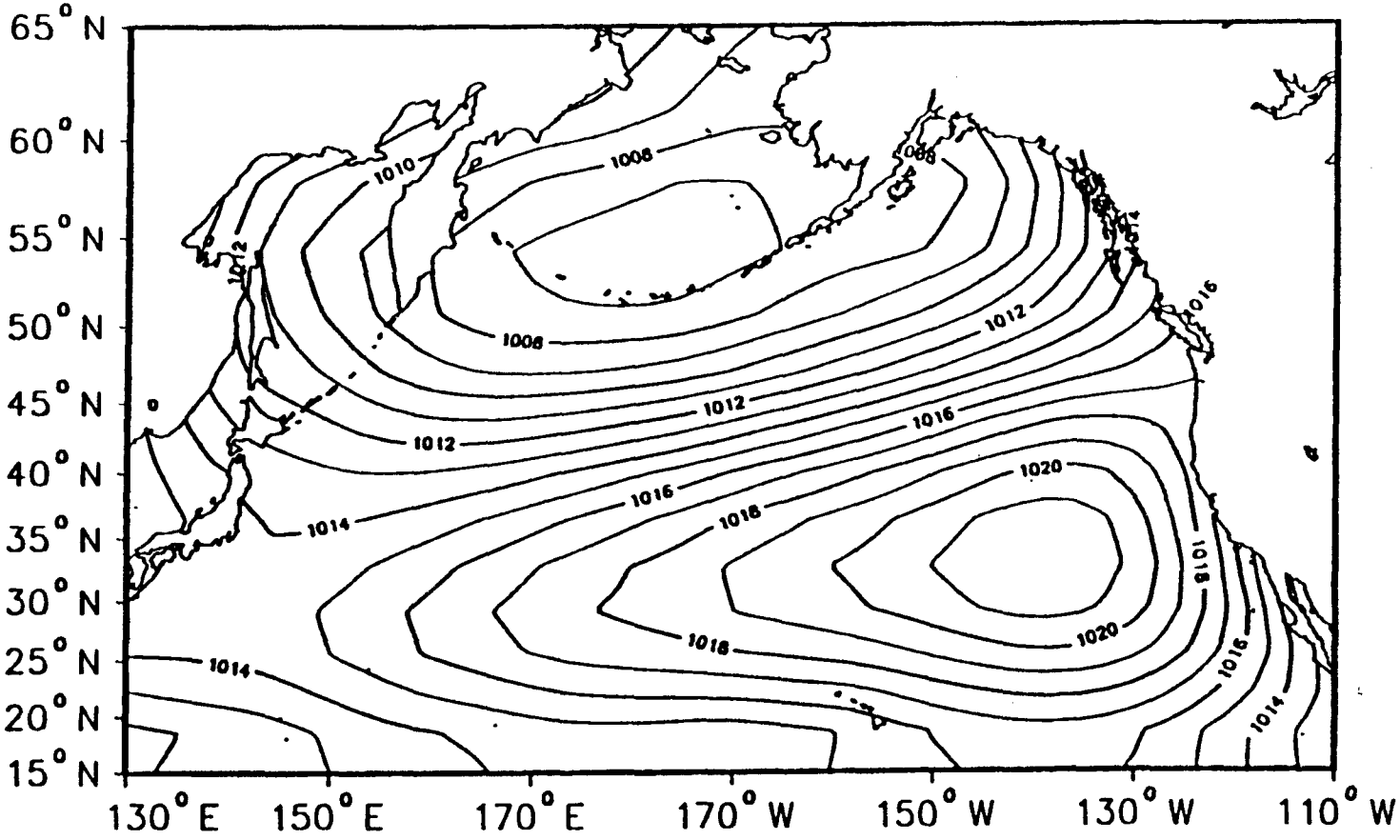

Figure 1.1 : Mean North Pacific sea level pressure 1946-1988. CI= 1 mb.

be 1002 mb. They find a central pressure of 1024 mb for the East Pacific High.

Annual Mean Curl

The annual mean of the wind stress curl for the period 1946-1988 (figure 1.2) shows basin and regional scale features. The northern section of the study area shows a basin scale region of positive curl bounded to the south by the zero contour which appears near 28°N in the western basin and slopes northeastward to about 49°N in the eastern basin. This positive curl is associated with storm systems occurring in the Aleutian Low. Hereafter, "Aleutian Low region" will be taken to be the region from 45°N to 60°N across the Pacific basin (excluding the Sea of Okhotsk). Basin scale negative curl representing winds in the subtropical anticyclone occurs to the south of the zero contour. Regional scale curl features consist of a thin band of positive curl along the California coast , a small region of positive curl off the Hawaiian Islands, and a small region of negative curl off the islands of Japan. The amplitude of the large scale positive wind stress curl generally increases poleward. The maximum values of positive curl (2.0 $*10^{-7}$newtons per cubic meter (N/m^3)) occur over the northern Gulf of Alaska. There is a secondary maximum over the western Bering Sea adjacent to the Kamchatka Peninsula. The maximum amplitudes occur north of 55°N in both regions. The meridional gradient of the positive curl is very weak except over the Gulf of

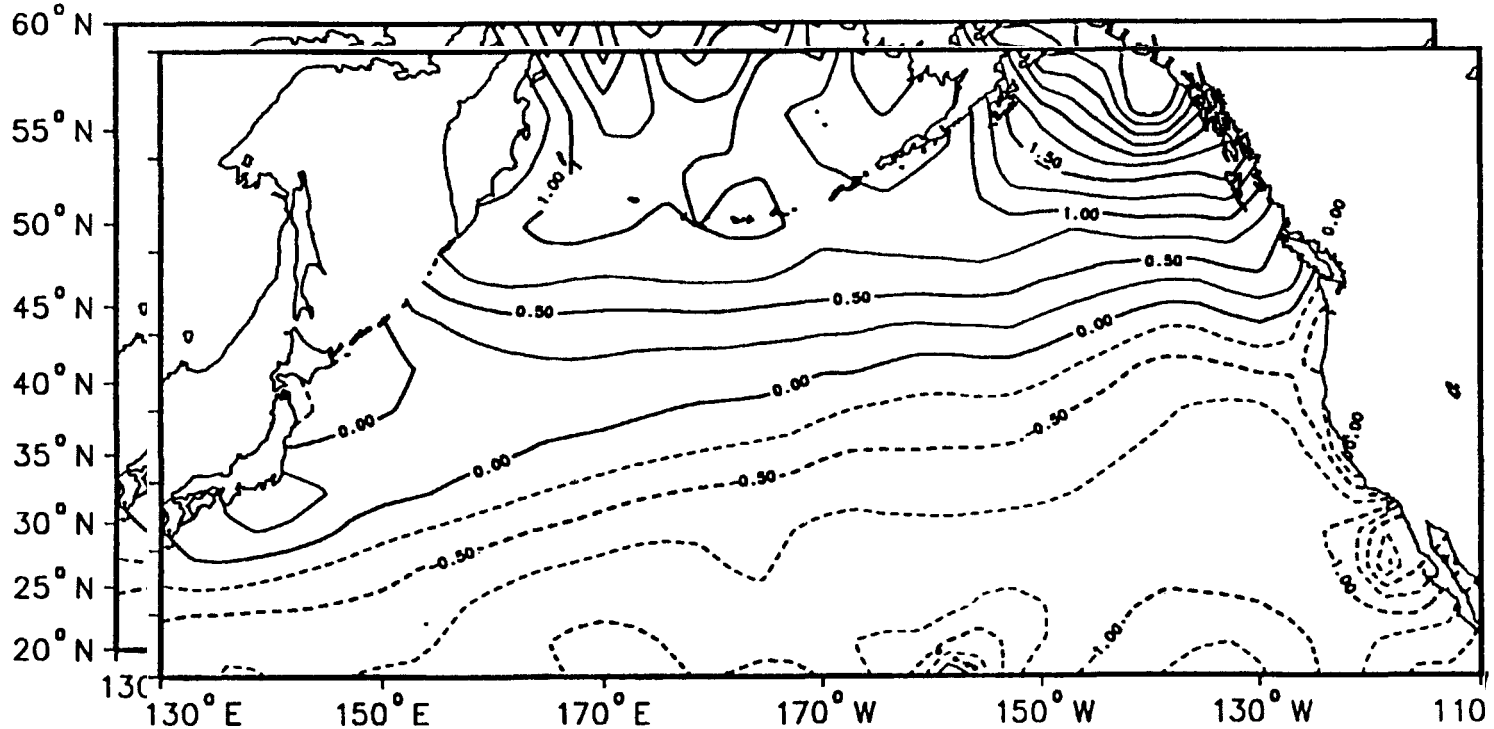

Figure 1.2: Mean North Pacific wind stress curl 1946-1988. CI= 0.25 * 10^{-7} N/m^3.

Alaska. The meridional gradient is weaker than the zonal gradient. The maximum gradient of the curl occurs over the Gulf of Alaska.

In contrast to the general poleward increase in the large scale positive curl field, the amplitude of the large scale negative curl field generally increases equatorward. There is a broad weak maximum between 20°N-25°N and 165°E-125°W. Maximum values of negative curl are about 1.0 $*10^{-7}$ N/m^3. The meridional and zonal gradients of the negative curl are small and nearly constant across the basin.

Mean Fields and Variance

In winter (December -February, figure 1.3a) large amplitude positive curl is present within the Aleutian Low region. The spatial maximum of the positive curl occurs over the northern Gulf of Alaska and a secondary maximum is present in the western Bering Sea near 57°N 175°E. The gradients are greatest over the Gulf of Alaska The zero contour of wind stress curl runs from 28°N in the western basin to 45°N in the eastern basin. This is the southernmost position that the zero contour occupies during the annual cycle. A negative curl maximum occurs in the western Pacific near 20°N 135°E, and there is a secondary maximum in the eastern Pacific at about 20°N 130°W. The largest negative curl gradients within the annual cycle occur in the western Pacific during winter. The positive curl observed near Hawaii in the mean curl field is not present during any of the winter months, while positive curl occurs off California during all of these months. Near Japan there is a local positive

curl maximum adjacent to a small region of negative curl. Within the annual cycle, the highest amplitudes of both the positive and negative basin scale curl occur during January.

During spring (March-May, figure 1.3b) the amplitude and meridional extent of the basin scale positive curl greatly decreases as the Aleutian Low weakens and the North Pacific High strengthens and broadens. The amplitude of the positive curl decreases through March and April. In May a weak maximum occurs along 50°N. This weak maximum reflects summer cyclone activity in the Bering Sea and Gulf of Alaska.The zero curl contour moves northward by about five degrees to between 45°N and 50°N in the central and eastern sections of the basin, and to between 40°N and 45°N in the western basin. The spatial extent of the negative curl expands poleward with the advancing high pressure. The amplitude of the negative curl field is slightly less than during winter over most of the ocean. During May the amplitude of the negative curl field adjacent to North America increases significantly. The region of negative curl observed off Japan in the winter expands to the east during March and merges with the large scale negative curl field in April and May. Positive curl is present near the Hawaiian Islands during all of spring, while the region of positive curl off California is present only during March.

In summer (June-August, figure 1.3c) the amplitude and spatial extent of the positive curl within the region of the Aleutian Low are at their annual minimum values. The annual maximum spatial extent of the basin scale negative curl occurs during the summer months. The

annual maximum of the amplitude of the negative curl field adjacent to North America (east of 130°W) occurs during July. The gradients of both the positive and negative curl are very weak except for the regional negative curl maximum adjacent to North America. Weak negative curl is observed over the northeastern Gulf of Alaska, eastern Bering Sea and off the northern Kamchatka Peninsula. The negative curl observed near Japan in winter and spring has moved slightly northward and has expanded further to the east, extending to about 160°E. Positive curl is observed near Hawaii during all of summer, and the annual maximum occurs near Hawaii during July. Positive curl is present off the California coast during July and August.

During fall (September-November, figure 1.3d), strengthened positive curl is present across the basin north of 45°N-50°N. Negative curl extends across most of the basin south of 45°N. The amplitude of the positive curl increases poleward and maxima occur in the northern Gulf of Alaska and eastern Bering Sea. Strong positive curl occurs over the Gulf of Alaska one to two months before strong curl develops over the Bering Sea. The spin-up begins in September in the Gulf of Alaska while a well developed cyclonic circulation pattern does not appear in the Bering Sea until October or November. Positive curl occurs to the south and southeast of Japan between 20°N-35°N and 130°E-155°E and a local maximum occurs in this region in October. Positive curl is present off California during all fall months. The annual maximum of the curl off California occurs during this time. Very weak positive curl occurs near Hawaii during September and November.

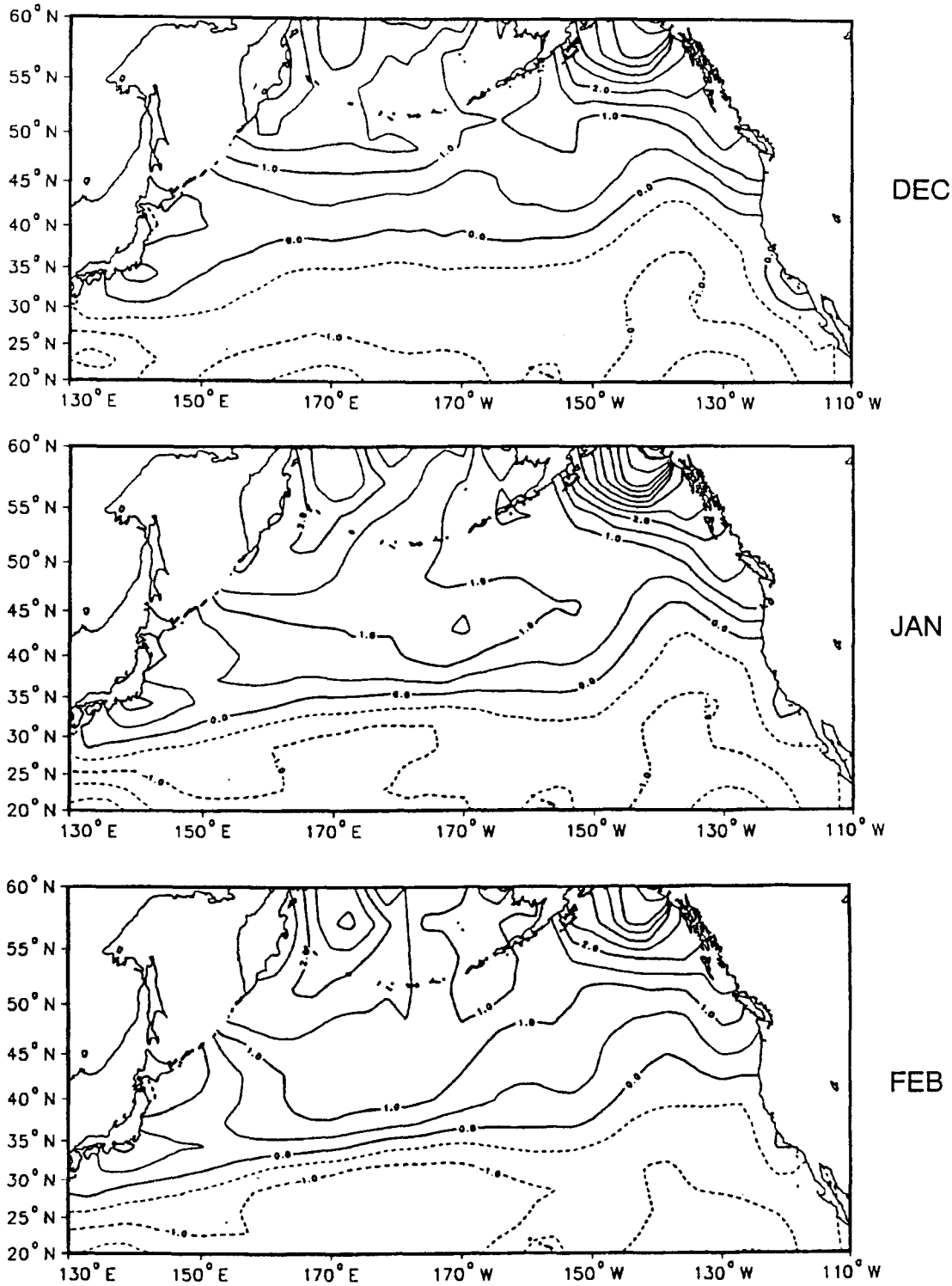

Figure 1.3a: Mean Wind Stress Curl., Dec.-Feb. CI= 0.5 * 10^{-7} N/m^3.

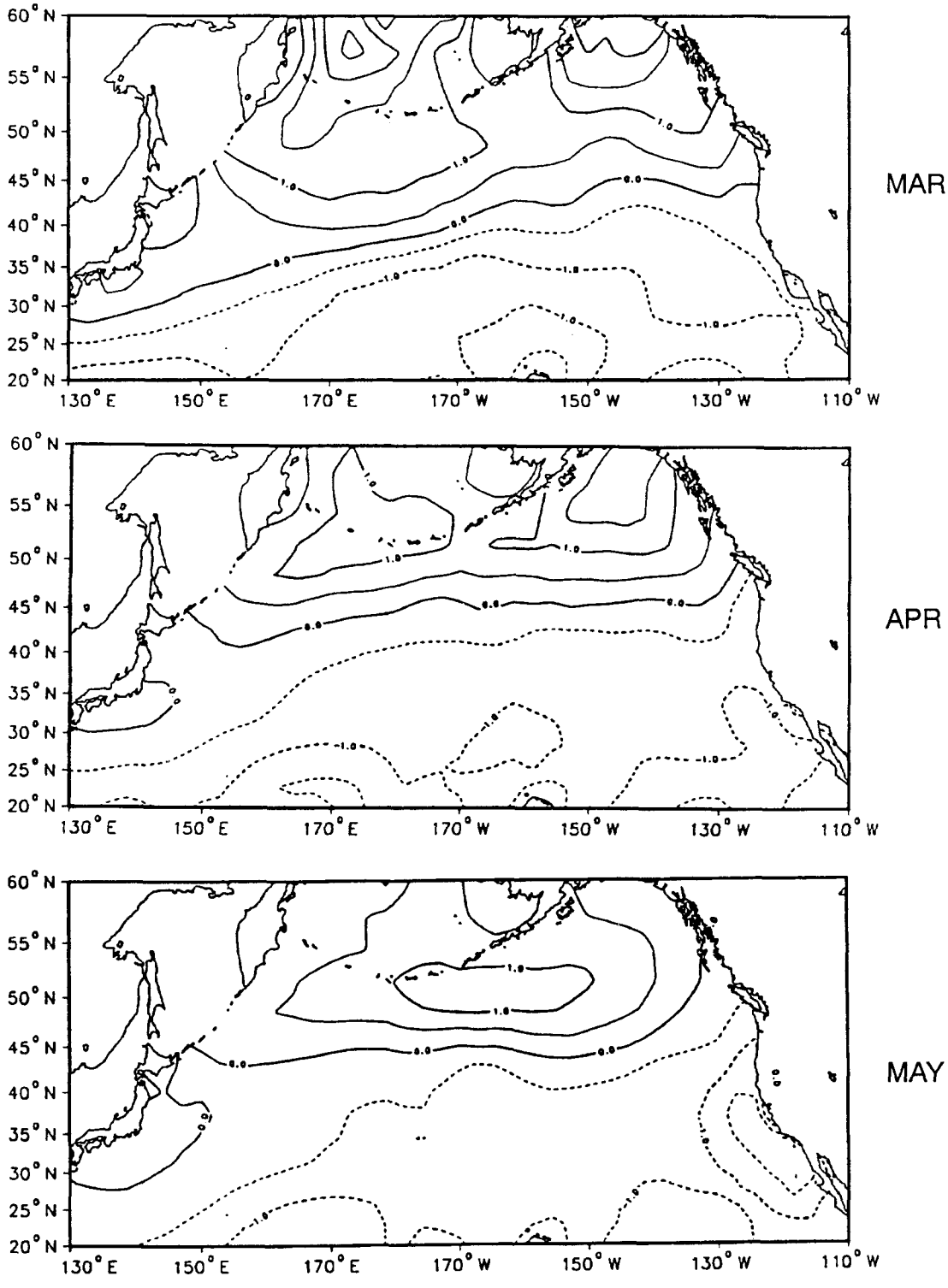

Figure 1.3b: Mean Wind Stress Curl., Mar.-May CI= 0.5 * 10^{-7} N/m^3.

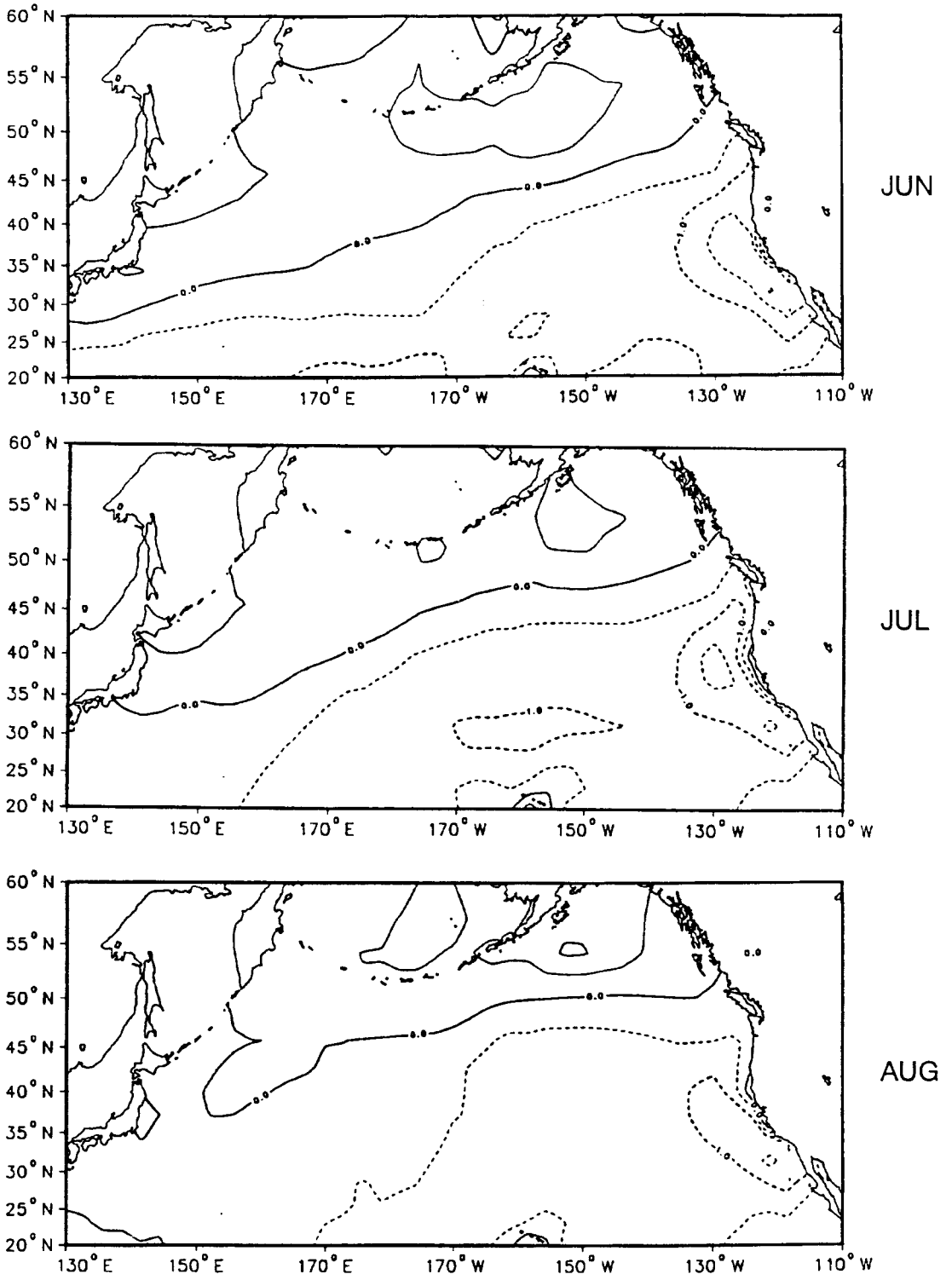

Figure 1.3c: Mean Wind Stress Curl., Jun.-Aug. CI= 0.5 * 10^{-7} N/m^3.

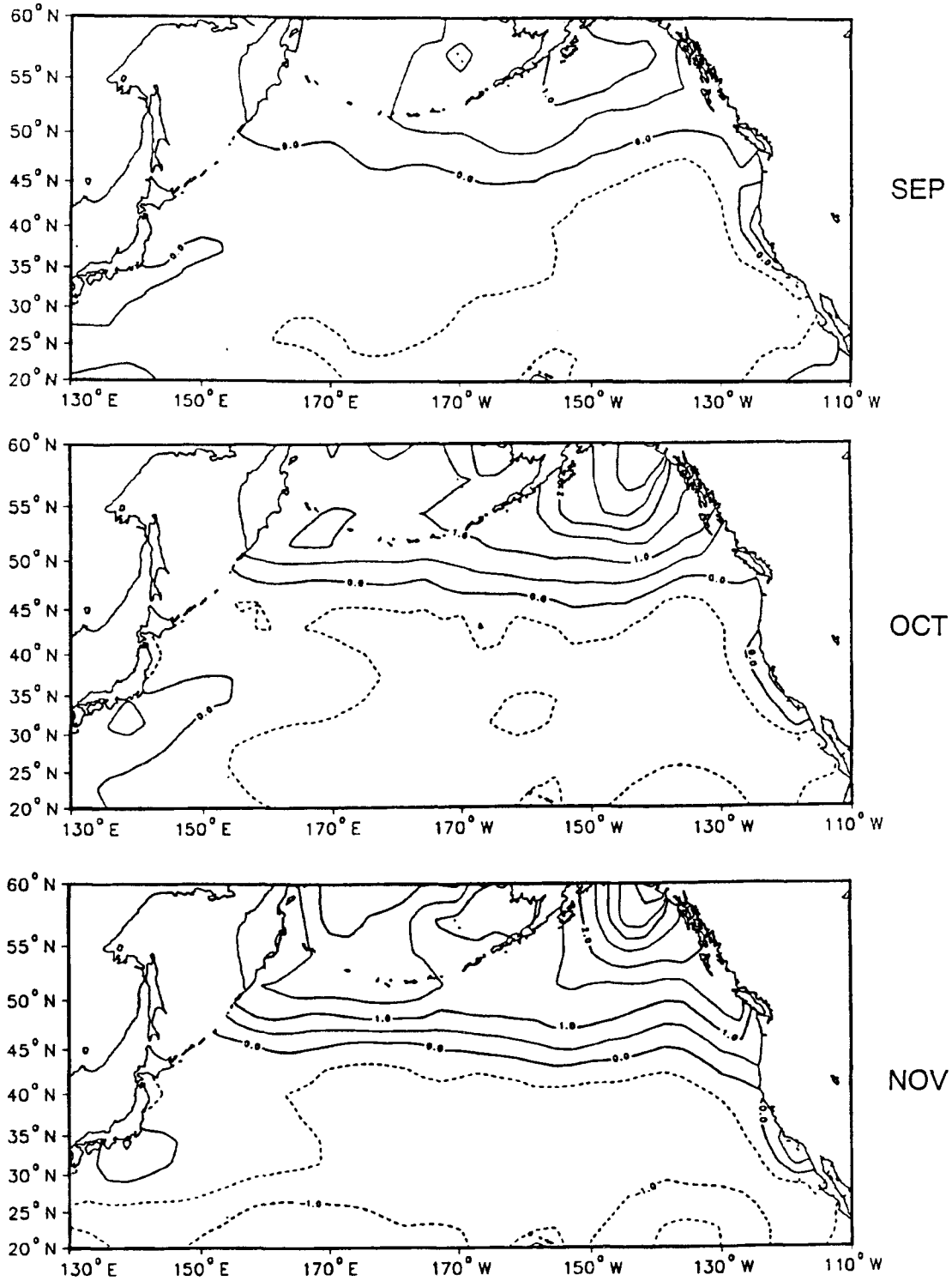

Figure 1.3d: Mean Wind Stress Curl., Sep.-Nov. CI= 0.5 * 10^{-7} N/m^3.

The variances of the monthly mean curl fields are shown in figure 1.4. During winter, the variance shows a general increase poleward from 20°N to 60°N (figure 1.4a). The variance is high within the entire Aleutian Low region, and the largest values occur across the basin north of 50°N. North of 50°N the annual maximum of the variance occurs during winter.

Throughout the spring and summer the variance steadily decreases within the region of the Aleutian Low (figure 1.4a and 1.4b). The magnitude of the variance is small and the spatial distribution is relatively homogeneous over most of the region from 20°N to 60°N from June through August. There is a local maximum off the Hawaiian Islands throughout the summer. There is also a local maximum off the coast of North America east of 130°W and between 20°N and 50°N. In this region the magnitude of the variance steadily increases beginning in March, and reaches maximum values during July and August. In fall, the variance begins to decrease adjacent to the coast of North America and continues to decrease throughout the months of fall and into winter (figure 1.4b). Within the region dominated by the Aleutian Low, the variance increases throughout fall and into winter. South of 30°N and away from the coast of North America the variance is small and nearly constant throughout the fall. The maximum amplitude of the variance occurs over the Gulf of Alaska and Bering Sea during winter. This maximum is associated with frequent and intense cyclone activity in the Aleutian Low. The largest values of the variance occur adjacent to the coast of North America during July. This appears to be associated with

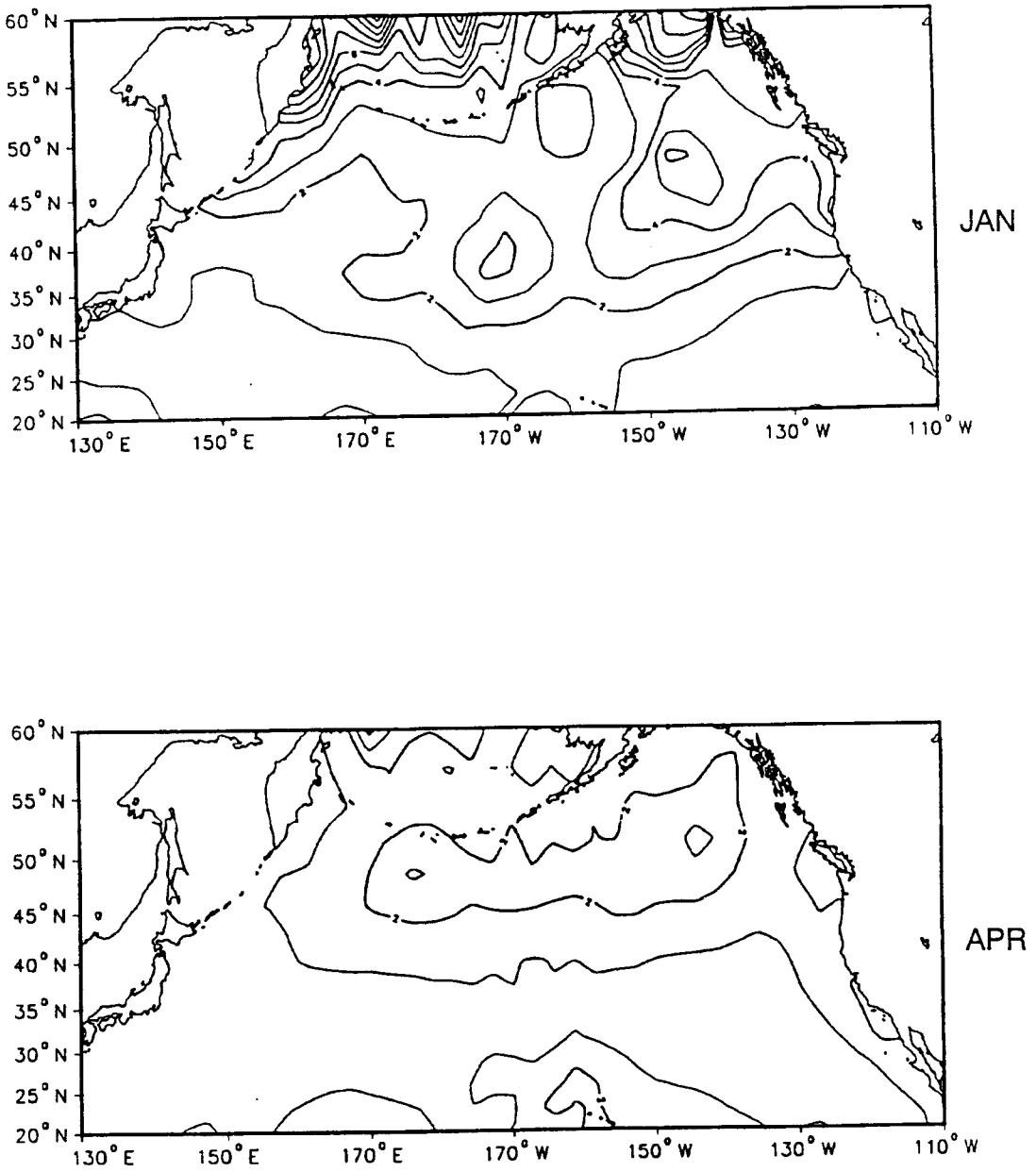

Figure 1.4a: Variance of Wind Stress Curl during winter and spring, CI= 1 unit.

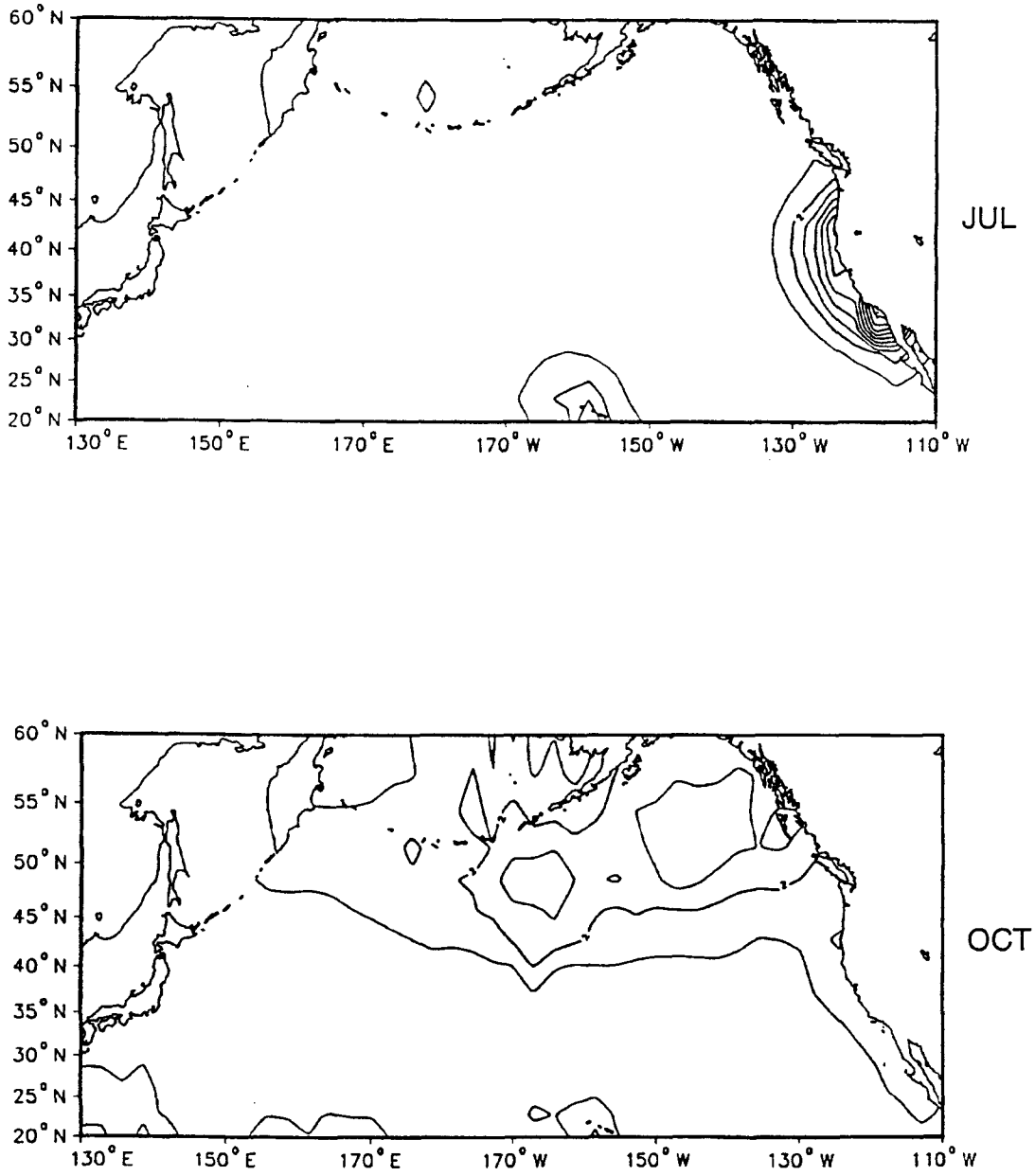

Figure 1.4b: Variance of Wind Stress Curl during summer and fall, CI= 1 unit.

the intensification of upwelling favorable winds that occurs during summer, and with the development of the southwest U. S. thermal low. Therefore, there is a phase difference of about six months between the occurrence of the maximum variance within the Aleutian Low and that off the west coast of North America. This phase difference arises as a result of the fact that the strongest atmospheric circulation occurs during winter over the Gulf of Alaska and Bering Sea, while the circulation is strongest adjacent to the west coast of North America during summer.

Annual and Semi-annual Harmonics and Spectral Energy

Power spectral analysis at points along several meridians demonstrated that the dominant signals in the power spectra of wind stress curl over most of the study area are the annual and semi-annual signals. The amplitude of the power spectral density of the annual signal (figure 1.5a) is highest over the Gulf of Alaska. Large amplitudes also occur over the Bering Sea and within about 500 to 900 km of the North American continent from Alaska to Baja California. The relative amplification of the field of wind stress curl adjacent to the coast of North America demonstrates that on annual time scales the wind field in the coastal zone of the eastern North Pacific differs significantly from the wind field over the open ocean. This is consistent with the result of Chao [1985], who notes that the alongshore jet in the wind field off North America has a width scale of 1000 km. A region of high amplitude energy at the annual period extends from the western Pacific to about 145°W

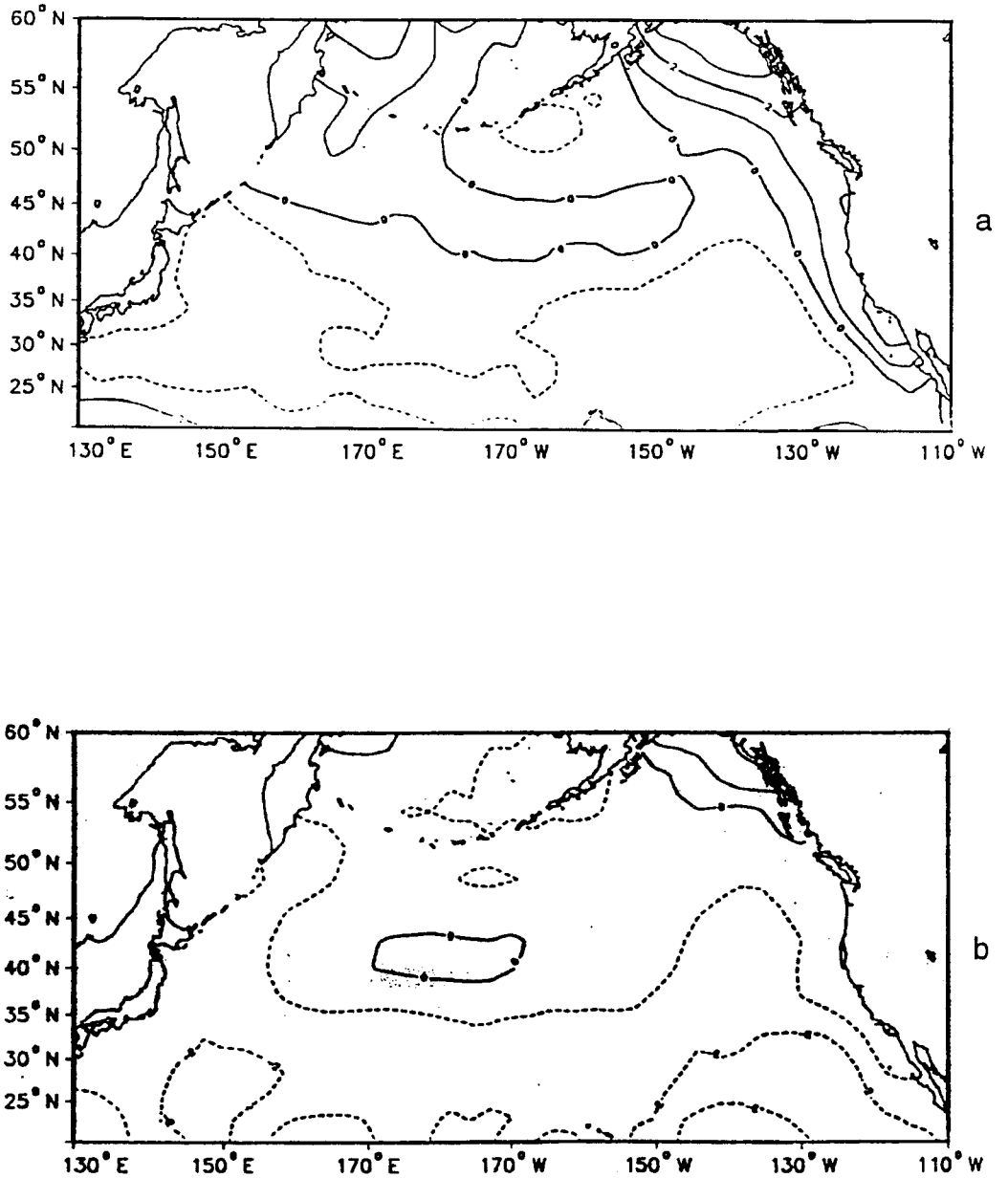

Figure 1.5: Logarithm of spectral energy of Wind Stress Curl CI= 1 unit.
a) Annual period; b) Semi-annual period.

between 45°N and 50°N. The energy of the annual signal is low and nearly constant over most of the basin south of 45°N, and in the central subarctic region between 180°W and 150°W.

In contrast to the energy of the annual signal, the power spectral energy of the semi-annual signal (figure 1.5b) is greatest over the Gulf of Alaska. There are secondary maxima adjacent to the northern Kamchatka Peninsula and over the open ocean between 40°N-45°N and 170°E-170°W. The open ocean maximum is probably associated with the region of intense open ocean cyclogenesis observed by Gyakum et al. [1989]. Amplitudes are small and nearly constant over much of the rest of the open ocean. Minimum values occur south of 30°N across most of the basin.

The seasonal cycle of the curl was removed from the data primarily to determine interannual variability in the residual anomaly time series. The largest amplitudes of the least squares fit to the annual harmonic of the curl (figure 1.6a) occur over the Gulf of Alaska. A secondary maximum is present over the western Bering Sea adjacent to the Kamchatka Peninsula. The amplitude of the maximum curl over the Gulf of Alaska is twice that of the maximum in the western Bering Sea. The amplitude of the annual harmonic is also large over the Kuroshio region and in a region extending from the coast of Canada to 170°E between 40°N and 45°N. The minimum amplitudes of the annual harmonic occur over most of the subtropical gyre and in the central subarctic from 45°N to 57°N and 170°E to 155°W. The maximum amplitude of the semiannual harmonic (figure 1.6b) occurs over the Gulf

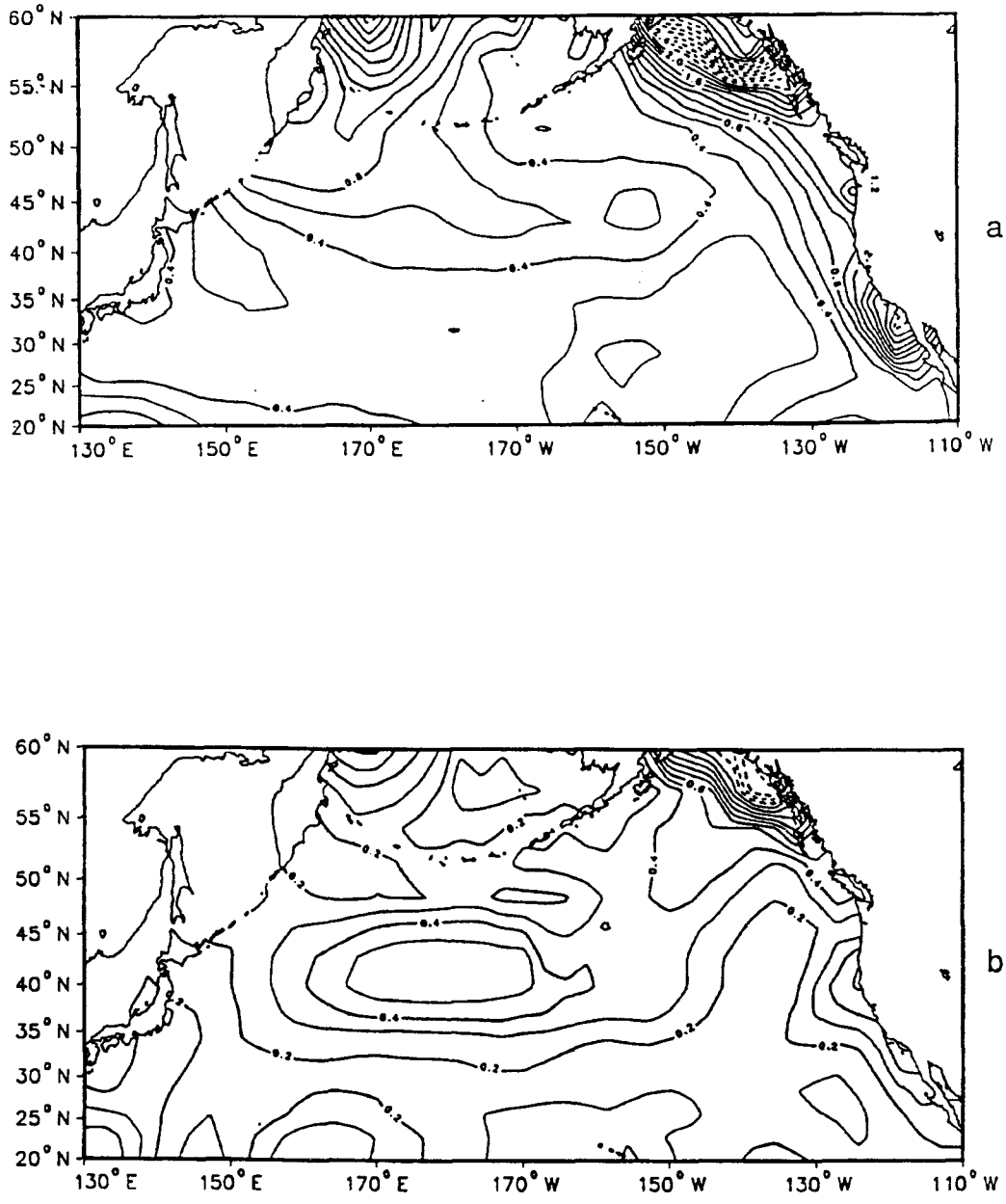

Figure 1.6: Amplitude of Wind Stress Curl CI= (a) .2 units, (b) .1 units.
a) Annual harmonic; b) Semi-annual harmonic.

of Alaska. A secondary maximum occurs over the central ocean between 35°N and 45°N from 160°E to 160°W. The maximum occurs because this is a region of frequent cyclogenesis as documented by Terada and Hanzawa [1984] and Gyakum et al. [1989].

Annual Cycle of Zonal Mean Curl

The annual mean of zonally averaged curl (figure 1.7) shows positive curl monotonically decreasing towards zero from 60°N to 45°N, while the negative curl becomes increasingly negative between 42°N and 24°N. Positive curl maxima occur at 57°N and 60°N while the negative curl maximum occurs over the region between 21°N and 30°N. The boundary between the subtropical and subarctic atmospheric circulation is between 42°N and 45°N as indicated by the latitude of zero wind stress curl.

The correlation matrix of annual mean values of the zonally averaged curl (table 1.1) shows that annual period fluctuations are coherent within the Aleutian Low region from 45°N to 60°N and within the subtropical anticyclone between 21°N and 27°N. The correlations between curl in the Aleutian Low all exceed 0.6 while those between 21°N to 27°N are greater than 0.7. These regions fluctuate out of phase with each other over the course of the annual cycle. In the Aleutian Low from 45°N to 60°N the maximum curl occurs during November through February and the annual minimum occurs from May through August. In the subtropical anticyclone between 21°N and 27°N the maximum negative curl occurs during winter as within the Aleutian Low, although the minimum values

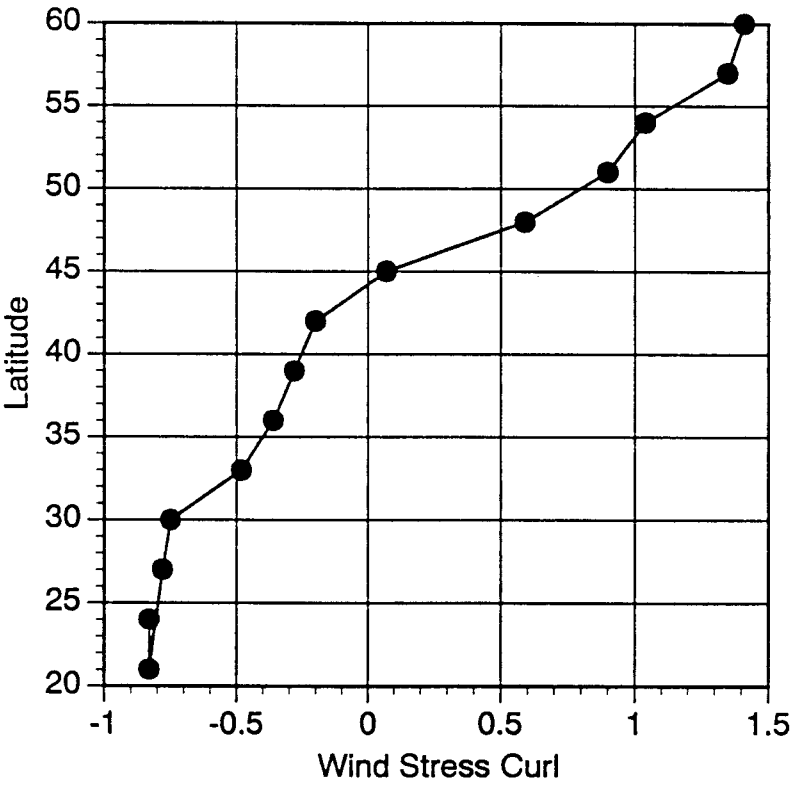

Figure 1.7: Annual mean of zonally averaged Wind Stress Curl. Units are 10^{-7} N/m^3.

	60°N	57°N	54°N	51°N	48°N	45°N	42°N	39°N
60°N	1							
57°N	.9822523	1						
54°N	.9072419	.9181823	1					
51°N	.837919	.8047402	.8999189	1				
48°N	.8842882	.8611853	.7664456	.8614479	1			
45°N	.7997342	.8203203	.6123796	.6163522	.9131	1		
42°N	.6703669	.7365838	.4932839	.3423719	.6899979	.9109893	1	
39°N	.5067123	.6001573	.3541292	.1096209	.4477573	.7291075	.9340484	1
36°N	.415487	.5230957	.2964641	.0194978	.2827893	.5467188	.7781024	.9360535
33°N	.5303422	.6144531	.633131	.457325	.3491392	.3246731	.3484426	.4331474
30°N	-.048514	-.087413	.1272327	.1103012	-.290062	-.534667	-.622508	-.574644
27°N	-.394261	-.414818	-.39987	-.581418	-.70884	-.688314	-.502933	-.308308
24°N	-.686922	-.626451	-.650705	-.851461	-.872639	-.680992	-.356463	-.072663
21°N	-.648106	-.636831	-.58558	-.742793	-.901127	-.840851	-.6065	-.340194

	36°N	33°N	30°N	27°N	24°N	21°N
36°N	1					
33°N	.603537	1				
30°N	-.371401	.3687113	1			
27°N	-.143429	-.089429	.5778864	1		
24°N	.0821599	-.203109	.1142987	.7490319	1	
21°N	-.129986	-.158245	.4363601	.8893136	.9180311	1

Table 1.1: Correlation matrix of zonal mean wind stress curl.

occur from July through September, which is one to two months later than when the minimum curl occurs in the Aleutian Low. At 30°N and 33°N negative curl maxima occur during mid-summer and minimum values are observed during fall and winter. The negative curl at 33°N and 30°N during summer is probably associated with a regional intensification of the curl occurring adjacent to the coast of North America. The wind stress curl at lower latitudes is nearly 180° out of phase with the Aleutian Low region. Between 33°N and 39°N, maximum negative values occur during spring and fall and negative minimum values during mid-summer. Negative zonal mean curl occurs during June and July at 60°N, while positive curl does not occur at any time south of 33°N in the zonal mean and negative curl does not occur at any time from 51°N to 57°N. Between 36°N and 48°N the curl oscillates between positive and negative during the annual cycle (figure 1.8a) as the North Pacific High and Aleutian Low shift their meridional positions. The range of the seasonal cycle (figure 1.8b) is largest in the Aleutian Low region and smallest in the subtropical anticyclone between 27°N and 33°N. The maximum range occurs at 60°N and is 8.5 times larger than the minimum range which occurs at 27°N. Over most of the other latitudes, the range is 2 to 3 times greater than the minimum range.

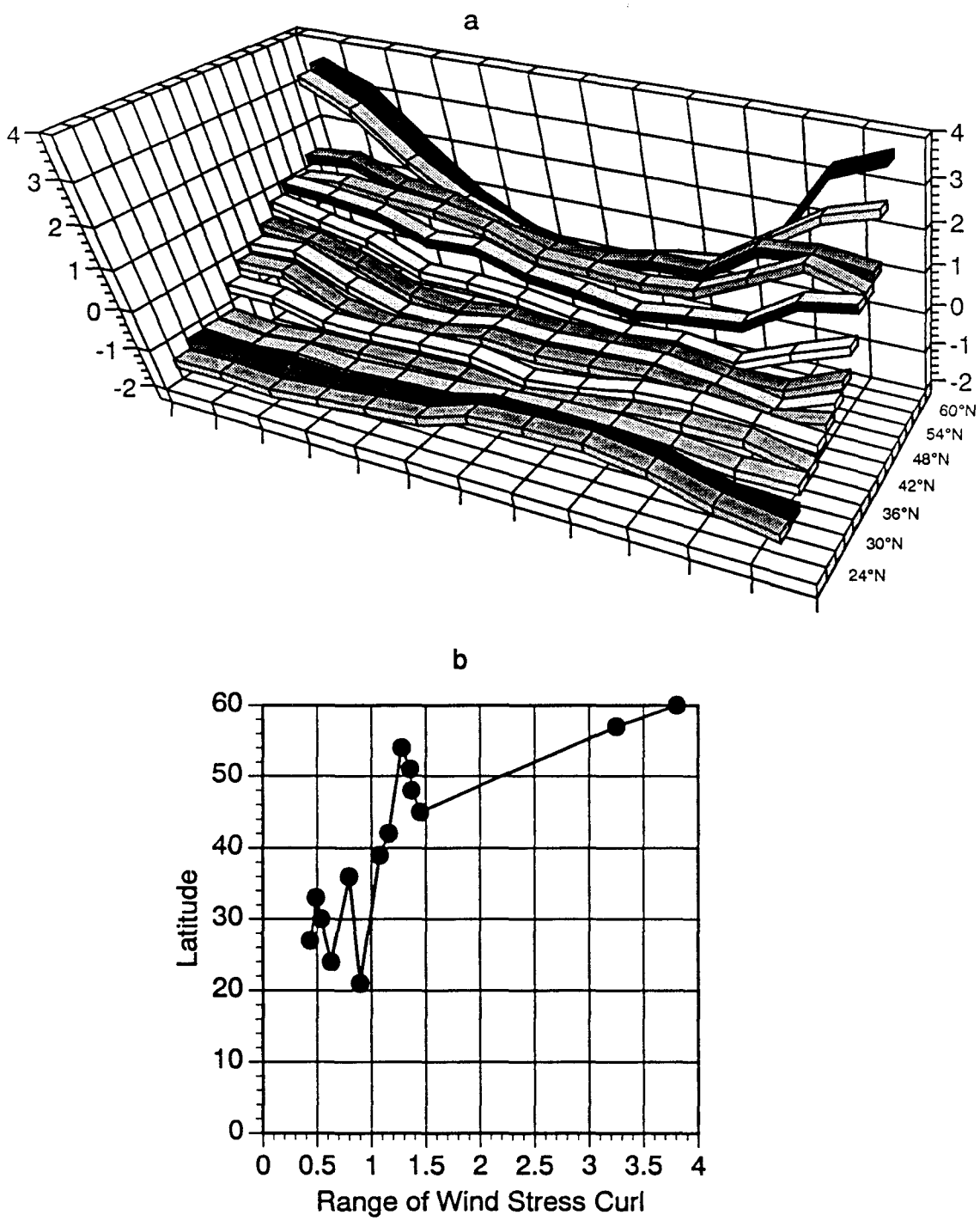

Figure 1.8: a) Annual cycle of zonal mean Wind Stress Curl. b) Range of zonal mean curl, Units are 10^{-7} N/m^3.

Annual Cycle North Pacific Sverdrup Transport

Integrated Sverdrup transports were computed across the Pacific basin along lines of latitude from the mean fields of the wind stress curl according to:

$$\Psi = \int \frac{\nabla x \bar{\tau}}{\beta} dx \qquad (1.4)$$

where Ψ is the meridional transport,

$\nabla x \bar{\tau}$ is the curl of the wind stress,

and β is the meridional gradient of the Coriolis parameter.

The annual mean Sverdrup transport (figure 1.9) shows that the boundary between the subarctic cyclonic circulation and the anticyclonic subtropical gyre lies roughly along 45°N across the basin. In the Kuroshio region the transport is about 45 Sverdrups (Sv) at 25°N. Transport in the Alaska Stream is about 15-20 Sv while the transport in the Kamchatka Current system is 35 Sv. The strongest flow gradients in the subtropical circulation occur in the region of the Kuroshio between 30°N and 35°N. The strongest gradients in the subarctic circulation occur in the Oyashio region between 45°N and 50°N and 155°E to 170°E. Monthly mean Sverdrup transport parallels the strength of the wind stress curl. The Sverdrup transport is strongest during winter, weakest during summer, and of intermediate strength during spring and fall (figure 1.10).

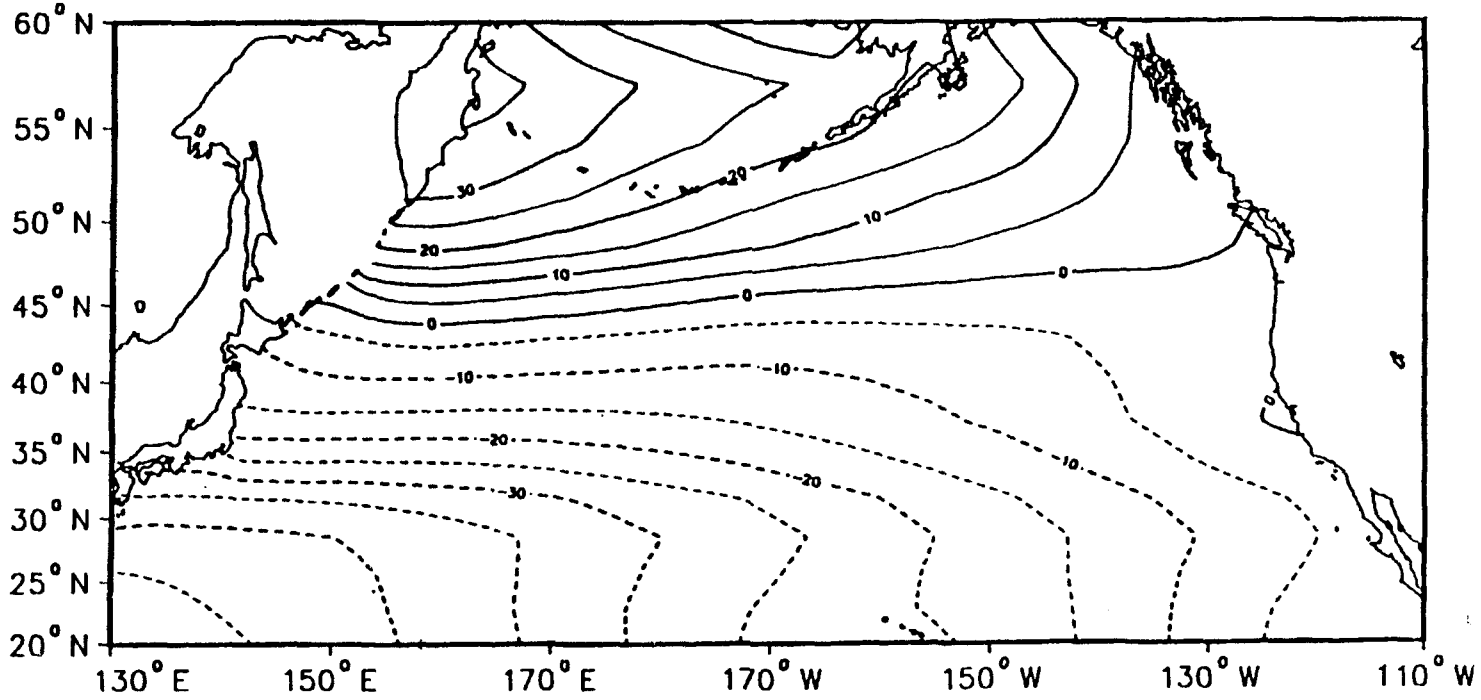

Figure 1.9: Annual mean Sverdrup transport. CI= $5.0*10^6$ m^3/s.

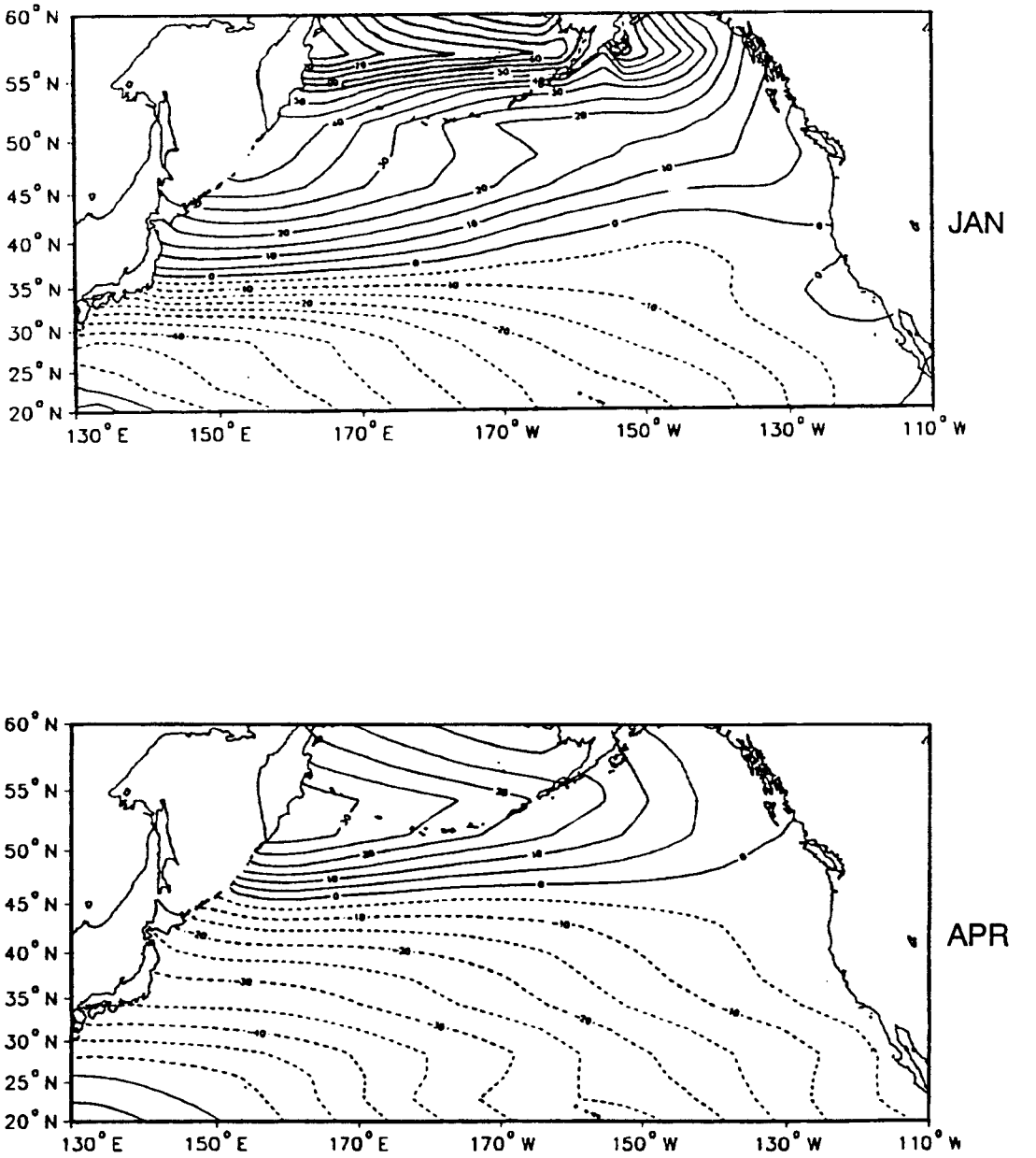

Figure 1.10a: Sverdrup transport during winter and spring, CI= $5.0*10^6$ m^3/s.

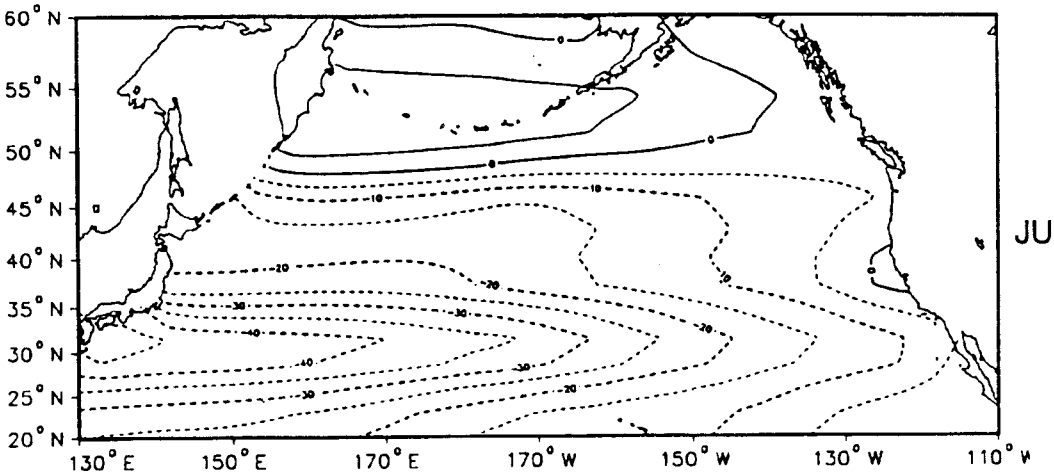

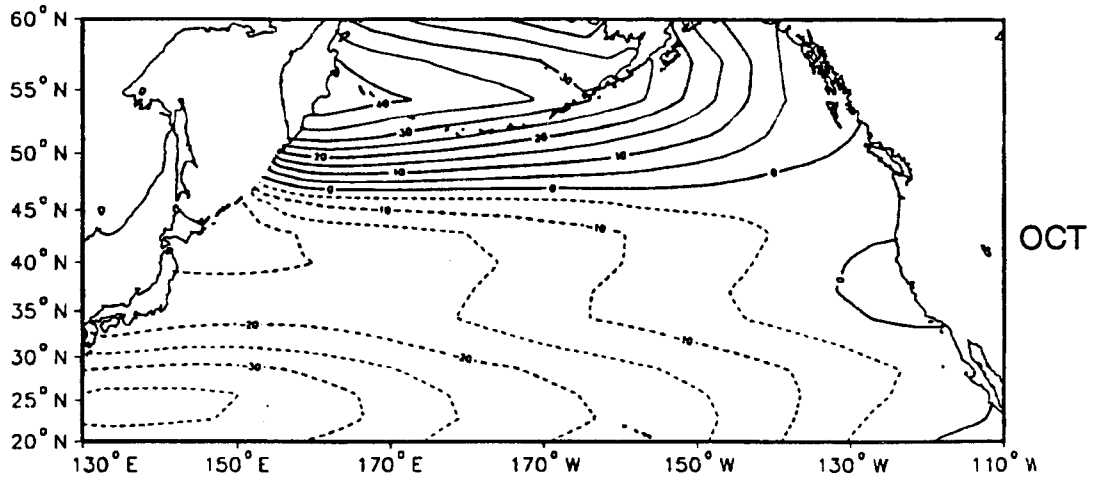

Figure 1.10b: Sverdrup transport during summer and fall, CI= $5.0*10^6$ m^3/s.

The Sverdrup relation is applicable in the open ocean away from the effects of boundaries. Transports in the western boundary current systems largely represent the return flows of the circulation in the Sverdrup interior. Therefore transport variations in the western boundary systems are used as indicators of the variability of the wind driven circulation. Seasonal variations in Sverdrup transport in the three western boundary current regions of the North Pacific are shown in figure 1.11. Seasonal transport variations are largest in the Kamchatka Current system of the western subarctic. The seasonal range in the Kamchatka Current is 70 Sv, while in the Kuroshio it is 35 Sv, and in the Alaska Stream the range is 30 Sv.

The contour of zero Sverdrup transport does not coincide with the zero contour of wind stress curl. The boundary between the subtropical and subarctic gyres is therefore taken to be the zero Sverdrup transport contour (after Talley, 1985). The boundary is displaced to its farthest south position during winter and migrates to its furthest north location during summer. During the annual cycle the boundary is displaced from 36°N to 50°N in the western Pacific and 45°N to 50°N in the eastern part of the basin. The zero contour is actually displaced to 60°N in the Gulf of Alaska during summer when negative curl is present in the mean field over the eastern gulf region.

The calculation of the Sverdrup transport used in this study assumes a flat bottomed ocean. It has recently been shown (Cummins 1989, Bang 1991) that the effects of sloping bottom topography in the

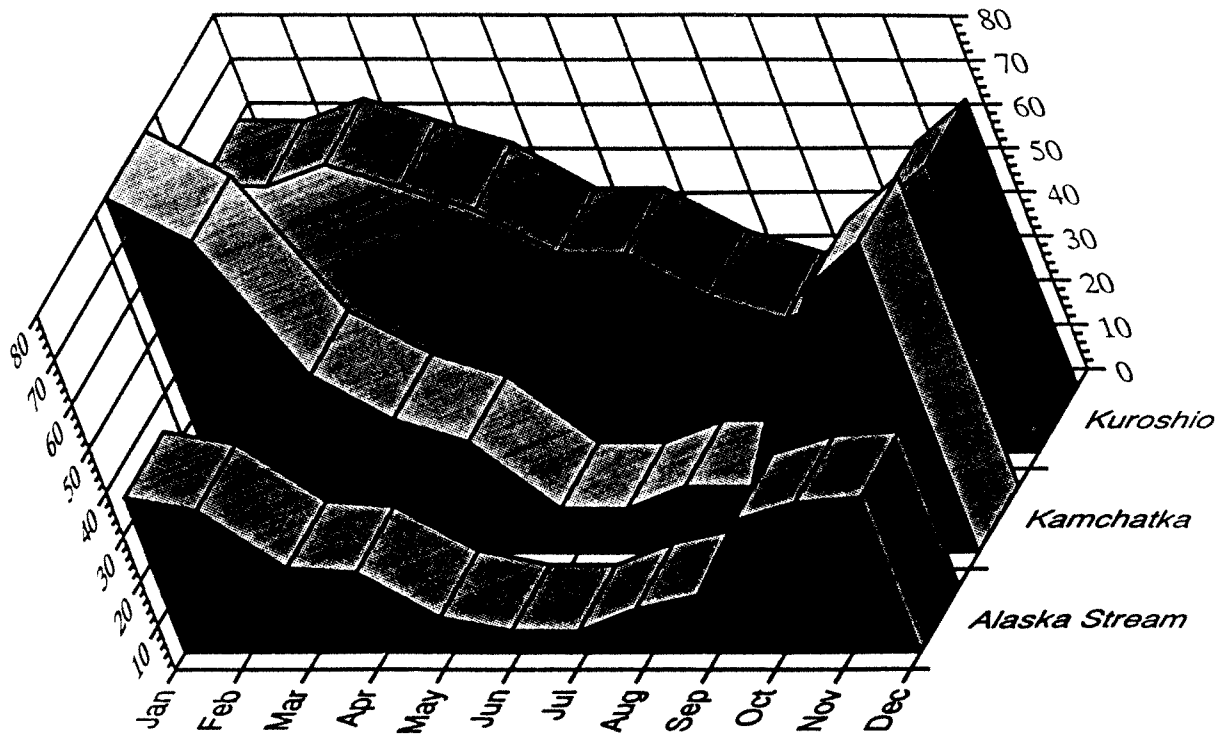

Figure 1.11 : Annual cycle of western boundary current transports . Units are 10^6 m^3/s.

subarctic North Pacific greatly reduce the large oceanic response to annual period wind stress curl forcing that the flat bottom Sverdrup balance predicts. The slope of the bottom topography effectively enhances the meridional gradient of the planetary vorticity (beta), thereby reducing the seasonal baroclinic response since the beta term is in the denominator of the Sverdrup relation (Equation 1.4). A significant improvement to the calculations presented in this work could be made by integrating along lines of constant potential vorticity (f/H) instead of along lines of constant planetary vorticity (f), thus including the effects of changes in bottom topography. This will be undertaken in a subsequent study.

Comparison with Previous Studies

The spatial structure of the mean wind stress curl field computed by Rienecker and Ehret [1988] using COADS for the period 1960-79 is quite similar to the spatial structure of the mean curl of this study, where the mean was computed for the period 1946-88. In both studies the subarctic region is characterized by maximum positive curl in the Gulf of Alaska with a secondary maximum in the western subarctic adjacent to the Kamchatka Peninsula. The location and slope of the zero contour are very similar across the basin. Differences occur in the structure of the subtropical anticyclone, where that of Rienecker and Ehret has a more gyre like structure than the subtropical anticyclone computed in this study. The region of positive curl adjacent to North America is more clearly evident in the mean field of Rienecker and Ehret than it is in the

present study. Positive curl that occurs off the Hawaiian archipelago is not present in the mean field of Rienecker and Ehret. The amplitudes of the maxima of this study are smaller than those computed by Rienecker and Ehret. They differ by 0.5 to 1.0 $*10^{-7}$ N/m^3 in both the subarctic circulation and the subtropical anticyclone. The results of this study underestimate the wind stress because of the constant drag coefficient. Rienecker and Ehret note that the drag coefficient they used results in an overestimate of the stress. Therefore it appears that differences in amplitude are partly accounted for by the use of different formulations of the drag coefficient.

Even though the wind stress curl used in this study has been systematically underestimated through the use of a constant drag coefficient, the characteristics of the computed field of wind stress curl are found to be qualitatively consistent with, and quantitatively similar to, those derived in recent studies of the North Pacific (e.g. Kutsuwada, 1982, Rienecker and Ehret, 1988) and global wind fields (e.g. Hellerman and Rosenstein, 1983, Harrison, 1989, Trenberth et. al, 1989). These previous studies exhibit significant variability between their respective numerical values of wind stress and wind stress curl, and differ in their representations of regional scale features, although the large scale spatial structures are similar. These variations are caused both by different formulations of the drag coefficient and by differences in the data sets employed in the calculations (e.g COADS, ECMWF, FNOC, TDF11, Japanese Meteorological Agency).

Kutsuwada [1982] characterizes the annual cycle of North Pacific wind stress curl between 0°N and 50°N on a two degree grid using fourteen years of ship observations from the Japanese Meteorological Agency (JMA). His numerical values of zonally averaged curl between 50°N and 20°N are used to compare with the zonally averaged curl computed from the FNOC SLP data. The comparisons are for every three degrees from 21°N to 48°N, and the JMA data were interpolated onto the three degree grid. The JMA data at 50°N were directly compared to the FNOC data at 51°N. The shapes of the respective annual curves are similar at most latitudes, although numerical values differ by up to a factor of two (figure 1.12). The seasonal range of the JMA data exceeds that of the FNOC data at all latitudes except 45°N. The mean values and standard deviations of the JMA curl are larger than the FNOC curl between 27°N and 39°N, while the FNOC means are larger at 21°N, 24°N, and from 42°N to 50°N. The above comparisons demonstrate that the curl calculated from the FNOC pressure field is qualitatively and quantitatively consistent with the results of other studies.

The annual average Sverdrup transports computed in this study are quantitatively similar to transports computed in previous studies [Kutsuwada 1982, Hellerman and Rosenstein 1983, Talley 1988, Harrison 1989, Trenberth et al. 1989]. A comparison of the annual average transport values in the three western boundary current regions of the North Pacific is shown in table 1.2. Maximum values of transport in the Kuroshio and Kamchatka regions were used, while the Alaska Stream transport was taken to be the transport at 50°N 170°W. The values

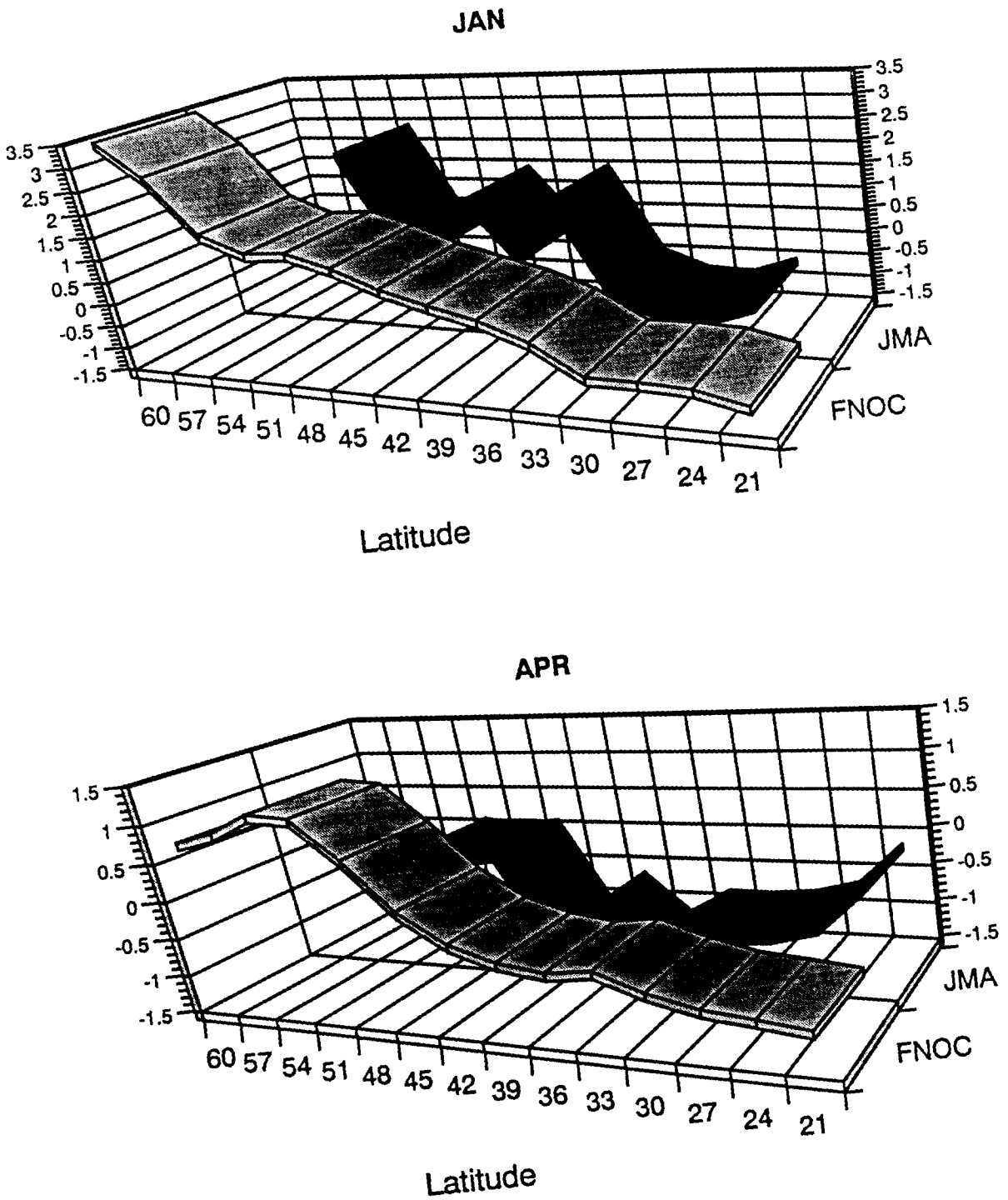

Figure 1.12a: Comparison of zonal mean curl during winter and spring using JMA and FNOC data, units are 10^{-7} N/m^3.

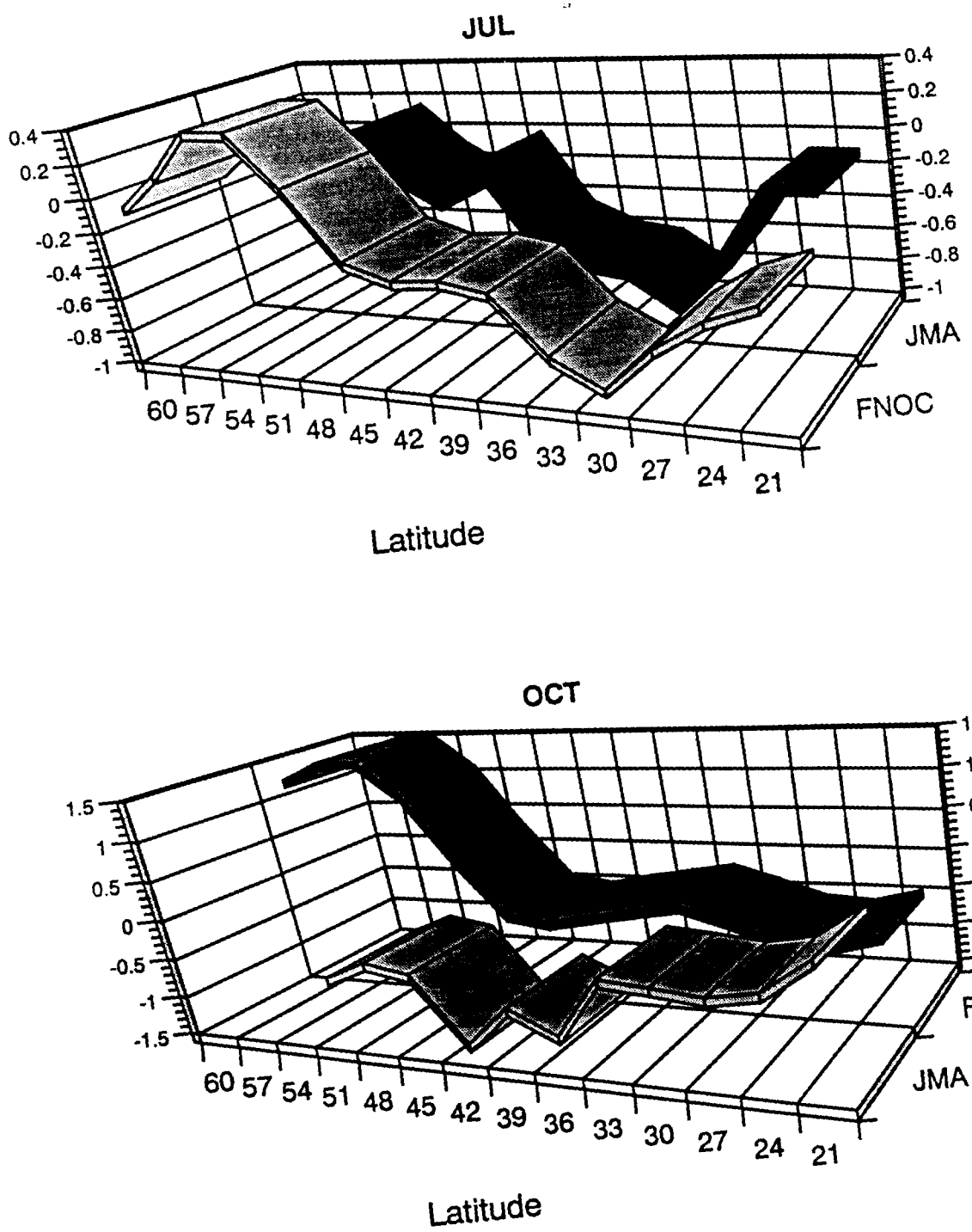

Figure 1.12b: Comparison of zonal mean curl during summer and fall using JMA and FNOC data, units are 10^{-7} N/m^3.

Study	Kuroshio	Kamchatka	Alaska Stream
Harrison (1989)	50	60	20
Hellerman and Rosenstein (1983)	55	40	15
Kutsuwada (1982)	40	20	20
Talley (1988)	50	30	15
Trenberth et al. (1989)	50	40	20
This Study	45	35	28

Table 1.2: Comparison of computed western boundary current transports in the subtropical and subarctic Pacific. Units are 10^6 m^3/s.

	GOA curl	Bering curl	East Pacific High curl	Western Pacific curl
GOA curl	1.00	--	--	--
Bering curl	-0.15	1.00	--	--
East Pacific High curl	-0.42	-0.27	1.00	--
West Pacific High curl	Not Significant	-0.41	0.27	1.00

Table 1.3: Correlation Matrix of wind stress curl series. Correlations are significant at the 99% confidence level.

computed in this study lie between the extreme values for each region and differ from the mean value of the other studies by 5, 3.8, and .5 Sv in the Kuroshio, Kamchatka Current and Alaska Stream regions respectively.

Empirical Orthogonal Function (EOF) Analyses

The EOF Method

EOF analysis is used to determine the spatial and temporal characteristics of the dominant large scale standing wave patterns in the field of wind stress curl. EOFs will be used to examine the possible effects of wind stress curl in driving and responding to oceanic variations. The method of EOF analysis separates the variability of the data into spatial patterns that are mutually orthogonal to each other. The spatial patterns generated by the EOF method are the eigenvectors of the covariance matrix. A time amplitude function (TAF) that modulates the spatial pattern is associated with each eigenvector. The eigenvector and time series together are known as a mode of variability [Barnier, 1986]. In this study a mode of variability will be referred to as an EOF. Each eigenvector also has an associated eigenvalue that represents the relative amount of the variance of the data set accounted for by the eigenvector. The utility of the EOF method is that a substantial percentage of the variance contained in the data can usually be accounted for by a relatively small number of EOFs (e.g. Davis, 1976, Weare et al., 1976, Barnier, 1986, Rienecker and Ehret, 1988, Breidenbach, 1990). The physical interpretation of the modes

beyond mode 1 is often rendered difficult due to the constraints imposed by the orthogonality conditions, since we do not expect physical processes to necessarily occur in such an ordered manner. A further weakness of the use of real EOFs (versus complex or imaginary EOFs) is that they do not allow for the detection of propagating features in the data set. Propagating features can be detected using complex EOF analysis. This study uses real EOFs and therefore will concentrate on the interpretation of the large scale standing wave patterns in the field of wind stress curl. In this part of the study two separate scalar EOF analyses (termed S1 and NS1) were performed using the monthly mean wind stress curl data. S1 is an experiment using the computed monthly mean wind stress curl data. NS1 is an analysis using the wind stress curl data with the seasonal cycle removed. The nonseasonal TAFs will be used later in this chapter to determine the regional importance of the dominant modes of interannual wind stress curl variability. They will also be used in later chapters to describe and quantify spatial and temporal interrelationships between wind stress curl, SST, air temperature, sea-ice cover, SLP variability, and several indices of oceanic and atmospheric variability in the tropical Pacific.

The original data set (427 individual time series of 516 observations each) for each experiment was reconstructed from the EOFs by recombining the temporal and spatial decompositions produced by the EOF analysis. The purpose of the reconstruction was to make sure that the modal decompositions produced by the EOF method faithfully represent the variability contained in the original data set. The

reconstruction reproduced all of the original data very accurately. It is therefore concluded that the EOFs and their associated time functions represent the information contained in the original data set in the sense that no information has been lost in the transformation to the EOFs.

Experiment S1

The first four modes of S1 represent a cumulative total of 41% of the variance of the curl data set. EOF1 explains 22% of the variance. The highest amplitudes, which are nondimensional, and largest gradients of the eigenvector of the first mode (figure 1.13) appear north of 50°N over the Gulf of Alaska. There are secondary local maxima between 55°N and 60°N in the western Bering Sea and adjacent to the west coast of North America between 25°N and 35°N. The amplitudes over much of the open ocean north of 30°N are small, as are the gradients. The zero contour lies between 30°N to 35°N over most of the basin. Between about 140°W and 110°W the zero contour slopes northwest to southeast from 35°N to 20°N. Amplitudes south of the zero contour are small and nearly constant across the basin. The TAF associated with the first eigenvector (figure 1.14a) is characterized by a very well defined annual cycle. The highest amplitudes of the curl occur during November through February. Large interannual variations primarily occur during these winter months. The range of the interannual variations associated with the positive extrema of the TAF is about seven times larger than the range of interannual variations of the negative extrema. The positive extrema occur primarily during winter

while the negative extrema occur in spring and summer. The large range of interannual variability during winter are associated with changes in the strength of the large scale atmospheric circulation and interannual variations in cyclone activity. The power spectrum of the mode 1 TAF (figure 1.14b) shows peaks that correspond to periods of 6 months, 9 months, 1 year, and 1.6 years. These peaks are significant at the 95% confidence level. Broad banded energy also occurs in the 2.5 to 5 year period band of the mode 1 TAF power spectrum although this energy is not significant at the 95% confidence level. The smoothed TAF also suggests that longer period oscillations might be present in this series that cannot be resolved because the record is too short. The peak at annual period has an amplitude that is an order of magnitude larger than the next most energetic peak, which occurs at the semi-annual period. The concentration of spectral energy at the six month and one year periods demonstrates that mode 1 mainly represents the seasonal cycle of the wind stress curl. Comparison of the annual harmonic of the curl (figure 1.6a) with the eigenvector of mode 1 shows that the patterns are nearly identical. This further confirms that mode 1 of S1 represents the seasonal changes in the field of wind stress curl. The seasonal cycle dominates the distribution of variance. The prominent role of the annual cycle in the distribution of the field variance has also been shown in EOF studies of several other atmospheric and oceanic parameters, [e.g. Weare et al., 1976; Barnier, 1986; Servain and Legler; 1986, Ehret and O'Brien, 1989; Breidenbach, 1990].

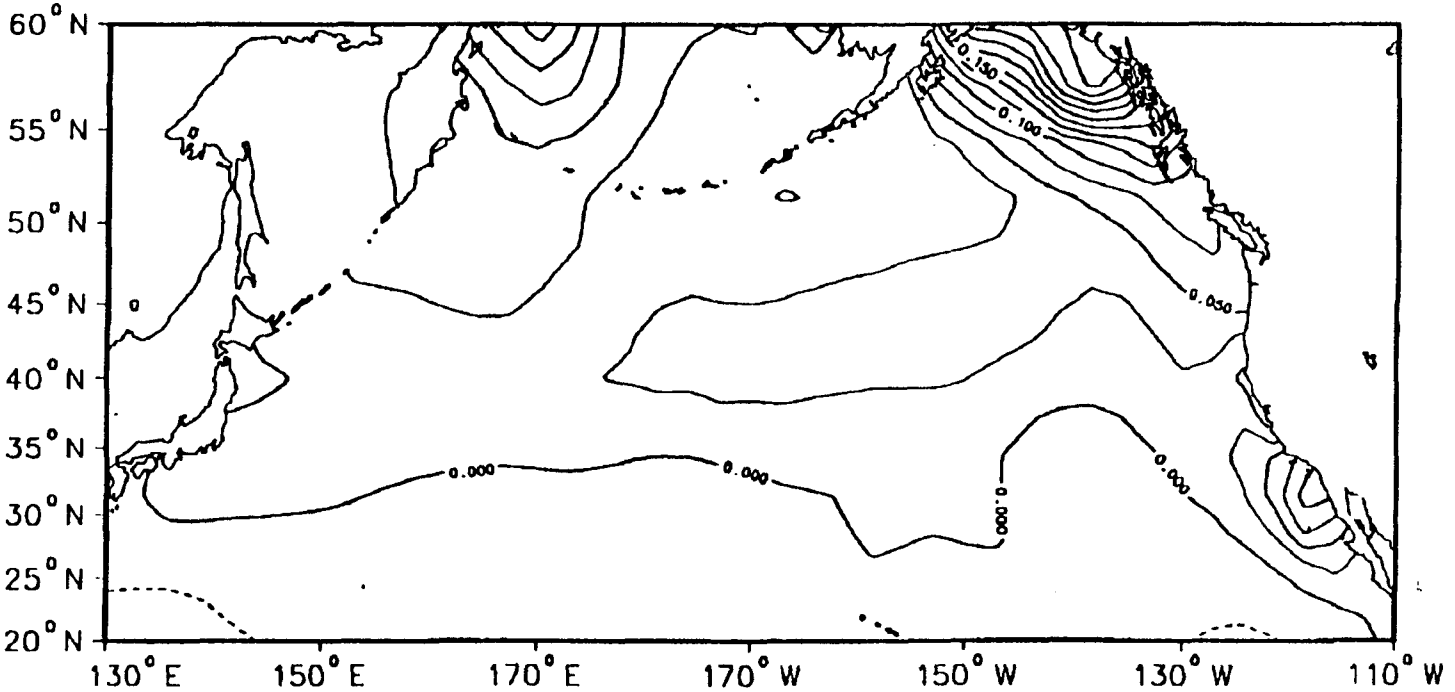

Figure 1.13: Mode 1 eigenvector of wind stress curl.
CI=0.025 dimensionless units.

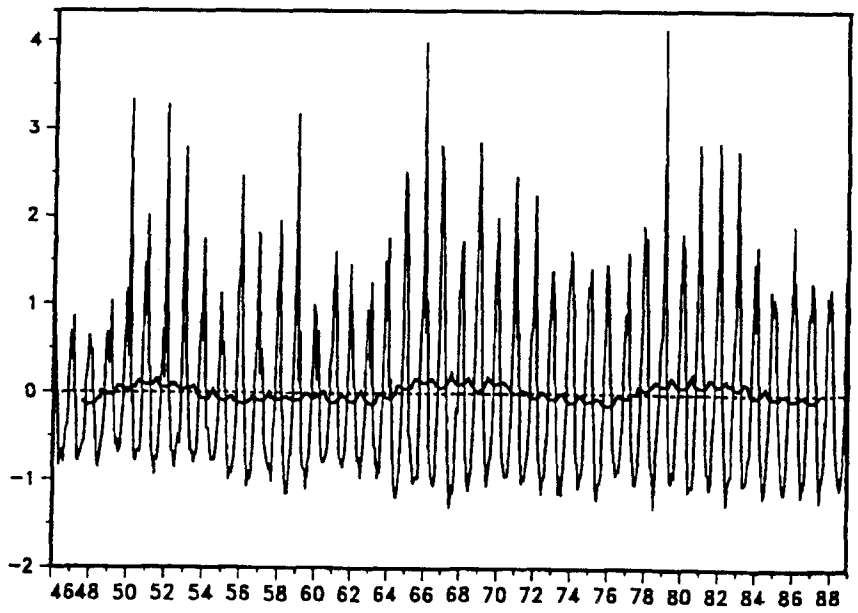

a)

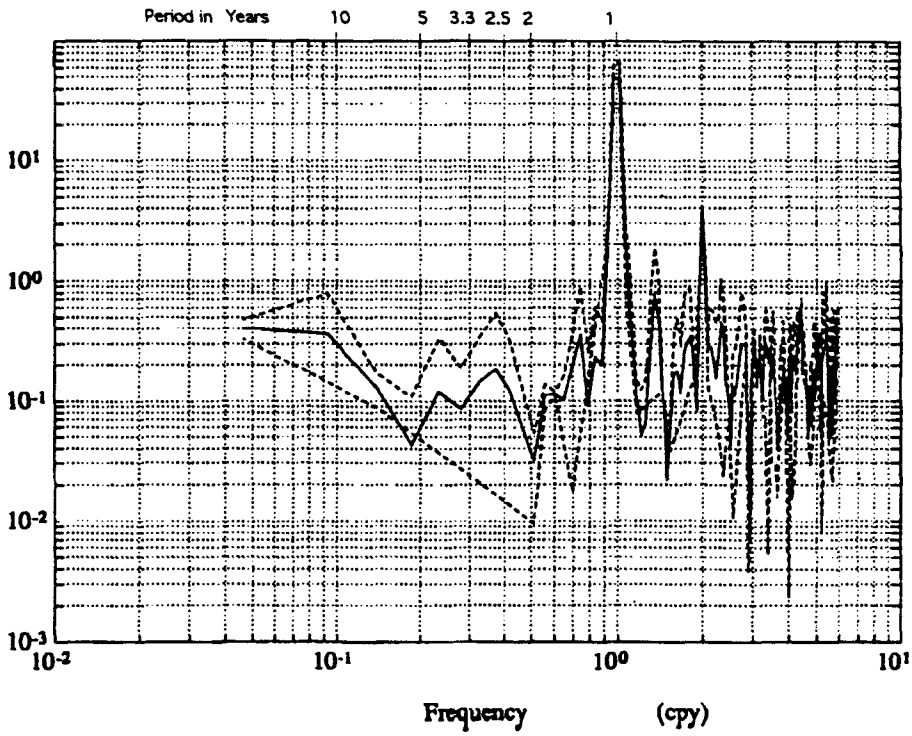

b)

Figure 1.14: a) Time amplitude function for mode 1.Units are 10^{-7} N/m^3
b) Power spectral density of mode 1 TAF.

EOF 2 explains 9% of the variance. The second eigenvector of the curl (figure 1.15) exhibits both east-west and north-south standing wave patterns. Between 20°N and 45°N and across the basin east of about 150°E there is a meridional oscillation that occurs between the regions occupied by the subtropical anticyclone and the Aleutian Low. The nodal line of this standing wave pattern is the zero contour that lies roughly along 42°N. Between 45°N and 60°N there is an east to west oscillation between the central/western North Pacific and the eastern North Pacific. This eigenvector appears to represent zonal fluctuations in the position of the Aleutian Low. The zero contour slopes northwest to southeast and lies between 150°W and the 135°W. The highest nondimensional positive amplitudes of eigenvector 2 occur across much of the northern Bering Sea. The Gulf of Alaska is out of phase with the Bering Sea and in phase with the subtropical anticyclone except adjacent to the North American continent. The highest negative amplitudes of this eigenvector occur over the northern Gulf of Alaska. The TAF of EOF 2 (figure 1.16a) shows large interannual fluctuations in both the positive and negative curl fields. The structure of the mode 2 EOF suggests that an anomalously weak Aleutian Low occurred from 1961 through 1968 across the Bering Sea and central North Pacific north of 42°N and west of about 140°W. During most of the period from 1976 to 1988 the Aleutian Low was anomalously strong in this over the central North Pacific and Bering Sea. The energy spectral density of the TAF associated with eigenvector 2 exhibits significant peaks at periods of 6 months, 1 year, 1.6 years, and 3.5 years (figure 1.16b). Spectral energy in the 10 to 11 year period band is not significant at the 95%

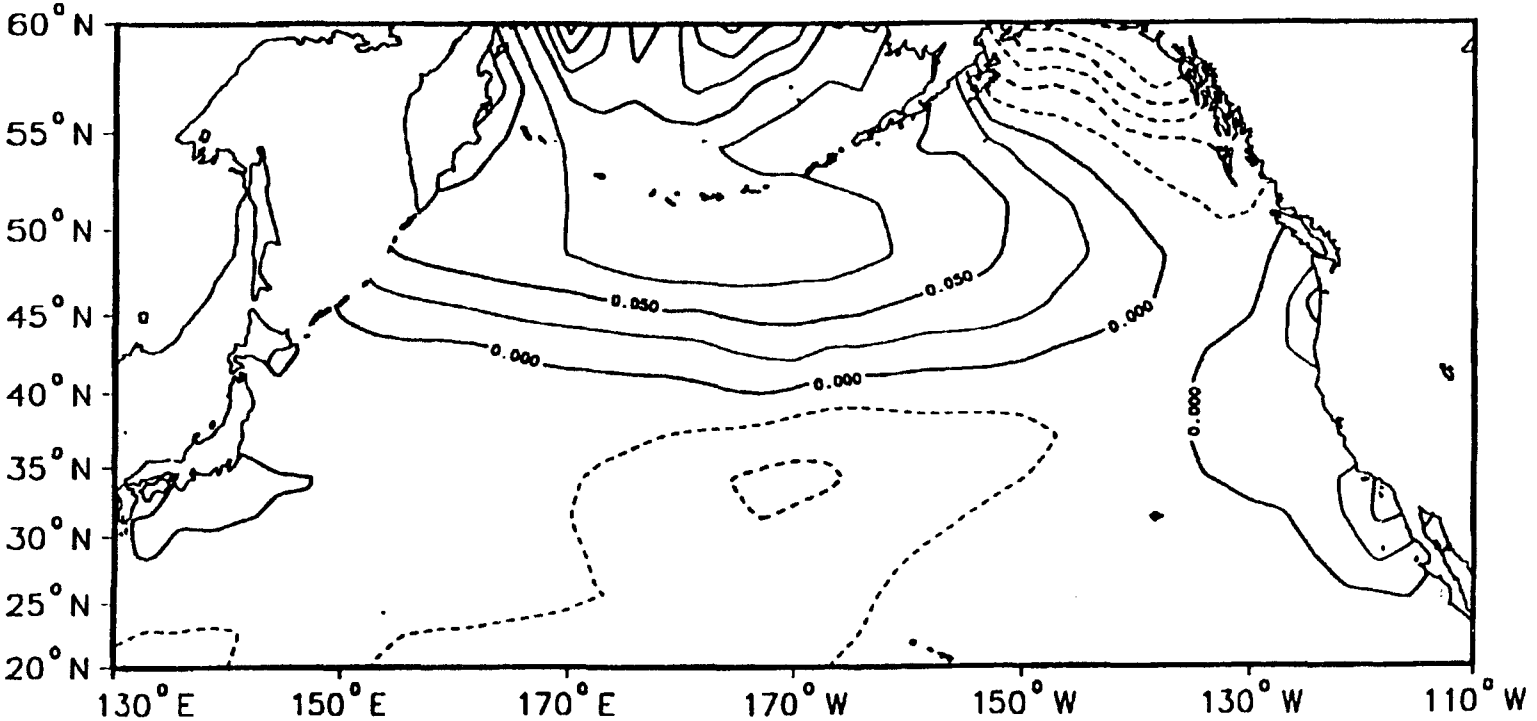

Figure 1.15: Mode 2 eigenvector of wind stress curl.
CI=0.025 dimensionless units.

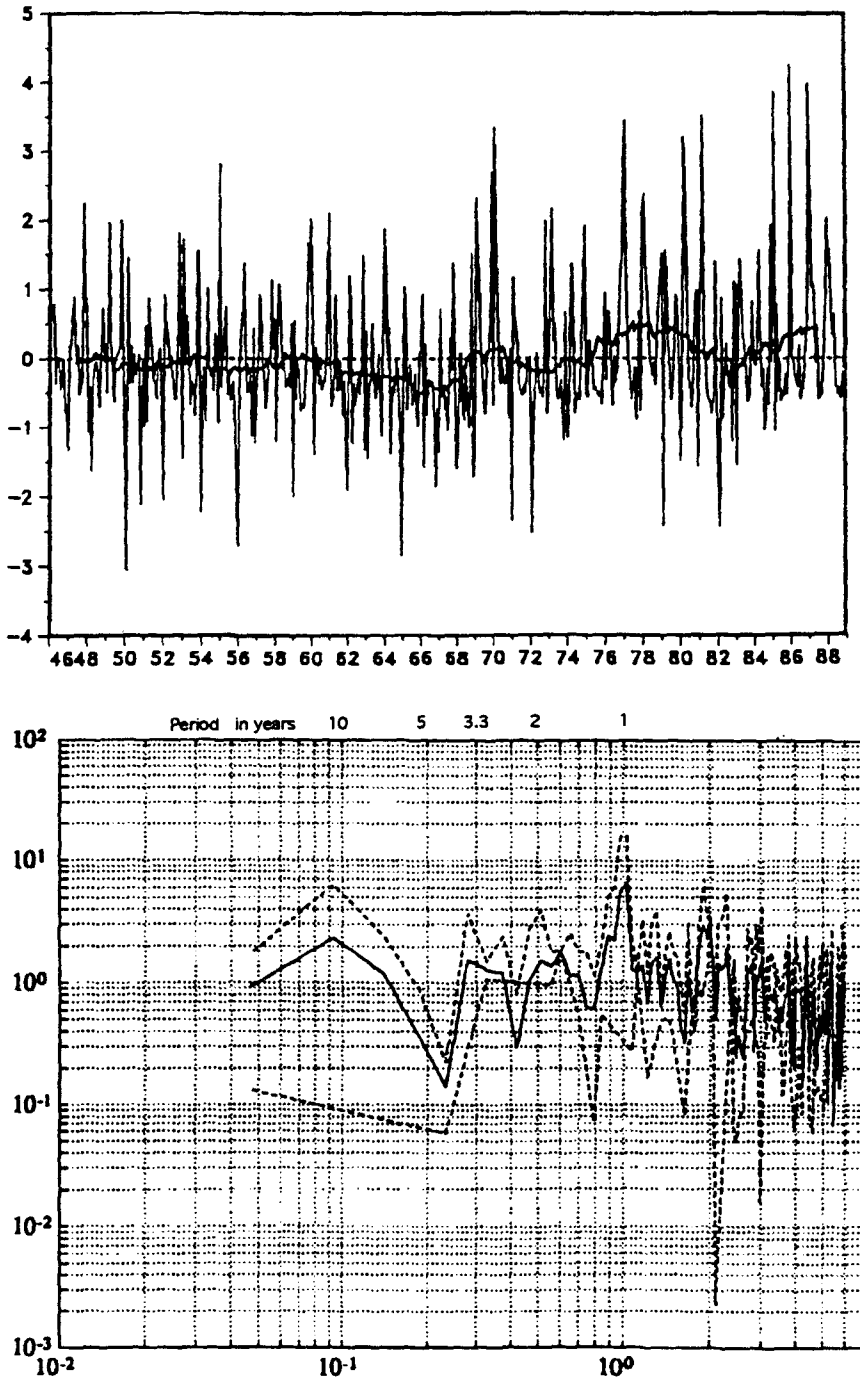

Figure 1.16: a) Mode 2 TAF of wind stress curl. Units are 10^{-7} N/m^3.
b) Power spectral density of mode 2 TAF.

confidence level, however the smoothed TAF curve does indicate once again that there are longer period fluctuations in the series than can be resolved with statistical confidence due to the length of the record.

EOF 3 accounts for 6% of the variance. The mode 3 eigenvector (figure 1.17a) shows a nearly basin scale north-south oscillation with zonally oriented nodes occurring roughly along 50°N and 30°N, suggesting that this mode represents fluctuations in the meridional positions and strengths of the trades and westerlies. The region of the northeast trades is in phase with the Bering Sea, Gulf of Alaska and with the western Pacific west of 150°E. The highest amplitudes of this mode occur in the central Pacific near 42°N 170°W and in the western Bering Sea. Significant peaks in the power spectrum of the TAF of eigenvector 3 occur at periods of 6 months, 1 year, and 2 years (figure 1.17b). The most energetic peak in the spectrum is the semi-annual signal. Broad banded energy that is not significant at the 95% level occurs in the 2.5 to 3.5 year period band.

EOF 4 explains 4% of the variance of the curl. The mode 4 eigenvector (figure 1.18a) shows a north-south standing wave pattern between the central and northwestern North Pacific. There is also an oscillation between the Bering Sea and and the central and eastern North Pacific north of 35°N and west of 155°E. The highest amplitudes in this mode occur between 55°N and 60°N in the western Bering Sea. Secondary maxima occur near 52°N 175°E and 36°N 175°E. This eigenvector also shows that the Gulf of Alaska out of phase with the Bering Sea. The spectrum of the TAF for eigenvector 4 (figure 1.18b) exhibits significant

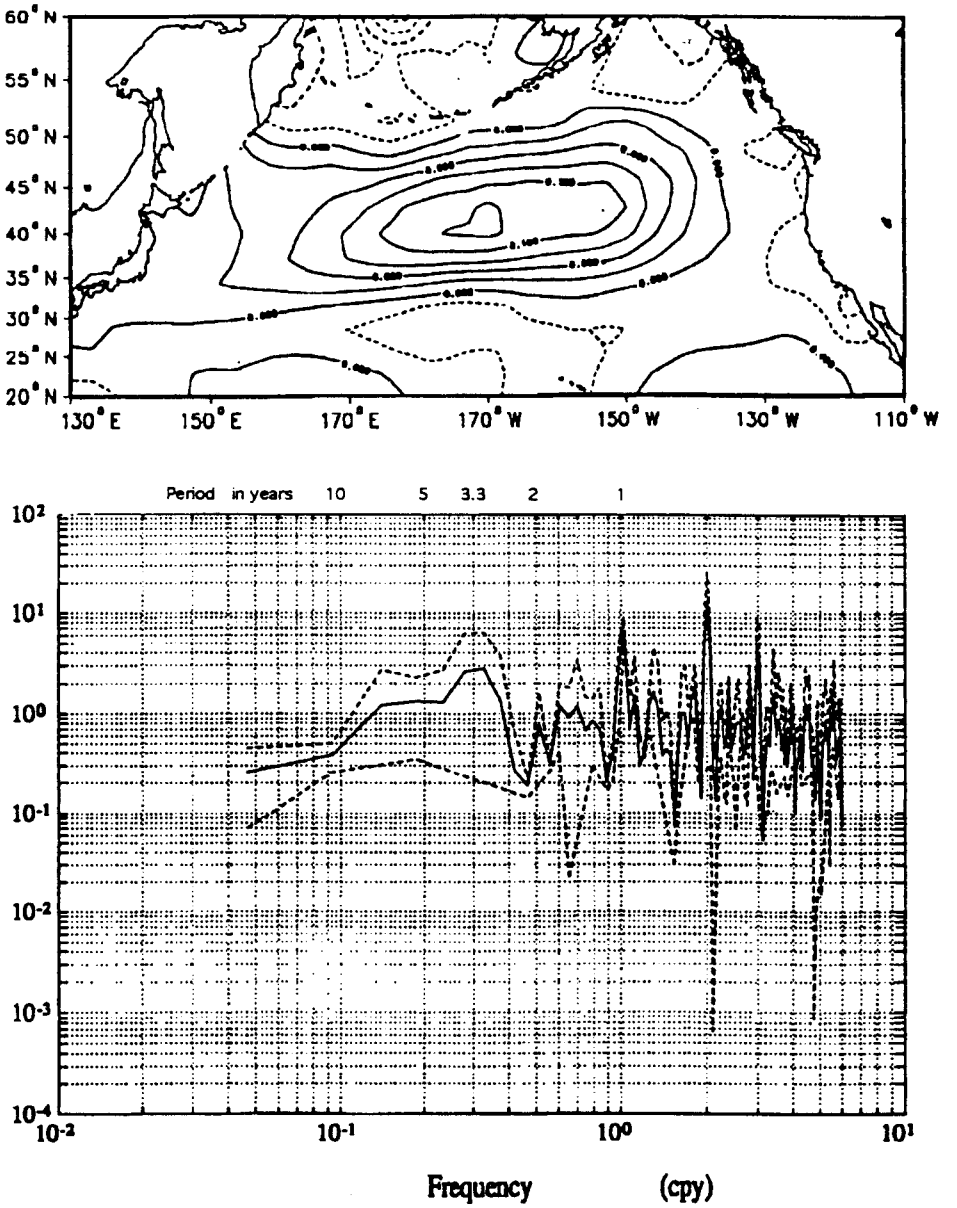

Figure 1.17: a) Mode 3 eigenvector of wind stress curl. CI=0.025 dimensionless units. b) Power spectral density of the mode 3 TAF.

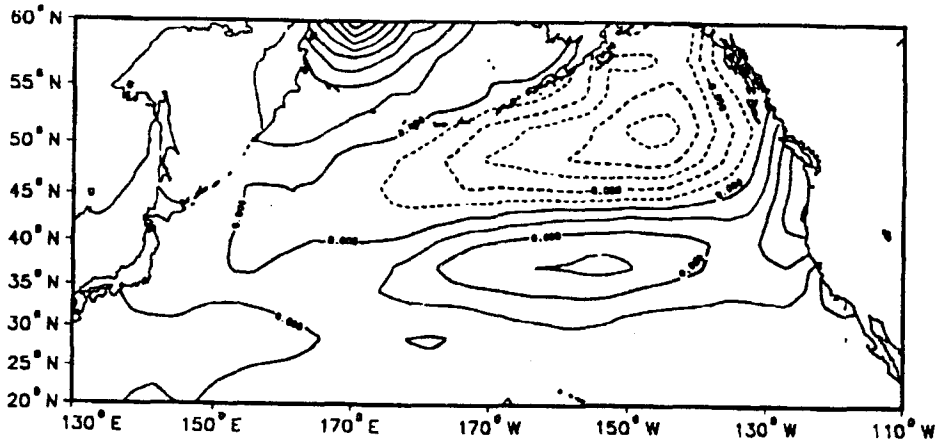

a)

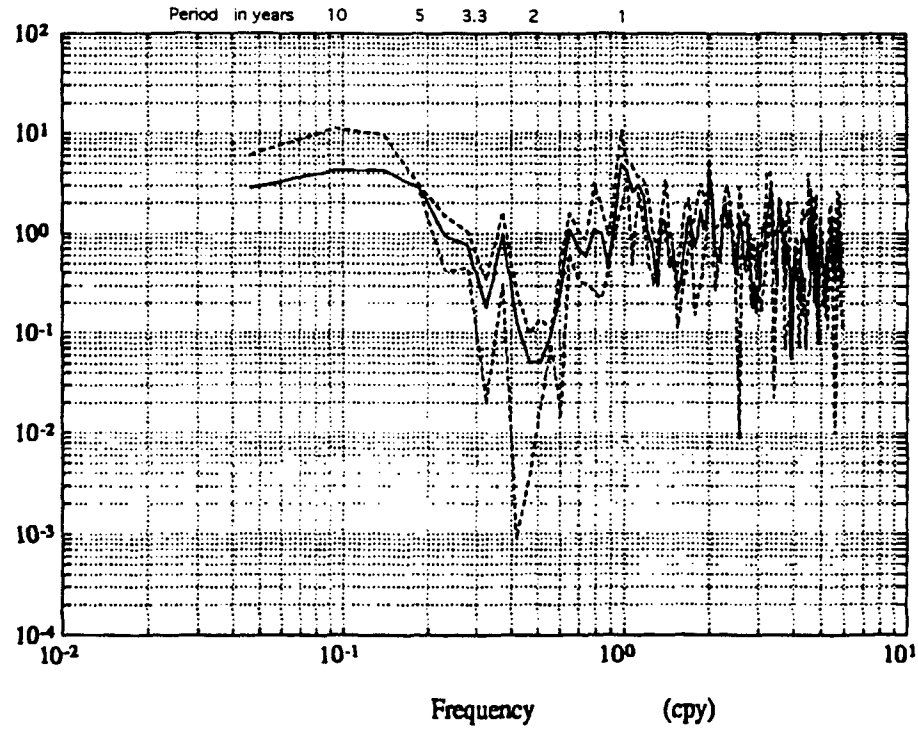

b)

Figure 1.18: a) Mode 4 eigenvector of wind stress curl. CI=.025 dimensionles units. b) Power spectral density of mode 4 TAF.

peaks at periods of 6 months, 9 months, 1 year, 20 months, and 2.6 years. The most energetic peaks occur at the annual and semi-annual periods.

Experiment NS1

The first four modes of NS1 together account for 30% of the nonseasonal variance. These modes explain 12%, 7%, 6%, and 5% of the variance respectively. Modes 1, 2, and 3, in this experiment (figure 1.19) are closely related to modes 2, 3, and 4 respectively of S1. The spatial structures of the respective eigenvectors are similar but not identical. Differences are more pronounced in the associated TAFs. Even though mode 1 of S1 was interpreted to largely represent the seasonal cycle, the seasonal distribution of variance is not fully contained in mode 1. Seasonal components exist in higher modes and therefore the removal of the seasonal cycle affects all of the modes in which there is a seasonal component. The differences between the eigenvectors and TAFs of these respective modes of S1 and NS1 are therefore largely attributable to seasonal variability, and the eigenvectors of NS1 represent the spatial structure of the interannual variability of the curl.

Comparison with Rienecker and Ehret

Rienecker and Ehret [1988] computed EOFs of nonseasonal North Pacific wind stress curl between 3°N and 55°N for the period 1950-79 (their figures 4 and 7). The mode 1 eigenvectors are quite similar in their large

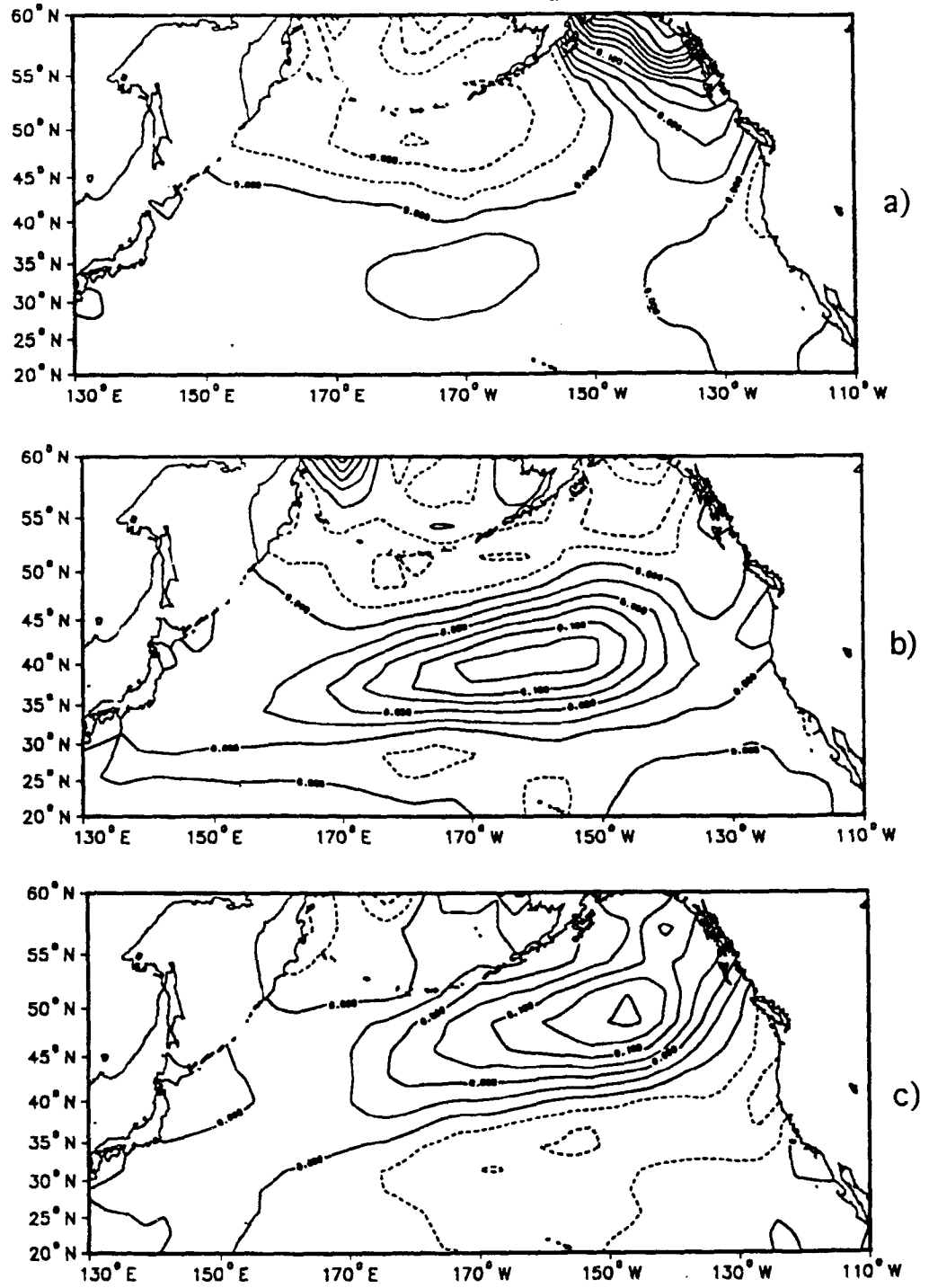

Figure 1.19: Eigenvectors of nonseasonal wind stress curl. Units are dimensionless. a) Mode 1 b) Mode 2 c) Mode 3.

scale structures, except off of the Kamchatka Peninsula. The main difference between the mode 1 eigenvectors is that the zero lines of the basin scale oscillation differ meridionally by about 10 degrees. Also, even after the nondimensional amplitudes are scaled to each other they are quite different. The structure of the mode 2 eigenvectors are very similar except near the Kamchatka Peninsula. The spatial structure of the mode 3 eigenvectors bear little resemblance to each other. There are at least 3 possible reasons for the differences in the spatial structures of the eigenvectors in this study and those of Rienecker and Ehret [1988]. The first is that this study includes data to 60°N while the study of Rienecker and Ehret includes data to 55°N. Since a substantial amount of the variance occurs between 55°N and 60°N (i.e. figure 1.4) it seems feasible that the large variance at high latitudes accounts for part of the difference in the spatial structure of the eigenvectors. The second reason is a function of the time periods used for the analyses. Since it appears that a climatic shift occurred in the high latitude wind field after 1975, it seems reasonable that the effects of this climatic shift might be manifested in the structure of the dominant modes of variability of the wind field. This climatic shift after 1975 is apparent in the TAFs of the 4 dominant EOFs computed in this study. This climatic shift is not strongly manifested in the EOFs of Rienecker and Ehret since their record ends in 1979. Therefore the longer record used in this study appears to account for some of the differences in the structure of the eigenvectors in this study and those of Rienecker and Ehret. Finally, the results of Rienecker and Ehret include gridpoints throughout the equatorial and tropical Pacific (i.e. from

0° to 20°N) while this study does not include that region. Differences in the temporal structures of the EOFs are therefore also attributable to the inclusion of the tropical region by Rienecker and Ehret and the exclusion of the tropics in this study.

Regional Interannual Variability of North Pacific Wind Stress Curl

Regional Wind Stress Curl Series

The 427 point domain of the wind stress curl field was separated into subregions encompassing the Aleutian Low, East Pacific High and western North Pacific subtropical anticyclone regions (figure 1.20). These subregions were selected on the basis that a preliminary analysis of wind stress curl at points along several meridians and lines of latitude qualitatively suggested that wind stress curl fluctuated coherently within each of the subdomains. Each subdomain consists of a collection of spatial gridpoints . With the exception of the East Pacific High region, each spatial gridpoint is composed of a 547 month time series of wind stress curl anomalies (i.e. the seasonal cycle has been removed). For the East Pacific High region the time series are 516 months long. A single time series representing each region was computed by averaging the collection of gridpoint time series over the region of the subdomain. The time series of wind stress curl in each subdomain are shown with a three year running mean superimposed on the anomaly time series. A three year

running mean was selected in order to smooth out the 2 to 2.5 year fluctuations observed in some of these regions, in order to concentrate on longer time scale variability. Unless stated otherwise, "running mean" will be understood to represent a three year running mean.

In the Aleutian Low region the running mean anomalies were strictly positive between 1976 and 1988 (figure 1.21a) indicating that an intensification of cyclone activity occurred during this period. Similarly during 1961-68 and 1971-75 the running mean anomalies were strictly negative, which suggests that cyclone activity was lower than normal during these periods. Therefore the Aleutian Low was anomalously weak during 1961-68 and 1971-75 and anomalously strong from 1976 to 1988. The latter result is consistent with that of Trenberth [1990] who shows using SLP data that the Aleutian Low has intensified in winter during the period 1977-88. This is also consistent with the results of Nitta and Yamada [1989], who note that 500 mb geopotential height anomalies over the North Pacific were persistently negative during winters in the 1980's. After 1988 the intensification appears to comes to an end as the sign of the mean curl anomalies becomes negative. From 1973 through 1980 the mean curl anomalies in the Aleutian Low region steadily increased from negative to positive. After 1981 intensification slackened and the trend reversed, although the mean anomalies remained positive for most of the period through 1987. The periods 1961-68 and 1976-88 are the longest in the record where the sign of the mean anomaly is persistently of one sign. Otherwise the curl changes sign on time scales of about 2 to 6 years. The power spectrum of the Aleutian Low time series shows no peaks at

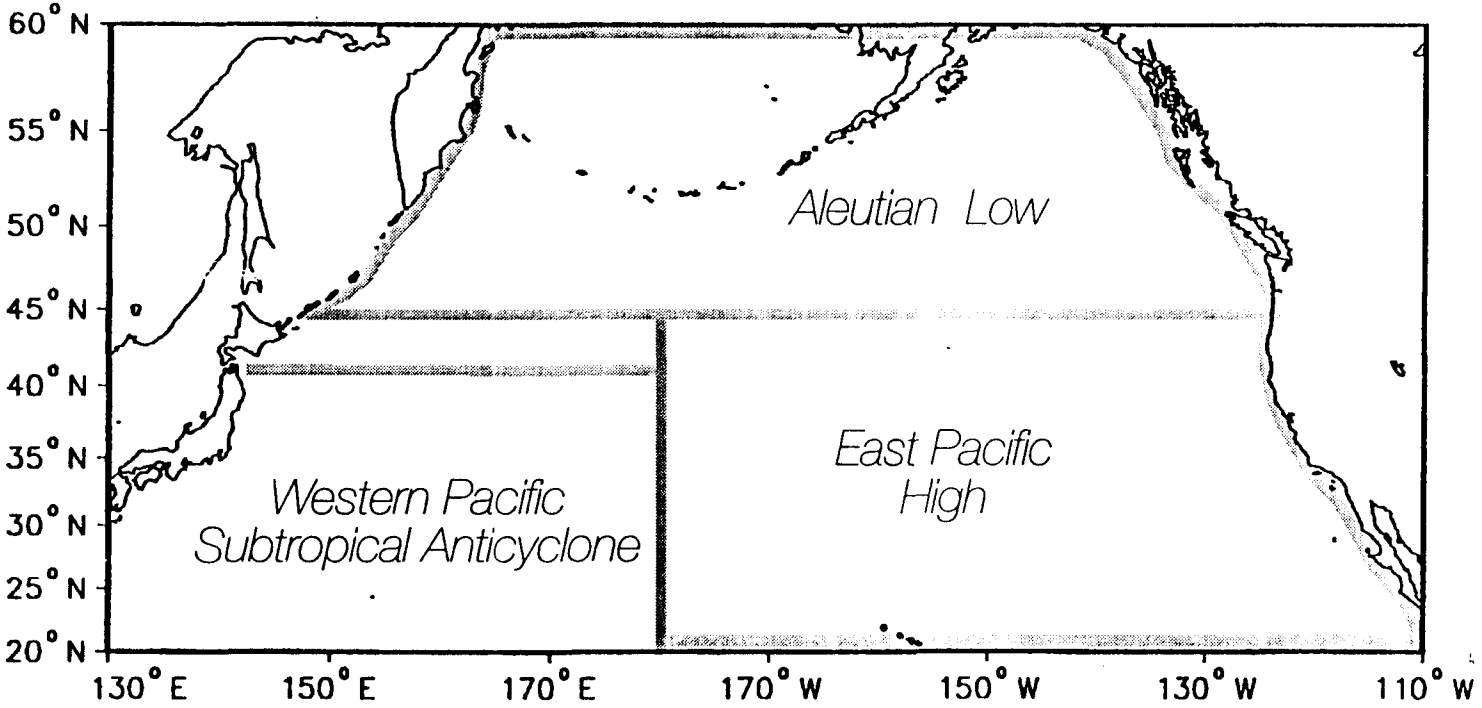

Figure 1.20 : Areas over which regional mean time series of wind stress curl were computed.

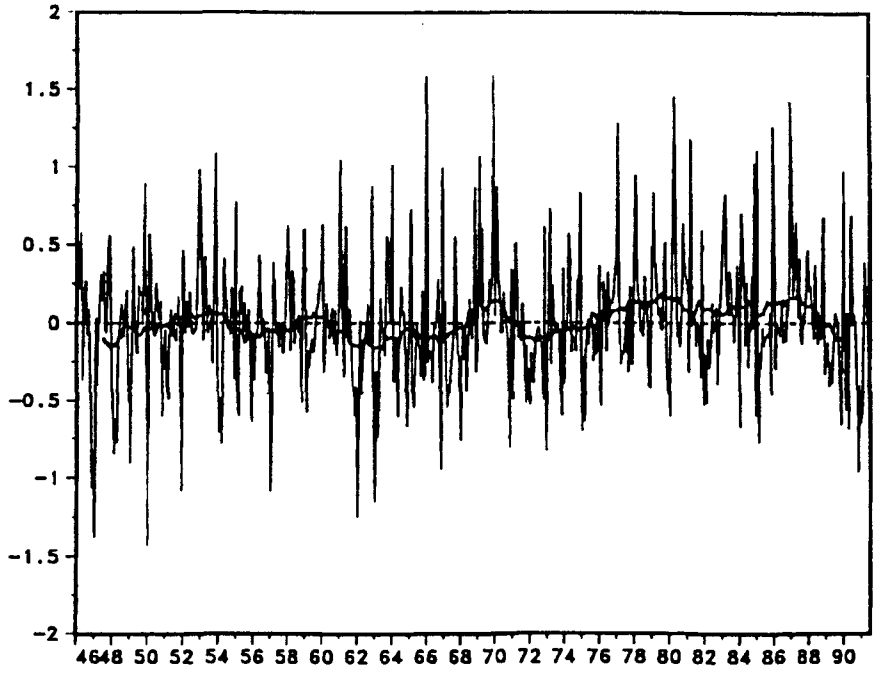

a)

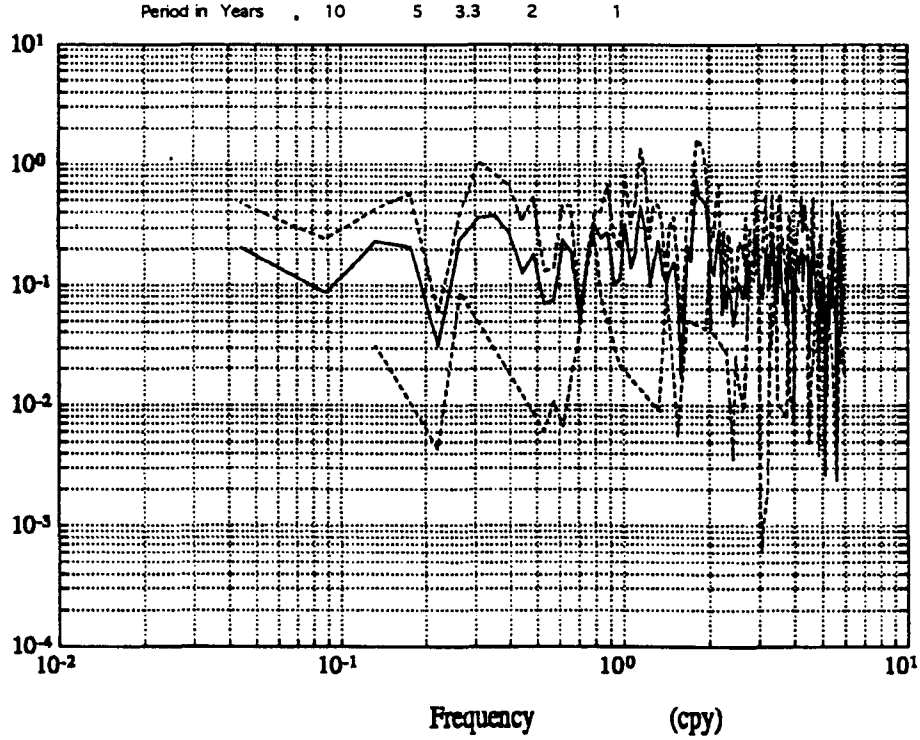

b)

Figure 1.21: a) Time series of Aleutian Low curl anomalies. Units are 10^{-7} N/m^3.

b) Power spectral density of Aleutian Low series.

frequencies lower than 0.5 cycles per year that are significant at the 95% confidence level (figure 1.21b). However, there is broad banded energy in the low frequency portion of the spectrum concentrated at 5 to 7 year and 2.5 to 3 year periods.

The East or North Pacific High time series (figure 1.22a) is characterized by running mean anomalies of magnitude less than 0.15 units. The sign of the anomaly of the running mean often persists for 4 to 8 years. Positive mean anomalies in the series indicate that the North Pacific High was anomalously weak from 1947 through 1952 and from 1961 through 1968. The latter period corresponds to the time period when the Aleutian Low was also anomalously weak. The eastern subtropical Pacific anticyclone was anomalously strong during most of the period 1969 to 1984. The correlation coefficient between curl anomalies in the East Pacific High region and those in the Aleutian Low region is -.31 at zero lag, which is significant at the 99% level. The sign of the coefficient indicates that there is a tendency for the East Pacific High to be intense when the Aleutian Low is intense and weak when the Aleutian Low is weak, although the small magnitude of the coefficient shows that the relationship is an imperfect one. The power spectrum of the East Pacific High curl time series shows significant energy occurs at periods of 2 years, 2.5 to 3 years and 5 to 6 years (figure 1.22b). These are the same periods that dominate the low frequency part of the power spectrum of Aleutian Low curl anomalies. This suggests that the meridional extent of low frequency wind stress curl fluctuations might have a very large spatial scale.

The time series of curl in the western subtropical Pacific indicates that a strong and abrupt climatic anomaly occurred in this region from 1976 through 1986 (figure 1.23a). The mean anomalies are generally small and the sign changes many times through the record although anomalies of one sign or the other may persist for three to six years. The amplitudes of the mean oscillations from 1976 to 1986 are the largest that occur in the entire record. The power spectrum of the western Pacific time series shows statistically significant peaks in the 2 to 2.5 year and 2.5 to 3 year period bands (figure 1.23b).

Dividing the western subtropical Pacific anticyclone region into northern (30°N-39°N) and southern (21°N-27°N) regions shows that the low frequency negative curl anomalies that observed during 1976-88 occurred primarily between 21°N and 27°N (figure 1.24a). These negative curl anomalies are interpreted to represent a weakening of the subtropical easterly wind field during this period. Similarly the positive anomalies observed in the subtropical anticyclone region during 1979-85 occurred primarily between 30°N and 39°N (figure 1.24b), probably associated with an intensification of the midlatitude westerlies, an expanded and intensified Aleutian Low and increased subtropical cyclogenesis during this period.

During the period 1976 to 1988 mean wind stress curl anomalies in the Aleutian Low region and the subtropical western Pacific underwent the most persistent and extreme fluctuations observed during the record since 1946. Individual anomalies in these regions during this period did not obtain their maximum values over the length of the record, which

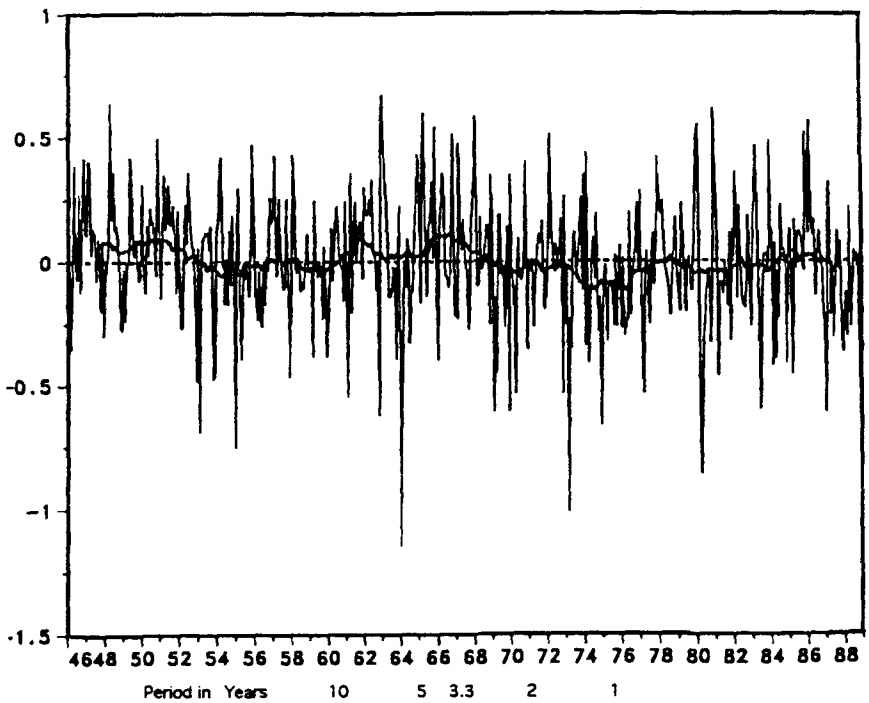

a)

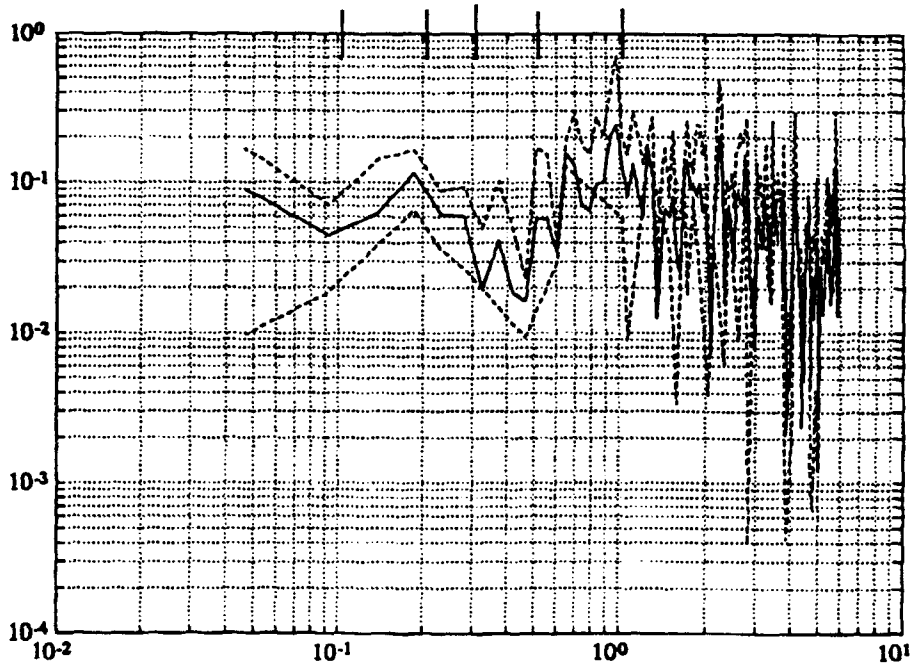

b)

Figure 1.22: a) Time series of East Pacific High curl anomalies. Units are 10^{-7} N/m^3. b) Power spectral density of East Pacific High series.

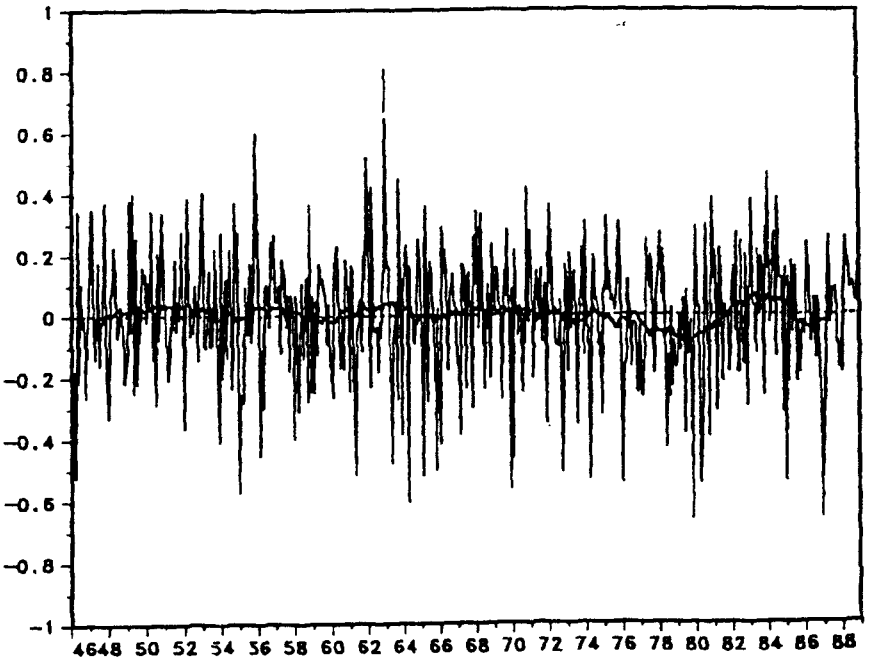

a)

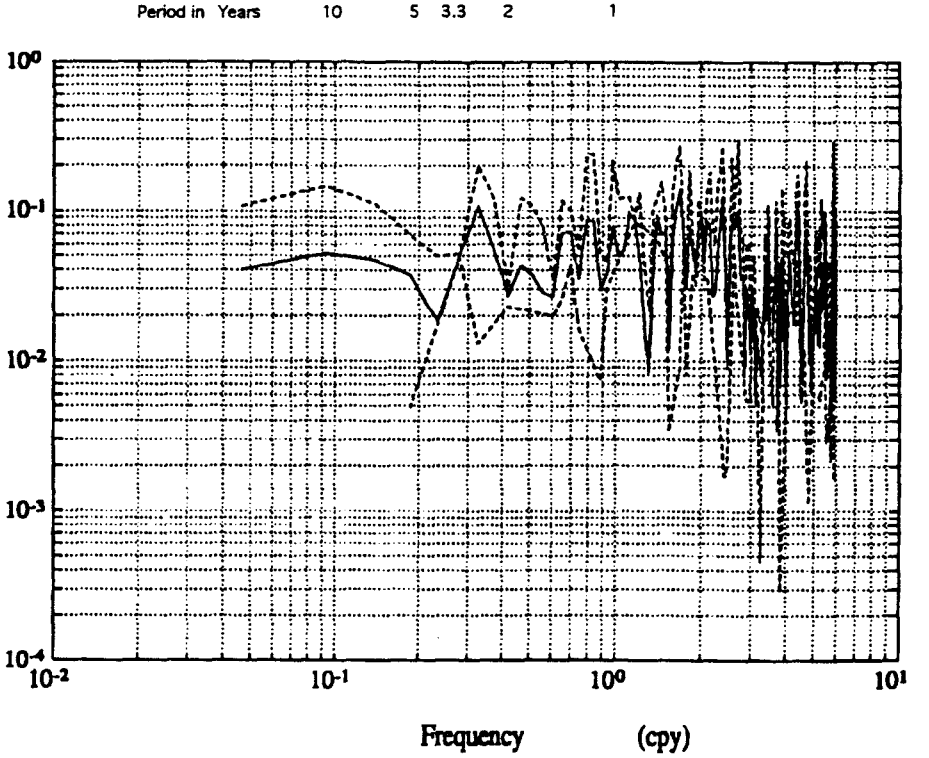

b)

Figure 1.23: a) Time series of Western Pacific subtropical anticyclone wind stress curl. Units are 10^{-7} N/m^3. b) Power spectral density of Western Pacific series.

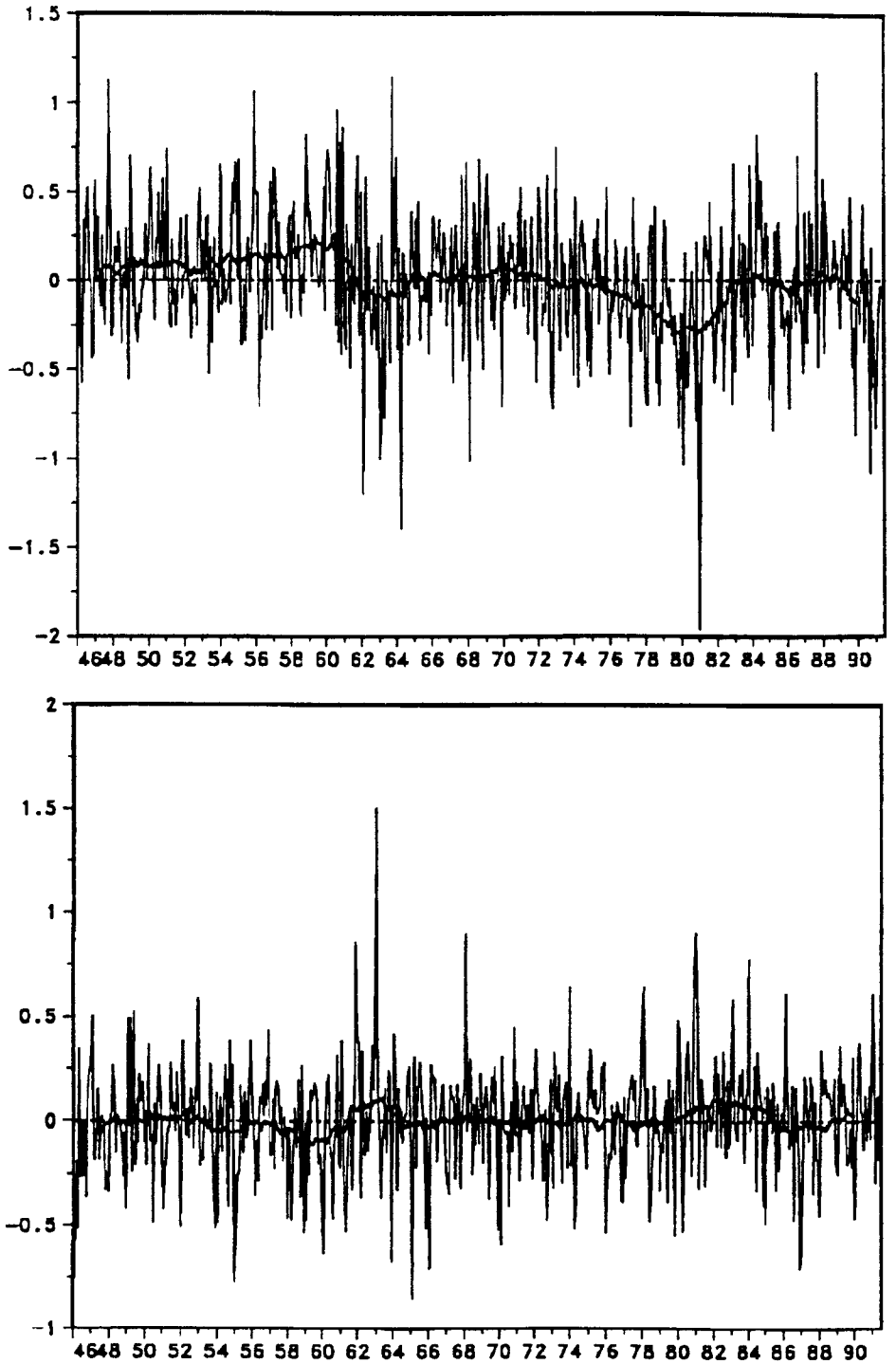

Figure 1.24: Wind stress curl anomalies in Western Pacific subtropical anticyclone. a) 21°N-27°N b) 30°N-39°N. Units are 10^{-7} N/m^3.

suggests that the observed extremes in the mean series are part of a climatic anomaly that endures for several years. Also since the large anomalies of the mean curl observed during 1976-88 are not restricted to occur only in the Aleutian Low region, the intensification observed in the Aleutian Low appears to be related to changes in the atmospheric circulation that have a spatial scale that is larger than that of the Aleutian Low.

Since the nonseasonal wind stress curl variations tend to fluctuate out of phase between the Bering Sea and Gulf of Alaska, the Aleutian Low region was divided into the Gulf of Alaska and Bering Sea subregions (figure 1.25). The running mean anomalies have been strictly positive over the Bering Sea during 1976-1988 (figure 1.26a) except briefly during 1982. In the Gulf of Alaska the anomalies are positive only between 1979 and 1987 (figure 1.26b), except briefly during 1985. During the period 1976-1981 the rate of intensification of the Aleutian Low over the Bering Sea was at a maximum, and the running mean anomalies attained their maximum positive values over the entire length of the record. The maximum amplitude of the mean curl anomalies exceeds 0.45 over the Bering Sea and is less than 0.2 over the Gulf of Alaska. Therefore it appears that while the intensification of the Aleutian Low has occurred in both subdomains, the recent strengthening of the low occurred to a greater extent in the Bering Sea than in the Gulf of Alaska.

Further differences in the curl fields over these two regions can be seen in the early years of the record. The mean anomalies over the Bering Sea were strictly negative during the entire period from 1952-1968, while

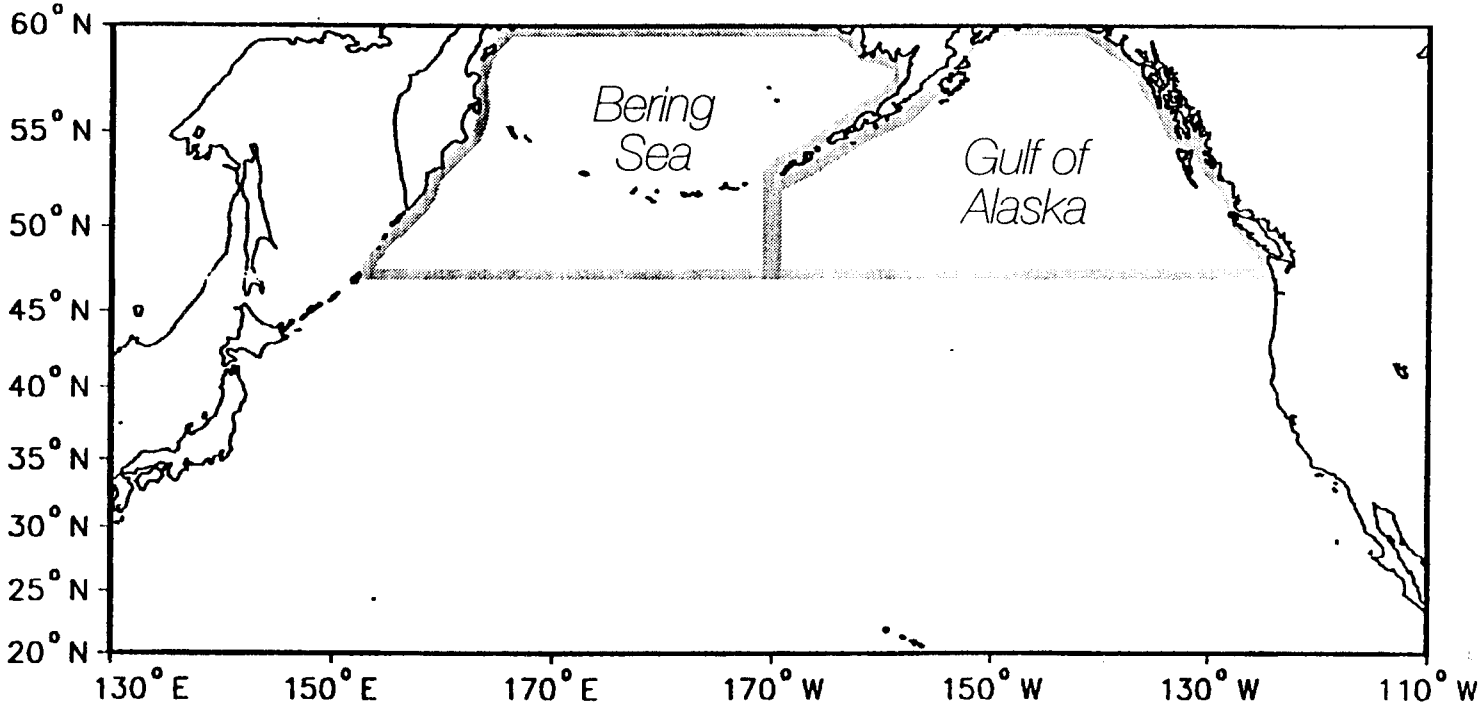

Figure 1.25 : Map showing division of Aleutian Low into Bering Sea and Gulf of Alaska Subregions.

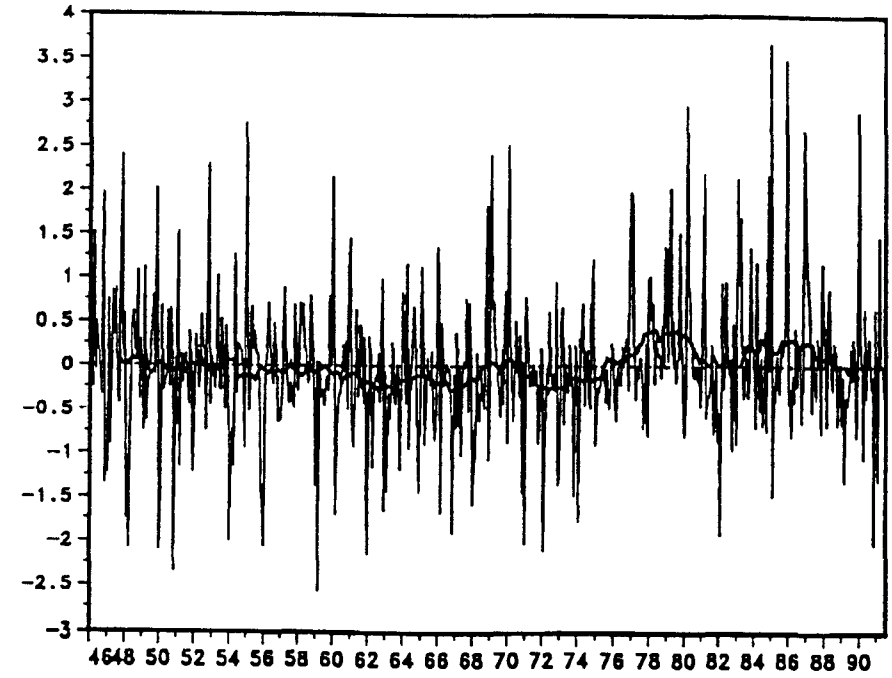

a)

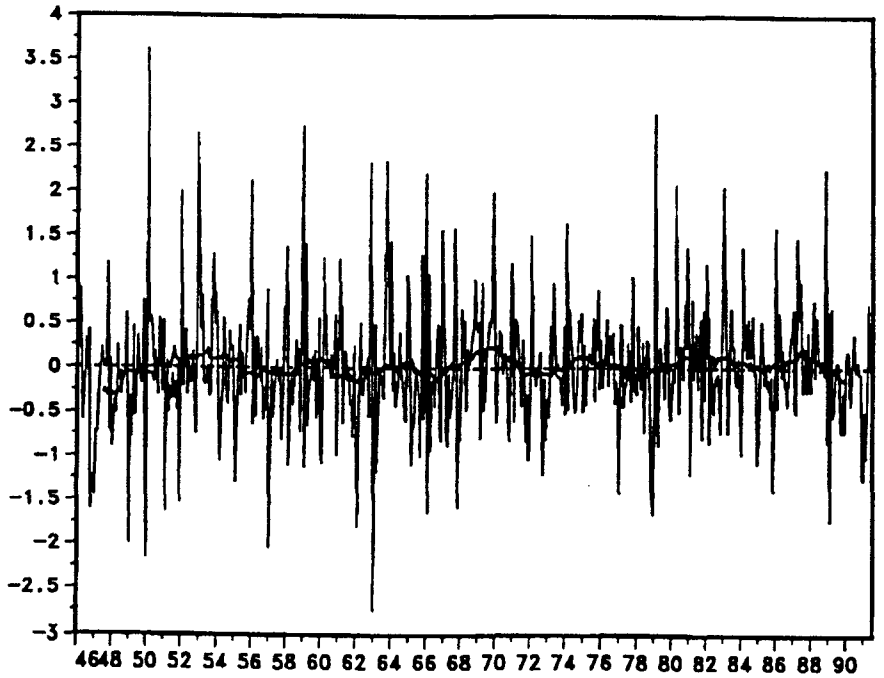

b)

Figure 1.26: a) Anomalies of Bering Sea wind stress curl.

b) Anomalies of Gulf of Alaska wind stress curl. Units are 10^{-7} N/m^3.

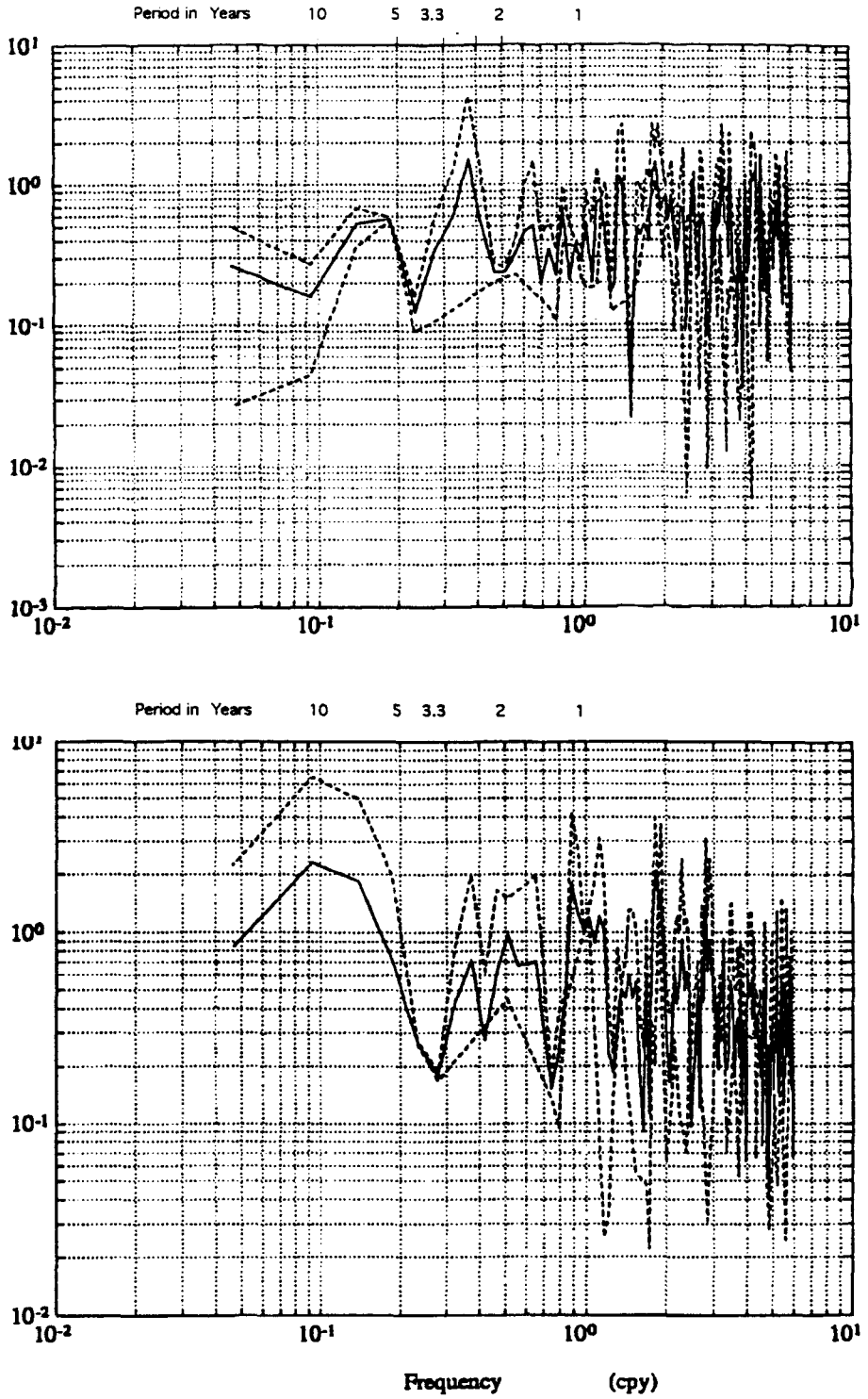

Figure 1.27: a) Power spectral density of Gulf of Alaska curl.
b) Power spectral density of Bering Sea curl.

the curl anomalies over the Gulf of Alaska oscillated from positive to negative several times during this same period. Power spectral analysis of these series shows that the two series oscillate on somewhat different time scales. There are peaks at periods of 2.5 to 3 years and 5 to 7 years in the power spectrum of the Gulf of Alaska curl (figure 1.27a) that are significant at the 95% level. The power spectrum of Bering Sea wind stress curl shows peaks at periods of 2 years and 2.5 to 3 years (figure 1.27b). These peaks are also significant at the 95% confidence level. There is also energy concentrated in the 10 to 11 year period band although it is not significant at the 95% level. However, the smoothed curve of the curl qualitatively suggests that oscillations of roughly 10 year period are present in Bering Sea wind stress curl. The regional time series show that zonal oscillations of the positive curl maximum within the Aleutian Low occur on interannual time scales, and the regional curl time series serves as an indicator of the long-term strength of the Aleutian Low.

Correlations and Coherence between Regional Curl Fields

The strongest correlations in the matrix of the regional time series of nonseasonal curl (table 1.3) are those between the Gulf of Alaska and East Pacific High, and those between the Bering Sea and western subtropical Pacific region. The Gulf of Alaska and Bering Sea are out of phase. Variations in the strength of the circulation in the Aleutian Low are out phase with those in the subtropical anticyclone.

Phase and coherence information between the regional curl series further confirms the above relationships and indicates those time scales for which these relations might be important (table 1.4). Fluctuations with periods of 2.5 to 3 years have been shown to occur in all of the regional spectra. On these time scales the fluctuations are strongly coherent with nearly zero phase difference over the entire Aleutian Low region and the eastern portion of the subtropical anticyclone. There is also strong coherence (0.96) between the Gulf of Alaska and Bering Sea at these periods but they are about ninety degrees out of phase. The coherence is not significant between the western portion of the subtropical anticyclone and the Aleutian Low, and the fluctuations are incoherent at these periods between the eastern and western regions of the subtropical anticyclone.

At the two year period, the eastern and western regions of the subtropical anticyclone are highly coherent (0.98) and ninety degrees out of phase. The coherences between the signal in these regions and the two year signal in the Bering Sea are not significant at the 95% level.

Finally, at the five to seven year period, the Gulf of Alaska and the eastern part of the subtropical anticyclone are strongly coherent (>0.9) and out of phase. These are the only regions where statistically significant energy occurs at periods of six to seven years. This further confirms that on nonseasonal time scales, in particular at periods of 2.5 to 3 and five to seven years, the meridional scales of wind stress curl variability are very large, and extend the length of the Pacific between 21°N and 60°N.

Correlations between regional curl fields and EOF Time Amplitude Functions

The matrix of correlations of the regional curl time series and the TAFs of the first four nonseasonal EOFs of the curl (table 1.5) is a measure of the importance of a particular EOF in explaining a portion of the variance in a specified region. Fifty percent of the variance of the nonseasonal curl in the Bering Sea region is explained by the TAF of nonseasonal EOF1, while only 10% to 17% of the variance is accounted for by this EOF in the other regions. EOF2 accounts for about one third and one tenth of the variance in the eastern and western subtropical anticyclones respectively, while less than 4% is accounted for across the subarctic region. EOF3 describes variability primarily in the eastern North Pacific. This mode explains 65% of the variance in the Gulf of Alaska and 30% in the East Pacific High region, while the correlation coefficients are small and not statistically significant in the Bering Sea and western subtropical Pacific. The nonseasonal EOFs 1, 3 ,and 4 are therefore strongly indicative of the principal modes of curl variability in the subarctic. In the subtropical anticyclone only EOF 3 explains a large amount of the variance. Furthermore, EOF 3 explains three times more of the variance in the eastern, than in the western region of the subtropical anticyclone. The variance of the curl in the western subtropical region is not strongly characterized by the dominant modes of the nonseasonal EOFs.

Regions	Periods (years)	Coherence	Phase (degrees)
Western Pacific & Bering	2.5 - 3	.60	0
Western Pac. & East Pac. High	2 2.5 - 3	.98 incoherent	90 --
GOA & Bering	2.5 - 3	.96	90
GOA & East Pac. High	2.5 - 3 5 - 7	.91 .92	180 180
GOA & Western Pac.	2.5 - 3	.70	90
East Pac. High & Bering	2.5 - 3	.80	90

Table 1.4: Phase and Coherence among regional wind stress curl series.

TAFs of nonseasonal wind stress curl

	Mode 1	Mode 2	Mode 3	Mode 4
GOA curl	0.41	-0.22	0.80	0.21
Bering curl	-0.71	-0.14	Not Signif.	0.55
East Pacific High curl	0.30	0.57	-0.55	Not Signif.
West Pacific High curl	0.40	0.32	Not Signif.	-0.18

Table 1.5: Correlations among regional curl time series and TAFs of nonseasonal wind stress curl EOF's.

Wind stress curl over the Bering And Chukchi Sea regions 1981-1990

The Seasonal Cycle

The annual mean field of Bering and Chukchi curl (figure 1.28) shows large scale negative curl occurring over most of the Chukchi region and positive curl over the Bering Sea. A negative curl maximum (i.e. the largest magnitude of the negative curl) occurs to the northwest of Bering Strait. A slight positive curl maximum occurs over the western Bering Sea near 60°N 170°E. The general features in the monthly mean fields consist of negative wind stress curl over most of the Chukchi Sea and positive wind stress curl over the Bering Sea (figure 1.29). The positive curl over the Bering Sea is of course associated with the Aleutian Low, while the negative curl over the Chukchi is associated with Arctic high pressure systems, in particular the eastern flank of the Siberian High and the western section of the Beaufort anticyclone. There is also a region of positive curl present over the Chukchi between 70°N-75°N and 160°E-175°E during the winter months. In November, December and January there are two local maxima over the Bering Sea, one over the northcentral Bering Sea, and the other adjacent to the Kamchatka Peninsula between 55°N and 60°N. The negative curl maximum is located to the northwest of Bering Strait between 67°N and 70°N from November through March. In February and March the only positive curl maximum present over the Bering Sea occurs adjacent to the Kamchatka Peninsula. In April the

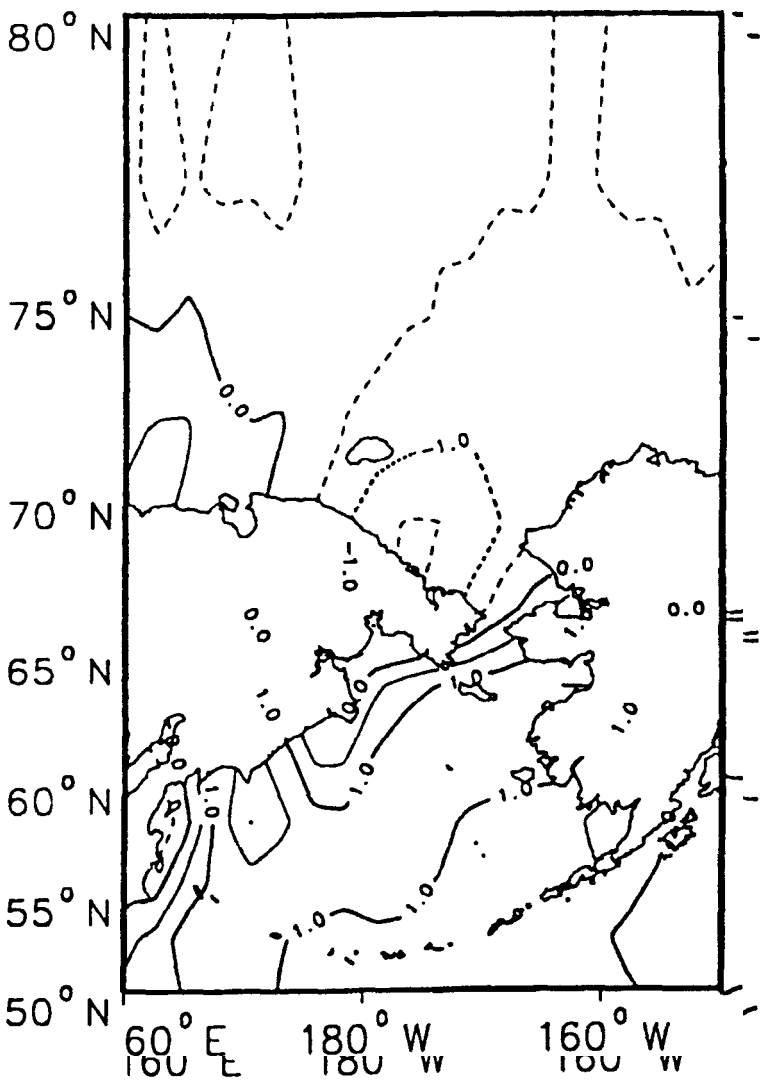

Figure 1.28: Annual mean wind stress curl over the Bering Sea and Chukchi Sea 1981-90. CI= 0.5* 10^{-7} N/m^3.

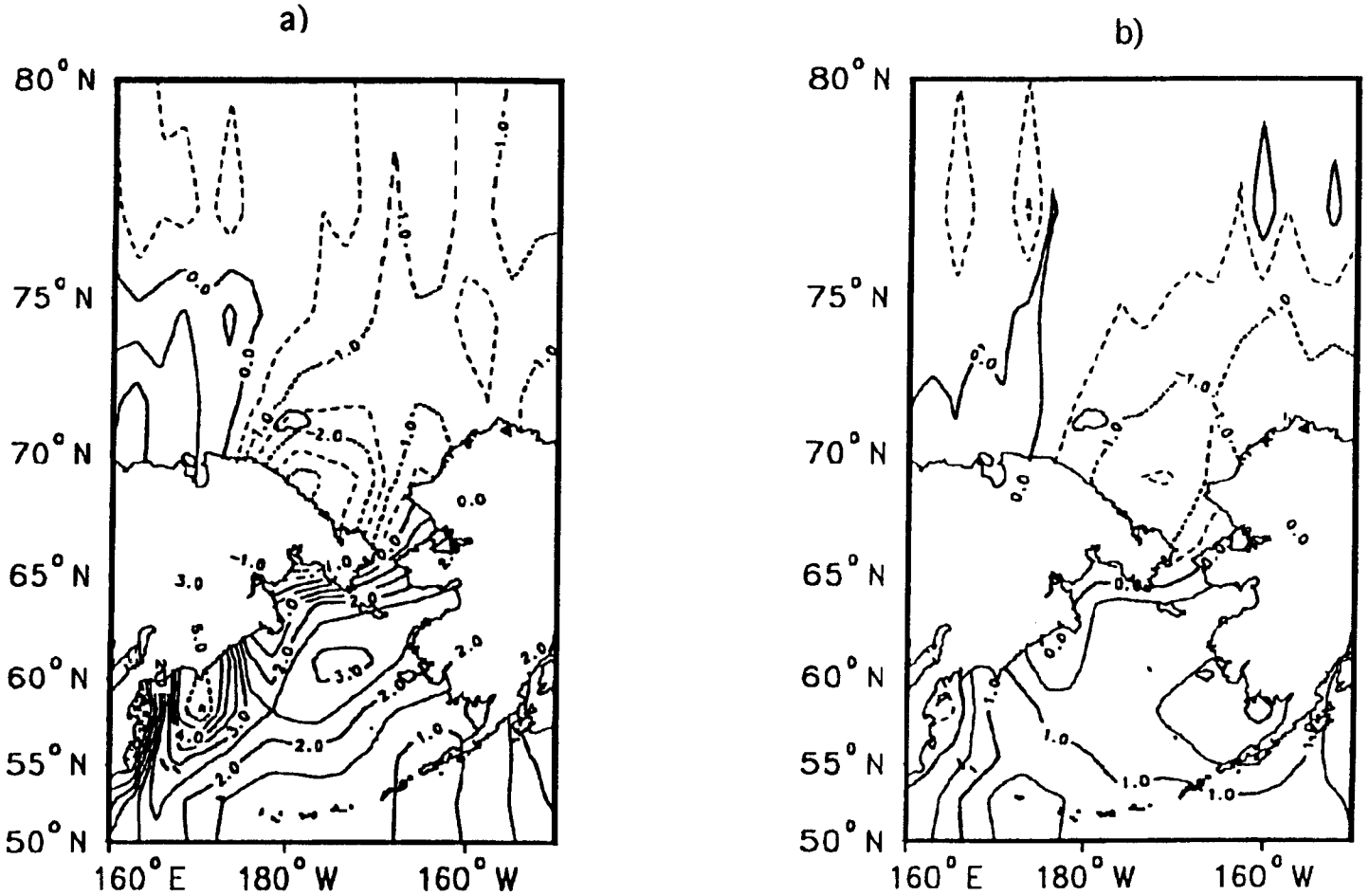

Figure 1.29: Mean wind stress curl over Bering Sea and Chukchi Sea1981-1990

a) January b) April. CI=0.5 * 10^{-7} N/m^3.

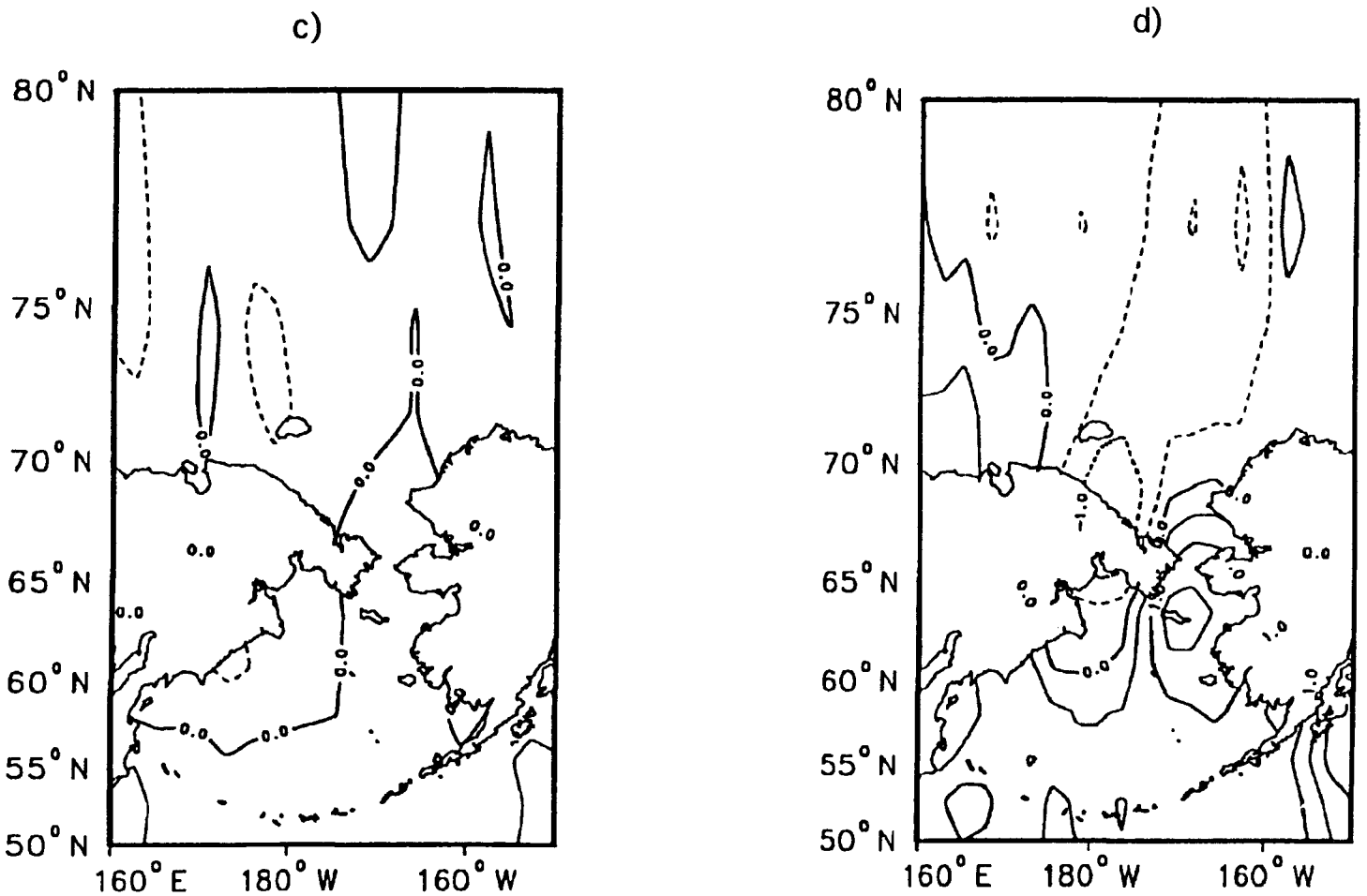

Figure 1.29 continued: Mean wind stress curl over Bering Sea and Chukchi Sea.
c) July d) October. CI= 0.5 * 10^{-7} N/m^3.

positive and negative curl still occupy generally the same regions as during winter, but the amplitudes have decreased by factors of from 1 to 4. During May, June, and July the amplitudes of the positive and negative curl weaken further, and negative curl occurs over much of the Bering Sea. During May and June positive curl is present over the Chukchi between 70°N and 80°N and 160°E to 165°E. In August and September the positive curl advances poleward in the Bering Sea as the Aleutian Low begins to deepen, and positive curl is present over much of the Chukchi basin between 75°N and 80°N. During October the positive and negative curl again occupy their respective winter regions, and the amplitudes begin to increase towards winter values.

The mean position of the zero contour of the curl is interpreted to roughly represent the boundary between the subarctic and Arctic wind fields. In November the boundary is located in its farthest northward position and lies near 68°N. During December and January the boundary slopes to the northeast from 64°N to 68°N passing through Bering Strait. In February and March the zero curl contour has shifted southward and lies well to the south of Bering Strait. From April through October the boundary lies over the Bering Sea with its southernmost points between 50°N and 60°N.

Interannual Variability

Individual time series of nonseasonal wind stress curl were averaged separately over the Bering Sea and Chukchi Sea regions to serve

as indicators of the strengths of the Aleutian Low and Arctic wind fields respectively. The dividing line was taken to lie along Bering Strait. Large positive anomalies present during most winters in the Bering Sea series (figure 1.30a) show that the Aleutian Low has been intense during much of the last decade, as has already been shown using a longer record and a slightly coarser grid. Negative anomalies associated with weak circulation occurred over the Bering Sea during winter in 1982, 1984, and 1989. Large negative anomalies in the time series of Chukchi wind stress curl (figure 1.30b) show that the Arctic wind field has also been intense during much of the last decade except for periods of persistently positive anomalies during winters of 1981-82, 1983-84, and 1988-89. The periods when the Arctic wind field was anomalously weak are the same periods when the Aleutian Low was weak. The similarity in the fluctuations of the mean anomalies qualitatively suggests that on interannual time scales the wind stress curl fields over the Bering and Chukchi regions fluctuate out of phase. The cross correlation coefficient for these time series is -0.41 at zero lag, which is significant at the 99% level. This shows that there is a statistical tendency for positive curl anomalies to be present in the Aleutian Low concurrent with negative anomalies in the Siberian High and vice-versa. Furthermore, the cross correlation coefficient for the time series of Chukchi Sea wind stress curl and wind stress curl averaged over the entire Aleutian Low region is -0.52 at zero lag and the 99% significance level. These correlations show that the strengths of Bering Sea and Arctic wind stress curl fields tend to fluctuate in concert on nonseasonal time scales during the 1980's.

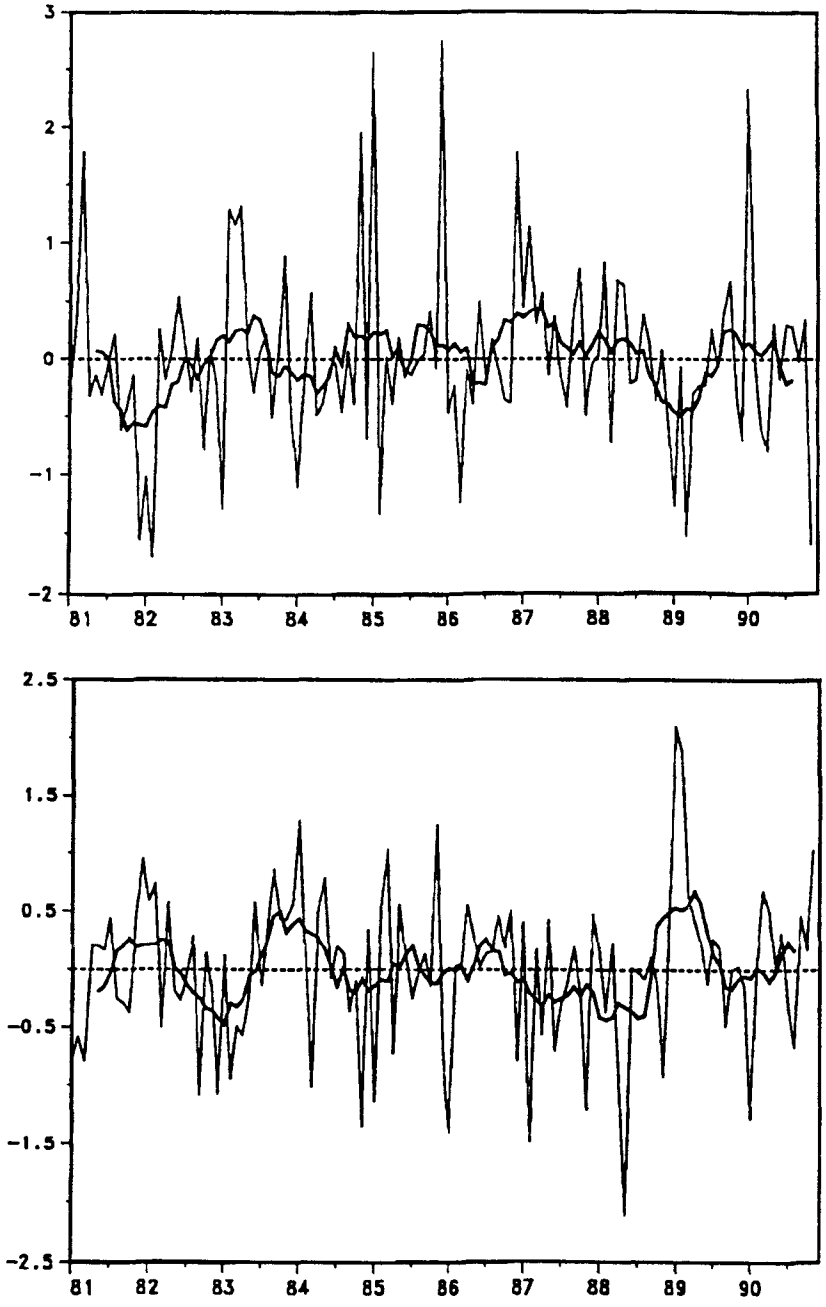

Figure 1.30: a) Bering Sea wind stress curl anomalies.
b) Chukchi Sea wind stress curl anomalies.
Units are 10^{-7} N/m^3.

EOF Analysis

EOF analyses were performed on the monthly mean wind stress curl data and on the monthly mean wind stress curl with the seasonal cycle removed. Hereafter these analyses will be referred to as S2 and NS2 respectively. The first four modes of S2 together account for 54% of the variance of the curl, while 47% of the nonseasonal variance is explained by the first four modes of NS2. The seasonal cycle explains only 7% of the curl variance, which shows that the amplitude of the seasonal cycle of the curl at this high latitude is small compared to the amplitudes of interannual variations.

Examination of the eigenvectors of the first four modes of both S2 and NS2 showed that the spatial patterns differ only slightly when placed in one to one correspondence with each other. This is another indication that the amplitude of the seasonal cycle of the curl is small compared to the amplitudes of the interannual variations. Most of the differences in the amplitudes of the seasonal and nonseasonal eigenvectors occur over the Bering Sea, which suggests that the seasonal cycle is stronger over the Bering Sea than it is at higher latitudes over the Chukchi.The eigenvectors of NS 2 are shown in figure 1.31. Since the eigenvectors of S2 and NS2 are quite similar, only the set of eigenvectors and TAFs from NS2 will be discussed. The first EOF explains 24% of the nonseasonal variance. The first eigenvector (figure 1.31a) strongly resembles the mean fields particularly during winter. It is interpreted to represent the quasi-

permanent positions of the wind fields associated with the Aleutian Low and Arctic high pressure systems. The mode 1 TAF (figure 1.32a) is characterized by large negative anomalies during most winters between 1981 and 1990, indicating that both the Aleutian Low and Arctic high pressure have been anomalously strong during these winters. Notable exceptions occur in 1982 and 1989 when large positive anomalies in the mode 1 TAF indicate that the circulation in the Aleutian Low and Siberian High was anomalously weak. EOF 1 mainly represents interannual variations in the strength of the Siberian High and Aleutian Low. Correlation coefficients between the mode 1 TAF and the nonseasonal series of Chukchi and Bering curl are 0.70 and -0.90 respectively indicating that about half of the nonseasonal variance of Chukchi curl is explained by this mode while about 80% of interannual Bering Sea curl variations can be explained by mode 1.

The second EOF (figure 1.31b) accounts for 10% of the nonseasonal variance. The second eigenvector shows a north-south oscillation with maximum amplitudes centered on the Bering Strait region. The curl over the southern Chukchi near Bering Strait is in phase with most of the Bering and out of phase with the rest of the Chukchi. The correspondence of the extrema in the TAF of mode 2 (figure 1.32b) and the Bering and Chukchi curl time series indicates that EOF 2 represents poleward intrusions of an intensified Aleutian Low into the southern Chukchi.

The third and fourth EOFs represent 7% and 6% of the nonseasonal variance respectively. The third eigenvector (figure 1.31c) shows that most of the Bering and Chukchi regions are in phase with each other and out of

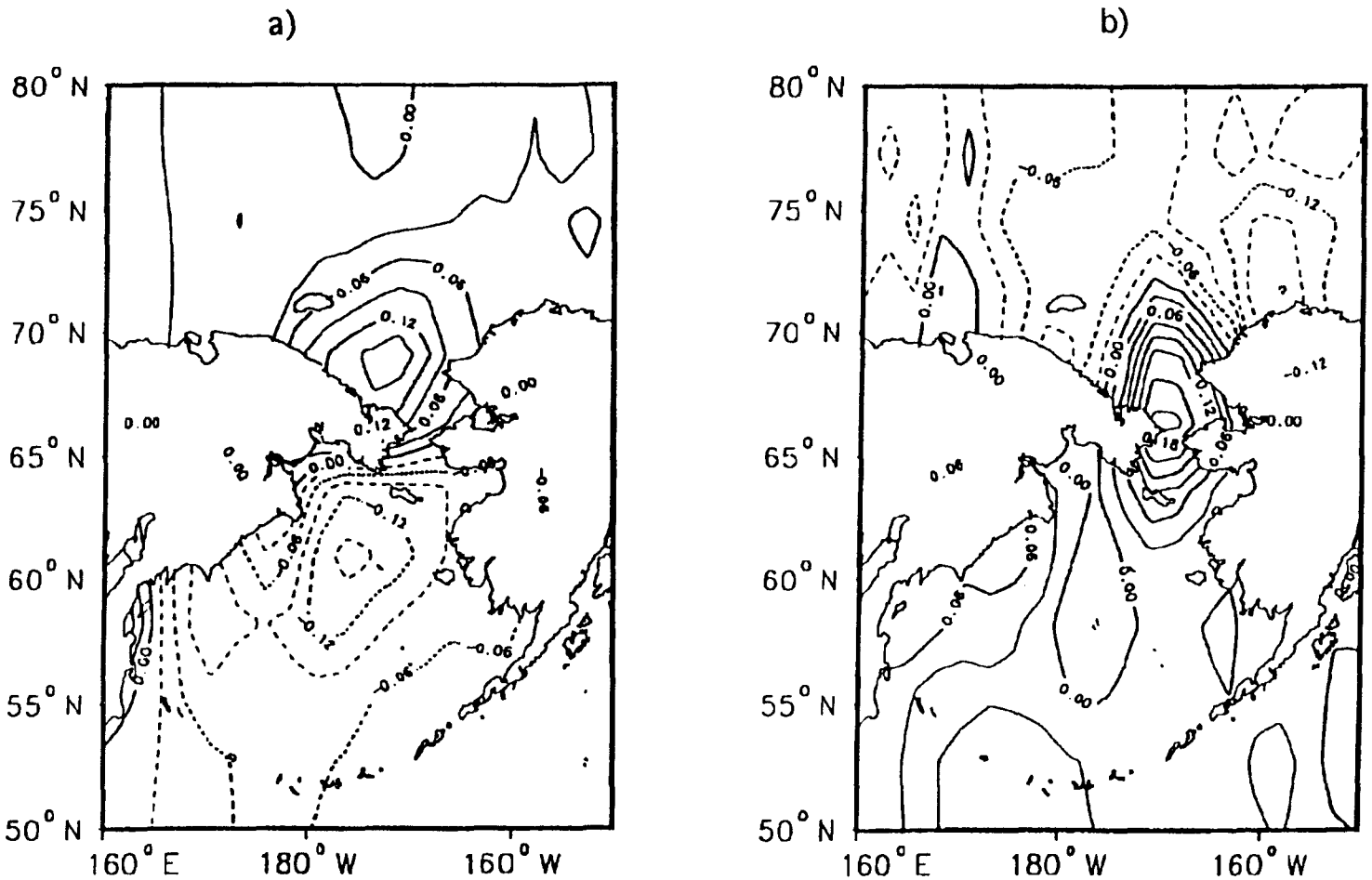

Figure 1.31: Eigenvectors of nonseasonal Bering Sea and Chukchi Sea wind stress curl. a) Mode 1 b) Mode 2. CI= 0. 03 dimensionless units.

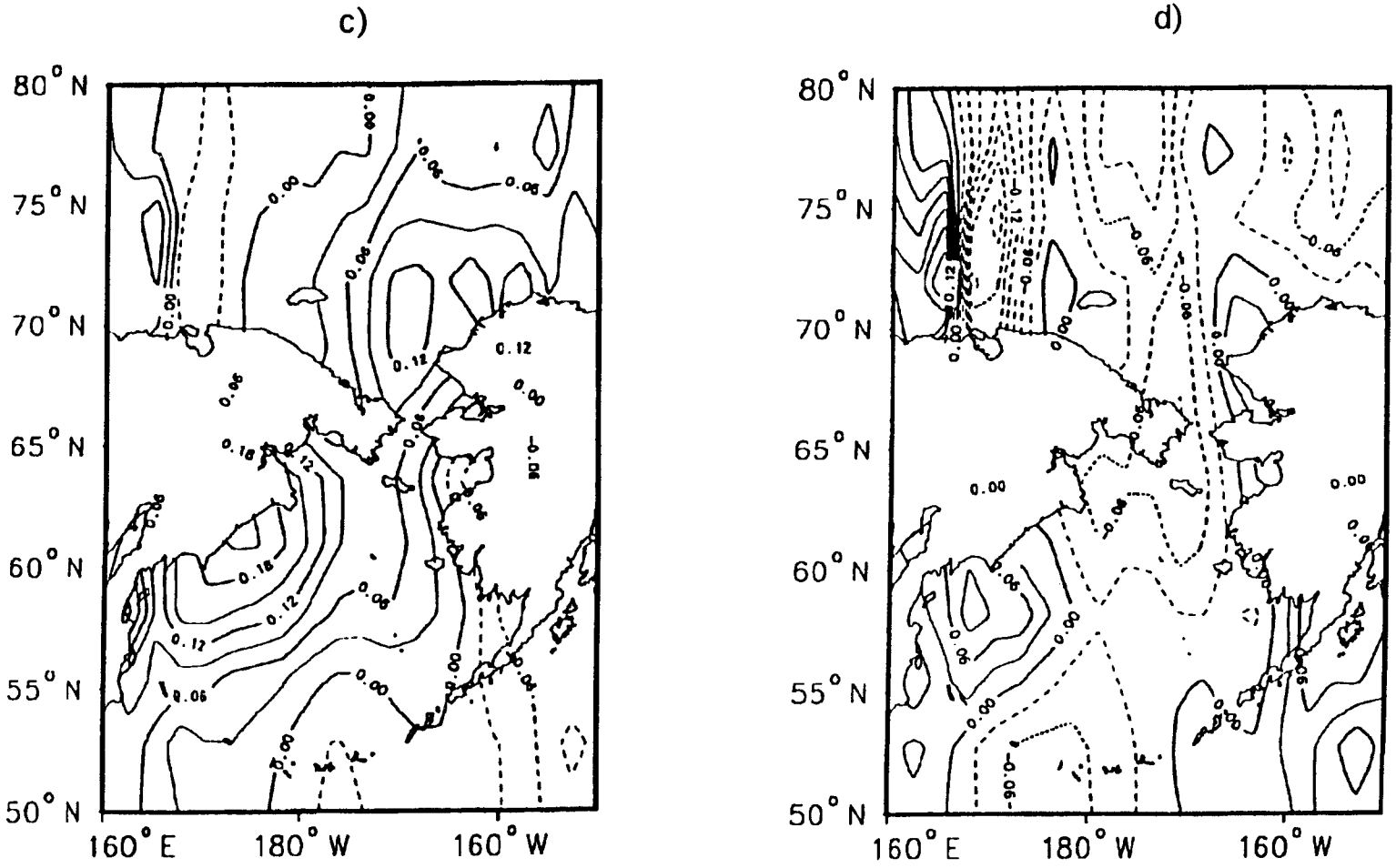

Figure 1.31 continued: Eigenvectors of nonseasonal Bering Sea and Chukchi Sea wind stress curl. c) Mode 3 d) Mode 4. CI= 0. 03 dimensionless units.

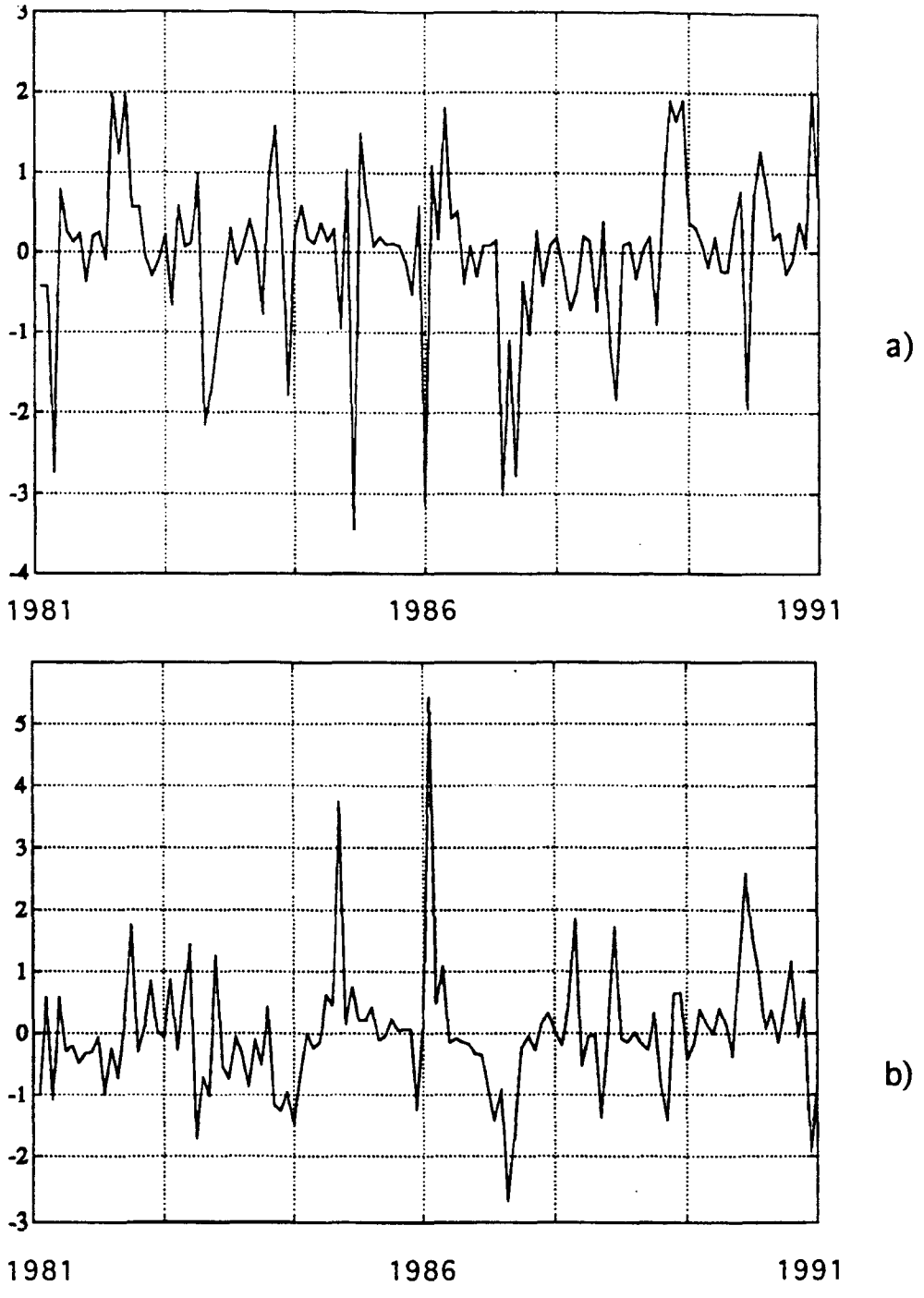

Figure 1.32: TAFs of nonseasonal curl over the Bering Sea and Chukchi Sea. a) Mode 1 b) Mode 2. Units are 10^{-7} N/m^3.

phase with the northwestern Gulf of Alaska, while the fourth eigenvector (figure 1.31d) shows largely the same structure except that the western Bering Sea is in phase with the northwestern Gulf of Alaska. The similarity in the spatial structure of the eigenvectors of these two modes indicates that they may represent similar physical processes. Overland and Pease [1982] note that EOFs with eigenvalues that are very close together may represent similar processes. The spatial similarity of these eigenvectors to each other, and their resemblance to the structure of the SLP field when marine blocking ridges occur over the Bering Sea suggests that EOFs 3 and 4 may represent the effects of marine ridging on the field of wind stress curl. Blocking ridges are discussed in chapter 3.

Oceanographic Effects of Wind Stress Curl Variability

Wind Stress Curl and Observed Transport and Property Variations in the Northeast Pacific

Tabata [1991a] notes that oceanographic properties such as temperature, salinity and dissolved oxygen at Ocean Station P (50°N 145°W) underwent interannual oscillations of 2 to 3 year period during 1956-66, while the period of the oscillations has doubled between 1966 and 1989 to about 6 to 7 years. Tabata [1991b] suggests that baroclinic transports along line P undergo oscillations with periods (3-4 and 6-7 years) that are similar to those of the property variations, although the spectral peaks of these oscillations are not statistically significant at the

95% level. The time series of Gulf of Alaska wind stress curl (figure 1.26b) qualitatively suggests that the time scales of Gulf of Alaska wind stress curl variability are similar to those observed in the ocean by Tabata [1991a, 1991b].

Cross correlation of Gulf of Alaska wind stress curl and the Line P transport time series (provided by S. Tabata) yielded a small (<0.2) correlation coefficient that is not statistically significant. The correlation was done only at zero lag because the oceanic transport series has a number of gaps. However, periods of strong and weak flow across Line P as categorized by Tabata [1991] tend to coincide with periods of positive and negative curl anomalies respectively. In 22 of 33 (66%) cases, strong and weak flow across Line P occurred in conjunction with positive and negative curl anomalies respectively in the Gulf of Alaska during winter. Also, the fact that there are significant peaks at periods of 2.5 to 3 years and 5 to 7 years in the power spectra of Gulf of Alaska and East Pacific High wind stress curl (figures 1.27a and 1.22b) suggests that the observed oceanographic fluctuations might be related to, or forced by interannual wind stress curl variability. To test this, the time series were each split into two time periods, 1946-66 and 1966-88, which overlap the time periods of the variable period oscillations observed by Tabata [1991a, 1991b]. The power spectrum of the 1946-66 time series of Gulf of Alaska curl (figure 1.33a) shows only one peak at frequencies lower than .5 cycles per year, and this occurs in the 2.5 to 3 year period band. There is a sharp drop off in power for periods longer than 3 years, in particular there is negligible energy at periods of 5 to 7 years in this spectrum. A broad banded peak

occurs in the 3.5 to 5.5 year band of the East Pacific High curl power spectrum for the 1946-66 period (figure 1.33b). These peaks are significant at the 95% confidence level. The power spectrum for the 1966-88 Gulf of Alaska series (figure 1.33c) shows a peak in the 5 to 7 year period band and no spectral peak in the 2.5 to 3 year period band. The peak at 5 to 7 year period is not quite significant at the 95% confidence level since the record is only 22 years long. However, the concentration of energy in the 5 to 7 year period band and the conspicuous lack of energy in the 2.5 to 3 year band suggest that 5 to 7 years is the dominant time scale of curl fluctuations over the Gulf of Alaska during 1966-1988. The only significant peak in the power spectrum of the East Pacific High series for 1966 to 1988 occurs at the 3.5 year period (figure 1.33d). There is very little energy at lower frequencies, in particular there is minimal energy in the five to seven year period band. Therefore the wind stress curl over the Gulf of Alaska has undergone interannual fluctuations with temporal characteristics very similar to those observed in the ocean by Tabata [1991a, b], while the fluctuations in East Pacific High curl show no such pattern. In particular from 1946 to 1966 Gulf of Alaska wind stress curl fluctuated at periods of 2.5 to 3 years as did properties along line P, while during 1966 to 1988 the period of the oscillations doubled to 5 to 7 years also in conjunction with a doubling of the period of the oscillations along line P. There is also a consistent relationship between the sign of the wind stress curl over the Gulf of Alaska and the interannual variations in the strength across line P. During the 33 year record of the strength of line P transport reported by Tabata [1991b], the average winter (November

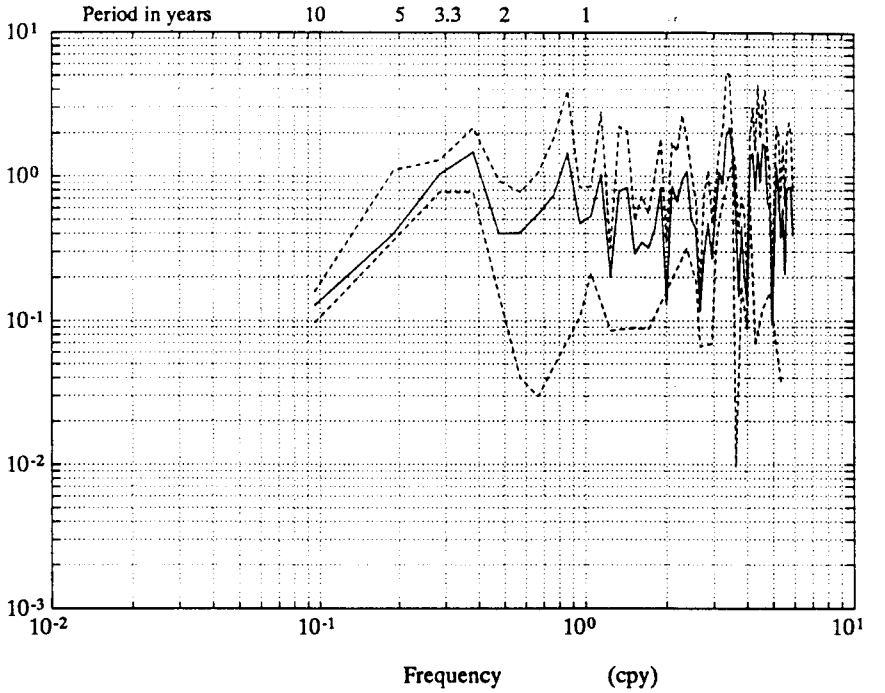

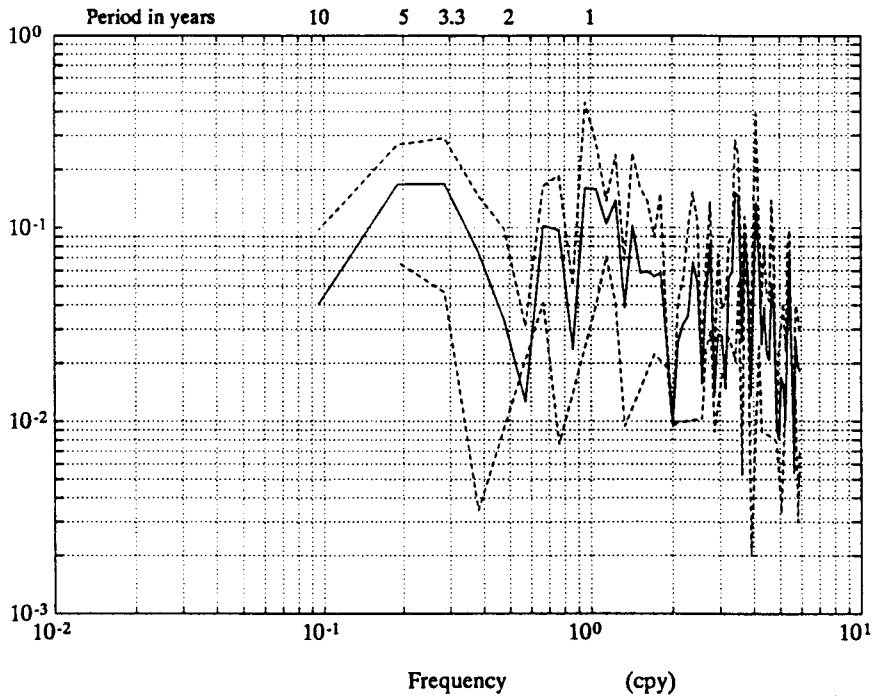

Figure 1.33: Power Spectra for the period 1946-1966.
a)Gulf of Alaska; b)East Pacific High.

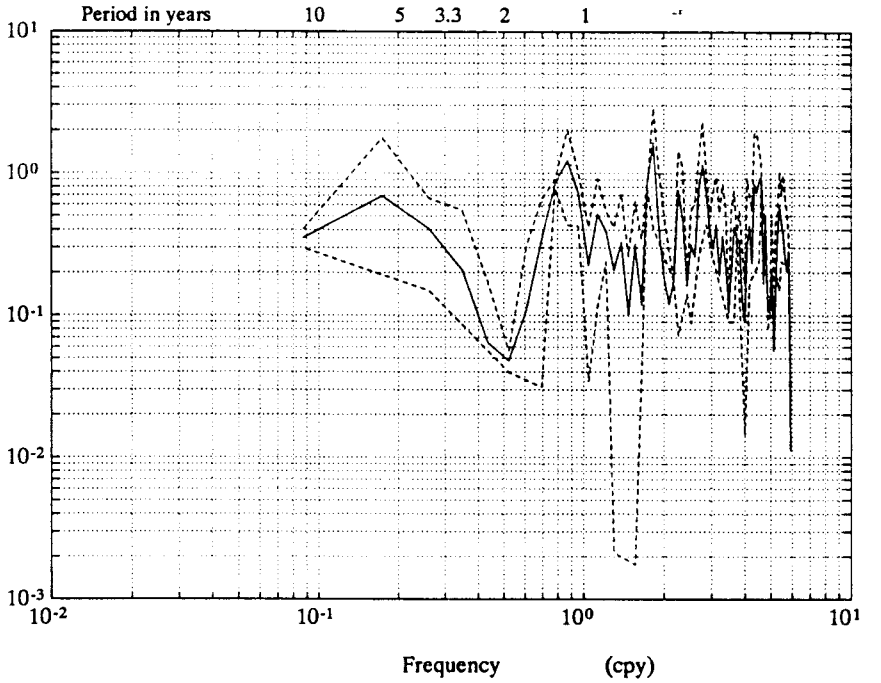

c

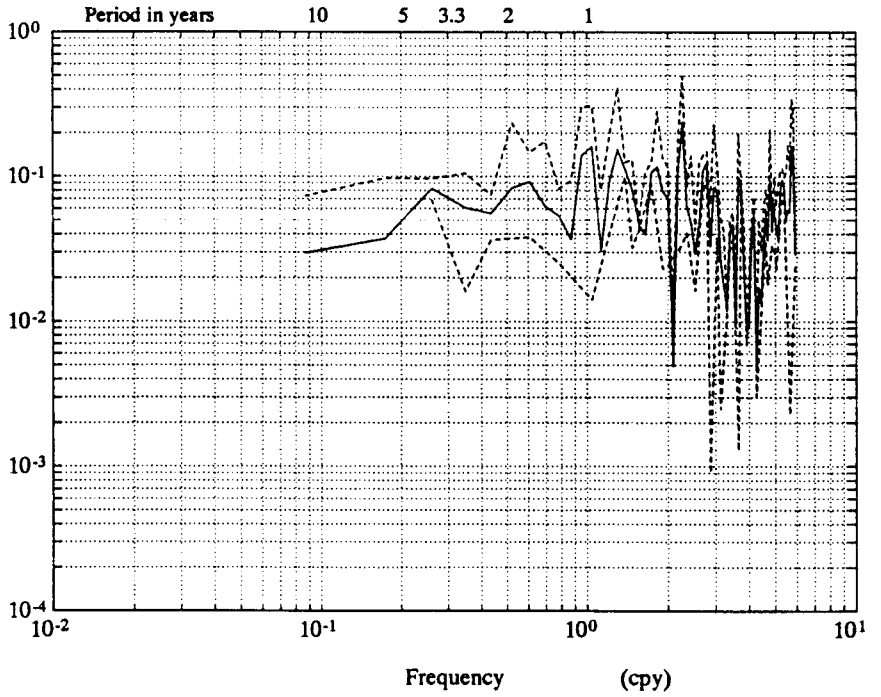

d

Figure 1.33 continued: Power Spectra for the period 1966-1988. c)Gulf of Alaska, d)East Pacific High.

through March) curl over the Gulf of Alaska was positive when transports were strong and negative when transports were weak. This occurred 66% of the time. Although the relationship is far from perfect it does show that the strength of line P transports often fluctuates in phase with Gulf of Alaska curl. This is also consistent with Sverdrup theory, which requires that intensified wind stress curl in the subarctic forces stronger poleward flow in the Sverdrup interior, while weaker curl weakens the flow. Therefore, on the basis of the arguments presented above it is suggested that the observed interannual transport and property variations along line P are, to some extent, forced by interannual variations of wind stress curl over the Gulf of Alaska.

Wind Stress Curl and Ocean Transports in the Western Subarctic Pacific

Positive wind stress curl anomalies over the Bering Sea during 1976-88 imply an increase in the northward Sverdrup transport in the Bering Sea. This in turn implies an intensification of the western boundary current system during 1976-88 via the continuity equation. Using data from Hanawa [1991, his figs. 4a, 4b], it is inferred that the observed western subarctic Pacific Ocean circulation has intensified and intruded further southward during 1976-88 in response to increased wind driven northward flow in the interior Bering Sea. The Oyashio current system has responded to this intensified wind stress curl over the western subarctic Pacific during 1976-88 by intruding further south than during years of weak wind stress curl forcing. Therefore, decadal scale

variability in subarctic North Pacific wind stress curl is manifested in the ocean circulation as intensified northward flow in the interior region of the Bering Sea, and intensified southward flow in the subarctic Pacific western boundary current system in response to the increased northward flow. This is consistent with the results of Sekine [1988, 1991], who has shown that on episodic time scales the Oyashio current intrudes 300-500 km southward of its mean position in response to anomalously strong north winds associated with an intensified Aleutian Low and Siberian High.

The western subarctic circulation might also respond to wind stress curl fluctuations on shorter time scales than a decade. The zonal oscillation between the eastern and western Bering Sea indicated by the first nonseasonal EOF of the curl was shown occur on 2.5 to 3 year as well as ten to eleven year time scales. Shirshov ridge is located approximately 450 km to the east of the Kamchatka Peninsula. The numerical results of Anderson and Corry [1985] in the Florida Current system suggest that the low frequency oceanic response of a boundary current to wind stress curl forcing might be a function of the distance between the forcing region and the boundary current. Localized wind stress curl forcing in the region of Shirshov ridge at 2.5 to 3 year period could generate baroclinic planetary waves in this period band. Planetary waves traveling at one to two centimeters per second, which is typical of the speeds of planetary wave like disturbances in the boundary current of the Gulf of Alaska [Okkonen, 1992] (where the latitude is similar to that off Kamchatka), would traverse the region between Shirshov ridge and the coast in 225 to 450 days, thus

inducing a response of the boundary current to interannual wind stress curl variations. Planetary waves generated far to the east of Shirshov ridge would not induce such a response because the travel time of the wave from the forcing region to the boundary region would likely exceed the period of the forcing. Also Shirshov ridge might effectively block the westward passage of energy through deflection and scattering effects. This suggests that the response of the western boundary current of the Kamchatka gyre to low frequency wind stress curl forcing might be coherent with the forcing when the Bering Sea wind stress curl maximum lies over and to the west of Shirshov ridge. When the wind stress curl maximum is displaced to the eastern Bering Sea or Gulf of Alaska no such response of the boundary current to the curl forcing is indicated. These results concerning the hypothetical response of the Kamchatka Current to low frequency curl fluctuations are largely speculative, and are based only on the characteristic fluctuations that are indicated to occur in the field of wind stress curl. Testing of these ideas will be relegated to numerical modelling efforts until sufficient oceanographic observations are available.

Wind Stress Curl and Planetary Waves in the Northeast Pacific

Tabata [1991b] shows that the strengths of transport across Line P and in the California Current are often weak during ENSO years. The California Current was weak during 11 of 13 ENSO years, while Transport across Line P was weak for 7 of 12 ENSO years [Tabata, 1991]. White and

Tabata [1987] find that interannual baroclinic long waves in the pycnocline along line P tend to be associated with ENSO events. White and Tabata [1987] suggest that anomalous wind stresses occurring in association with meridional teleconnections prior to and during ENSO events are important in driving these baroclinic long wave motions in the Northeast Pacific. White and Tabata [1987] explicitly make no causal connection between long wave activity at 50°N and wind stress curl even though White [1985] has shown that oceanic baroclinic long wave activity at 40°N is related to wind stress curl through a resonant response of the waves to the forcing, and White and Saur [1983] show that wind stress curl root mean square variability is greater at 50°N than at 40°N. These results suggest that long wave activity might also be greater at 50°N than at 40°N. White and Tabata [1987] note that the intensification of both baroclinic long wave activity and wind stress curl near the coast suggests that the variability at the coast is wind driven.

It was shown earlier that the field of curl in the Aleutian Low region, particularly in the Gulf of Alaska, oscillates at periods of 2.5 to 3 and 5 to 7 years. These periods correspond very closely to the two most energetic peaks in the power spectrum of the Southern Oscillation index, which occur at periods of 2.5 to 3 years and 5 years (figure 1.34). This indicates that the anomalous wind stresses that occur in meridional teleconnection to ENSO events as suggested by White and Tabata [1987], occur in conjunction with anomalies of wind stress curl that are apparently linked to the Southern Oscillation and hence to ENSO events. During ten of eleven ENSO events that occurred during the curl record, the pre-ENSO

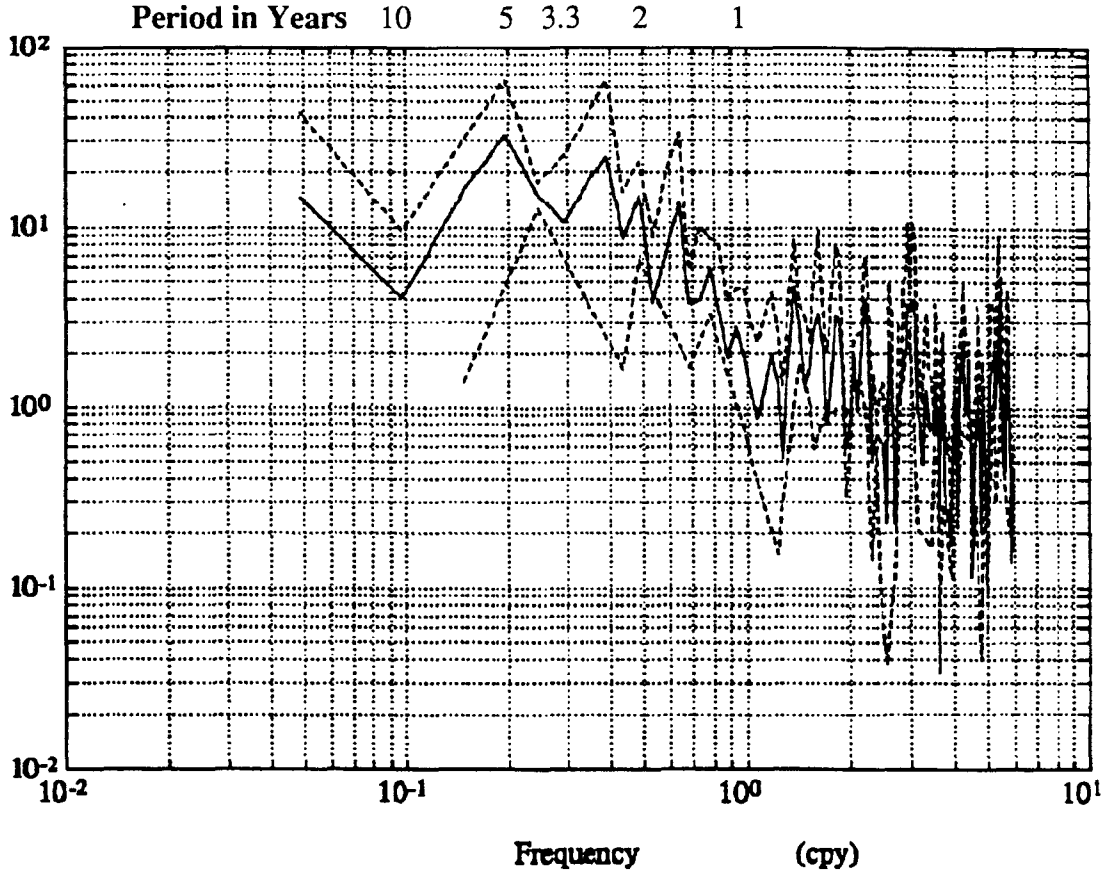

Figure 1.34: Power spectrum of the Southern Oscillation Index.

year winter is characterized by weaker curl in the Aleutian Low than during winter of the ENSO year. Therefore, there is a consistent relationship between the relative strength of Aleutian Low curl and ENSO events. Also, it can be shown by appropriately manipulating the equations of motion, that on long time scales the curl of the wind stress is a more important mechanism than wind stress in forcing low frequency baroclinic planetary waves in the ocean [e.g. Gill, 1982]. Based on the arguments given above, it is suggested that anomalous wind stress curl rather than wind stress during ENSO events might be forcing the long wave activity observed by White and Tabata [1987] along 50°N.

Summary and Discussion

In the North Pacific annual maxima of positive wind stress curl occur over the Gulf of Alaska and western Bering Sea, while negative maxima occur in the subtropical anticyclone between 21°N and 27°N across much of the basin. These maxima occur during the winter months of November through March. Maximum variance within the Aleutian Low region occurs during the winter months, while the variance of the curl in the subtropical anticyclone is small except adjacent to the coast of North America between 27°N and 36°N where the variance is large and the maximum variance occurs during summer. On the annual time scale the field of curl is intensified between about 500 and 900 km offshore of the coast of North America. The annual mean of zonally averaged curl

decreases monotonically between 60°N and 24°N. The maximum and minimum range of the seasonal cycle occur at 60°N and 27°N respectively.

EOF analysis shows that the annual cycle is the dominant mode of variability in North Pacific wind stress curl. Twenty two percent of the total variance is explained by the seasonal cycle, while the first 3 nonseasonal modes combined explain 19% of the total variance and 25% of the nonseasonal variance. The nonseasonal modes are characterized by both meridional and zonal oscillations in the region of the Aleutian Low and principally meridional oscillations in the subtropical anticyclone. On nonseasonal time scales the fields of wind stress curl in the Aleutian Low and North Pacific High tend to fluctuate in concert with each other, as does the curl within the Aleutian Low and Siberian High systems.

Regional wind stress curl variability during 1946-91 serves as an indicator of the strength of the Aleutian Low during this period. The regional curl time series shows that the Aleutian Low was anomalously strong from 1976 to 1988 and anomalously weak during most of the period 1954-75. After 1988 the intensification appears to have reversed and mean anomalies have been negative since 1989. Periods of weakened or strengthened wind stress curl in the Aleutian Low tend to occur on time scales of two to six years. Statistically significant fluctuations of the curl occur at periods of 2.5 to 3 and 6 to 7 years in the Gulf of Alaska and 2.5 to 3 years over the Bering Sea. The intensified Aleutian Low of 1976-88 occurred to a greater extent over the Bering Sea than in the Gulf of Alaska, although the curl was intense over the Gulf of Alaska from about 1979-86. Changes in North Pacific Sverdrup transports can be inferred

from long term changes in the strength of the curl within the Aleutian Low and the subtropical anticyclone. In particular, persistently weakened and strengthened transports occurred during 1961-68 and 1976-88 respectively, especially in the subarctic and western subtropical North Pacific.

During 1976-88 individual and running mean wind stress curl anomalies attained their maximum values over the course of the record across the Aleutian Low region, and in the western subtropical Pacific. In particular, during 1976-80 a persistent and large amplitude positive curl anomaly occurred over the Bering Sea and a persistent and large amplitude negative anomaly occurred in the western Pacific subtropical anticyclone, indicating a strengthening of the curl in each of these region. This also indicates that the recent observed strengthening of the Aleutian Low occurred as part of a climatic event or regime that has a larger spatial scale than that of the Aleutian Low.

Similarities in the time scales and phases of fluctuations of physical oceanographic properties and wind stress curl in the Gulf of Alaska suggest that anomalous wind stress curl might be important in driving observed interannual oceanographic variations at high latitudes in the Northeast Pacific. Anomalous wind stress curl occurring in conjunction with ENSO events was suggested as a generating mechanism for the two to five year period baroclinic planetary waves that have been observed by White and Tabata [1987] in the pycnocline of the Northeast Pacific Ocean.

Relationships between wind stress curl and oceanic fluctuations in the Gulf of Alaska and western subarctic Pacific were established and

qualitatively suggest that wind stress curl variability drives oceanic variability on interannual to decadal time scales in the subarctic Pacific. While the atmospheric data are relatively complete, the oceanographic observations are sparse, particularly during early periods of observation. More quantitative assessments await the acquisition of longer and more complete time series of oceanographic measurements.

Chapter Two

Interannual Variability in the North Pacific Climate System

Introduction

The dynamic and thermodynamic couplings between the atmosphere and ocean have tremendous effects on the global weather and climate. One of the most important examples is the occurrence of the El Niño-Southern Oscillation phenomenon, the effects of which are global in scale and affect not only weather and climate but the ecology and economy of the globe. On more regional scales, the fluxes of heat, moisture, and momentum between the ocean and atmosphere directly determine the climate of the maritime environment including the adjacent and heavily populated continental boundary regions. A knowledge of the mechanisms and time scales of oceanic and atmospheric climate variations is therefore important for the prediction of, and preparation for future environmental conditions.

This part of the study will describe interannual variations that have occurred over the past twenty to fifty years in North Pacific climate variables. Attention will be focused on the relationships between the various climate variables and the curl of the wind stress since wind stress curl was shown to be an indicator of the strength of the atmospheric

circulation, particularly in the Aleutian Low. Thus wind stress curl serves as a climate variable and the long time series (forty five years) of monthly wind stress curl anomalies will be used to assess the role of wind stress curl in the North Pacific climate system. A wind stress curl series of this length has not been available previously for examining the interrelationships between atmospheric and oceanic parameters in the North Pacific.

It will be shown that fluctuations in extratropical North Pacific wind stress curl, SST, air temperature, sea ice cover, and several tropical Pacific indices are strongly coupled on time scales of years, particularly during the period 1976-88. This period is characterized by strong and persistent anomalies in both the atmosphere and ocean of the Pacific region. These anomalies occur from the tropical to the high latitude North Pacific, and are suggestive of a climate anomaly with very large spatial scales.

Previous Studies

Interannual North Pacific SST variability has been studied by a number of investigators using EOF analysis or related methods (e.g. Davis, 1976, Weare et al., 1976, Douglas et al., 1982, Kawamura, 1984, Iwasaka et al., 1987,1988, Namias et al., 1988, Lau and Nath, 1990, Wallace et al.,1990). Many of these studies have examined the interactions between the lower atmosphere and the surface ocean through simultaneous correlation analyses of SLP and geopotential height

variations in relation to SST variability. These studies have shown that North Pacific SLP variations and geopotential height fluctuations at 500 mb and 700 mb tend to be strongly correlated to variations in the North Pacific SST field. Kawamura [1984] and Iwasaka et al. [1987] show that the dominant mode of nonseasonal North Pacific SST variability is highly correlated to the Pacific North American (PNA) pattern in the 500 mb geopotential height field. Iwasaka et al. [1987] use lagged correlation analysis to show that the PNA leads variations in North Pacific SST by one month, and conclude that the PNA forces SST anomalies represented by the dominant mode EOF. This is an indication that large scale atmospheric variability over the North Pacific forces large scale SST anomalies. On the other hand, Chen and Reiter [1986] find that SST anomalies in the Kuroshio region have a major effect on the strength and location of the Aleutian Low and the subtropical anticyclone, and hence on cyclone tracks downstream. In this case large scale SST anomalies control large scale atmospheric variations. Wallace et al. [1990] note that most of the oceanographic literature concerning atmosphere-ocean interactions has emphasized the role of the atmosphere forcing the ocean, while the atmospheric literature in the last decade has emphasized the forcing of the atmosphere by the ocean, in particular by SST anomalies. It appears that both the atmospheric forcing of oceanic variability and the oceanic forcing of atmospheric variations are manifested in processes that are important in determining interannual variability in large scale North Pacific weather and climate.

Data and Methods

Monthly mean North Pacific SST data for the period 1953 through 1990 were obtained from the Long Range Forecasting Group at Scripps Institution of Oceanography. The grid is spaced five degrees in latitude and longitude between 20°N and 60°N. Tropical SST for the period 1970 through 1990 was obtained from the NOAA/NWS Climate Analysis Center for the Niño 1+2 region of the eastern tropical Pacific. The Niño 1+2 region is bounded by the west coast of South America and the 90°W meridian and lies between the Equator to 10°S. A time series of the Southern Oscillation Index for the period 1950 through 1990 was also obtained from the NOAA/NWS Climate Analysis Center. Air temperature data for Sitka, Alaska and Saint Paul, Alaska were obtained from the NOAA/NWS Local Climatological Data monthly summaries. The Sitka time series covers the period 1940 to 1990 and the Saint Paul series is for the period 1953 to 1989. The Pacific North American Index was obtained from the Data Support Center at NCAR. The time series consists of 500 mb geopotential height data for the period 1946 through 1988. Bering Sea ice cover data was obtained from the western Arctic analyses of the Navy/NOAA Joint Ice Center. The ice cover time series is for the period 1953 through 1988.

The EOF method employed in this section uses the same procedures as those applied to the wind stress curl in chapter one and has been described previously. Cross spectral analysis and lagged cross correlations are used to describe interrelationships between the various

data sets. Unless stated otherwise, confidence limits of cross correlations are statistically significant at the 99% confidence level while power spectral estimates are statistically significant at the 95% level. The term "significant" will imply statistical significance at the level appropriate to the parameter in question. Time series plots of most of the variables are shown with a three year running mean curve superimposed on the anomaly series. Unless stated otherwise "running mean" will be taken to represent a three year running mean.

Analysis

Regional Interannual SST Variability

The North Pacific Ocean between 20°N and 60°N was divided into three regions of coherently fluctuating anomalies of SST based on the results of the cluster analysis of Iwasaka et al. [1988] (figure 2.1). The WNP and CNP regions are not significantly correlated with the ENP region although they are highly correlated with each other (table 2.1). The regional time series suggest there is a tendency for the ENP to fluctuate out of phase with the CNP and WNP regions although this relationship is not perfect. In the CNP region the three year running mean anomalies are strictly positive between 1955 and 1973 and strictly negative from 1975 through 1988 (figure 2.2a). A decreasing trend with an amplitude of nearly one degree in the running mean began in 1969 and ended in 1987. The power spectrum of the CNP series shows significant low frequency

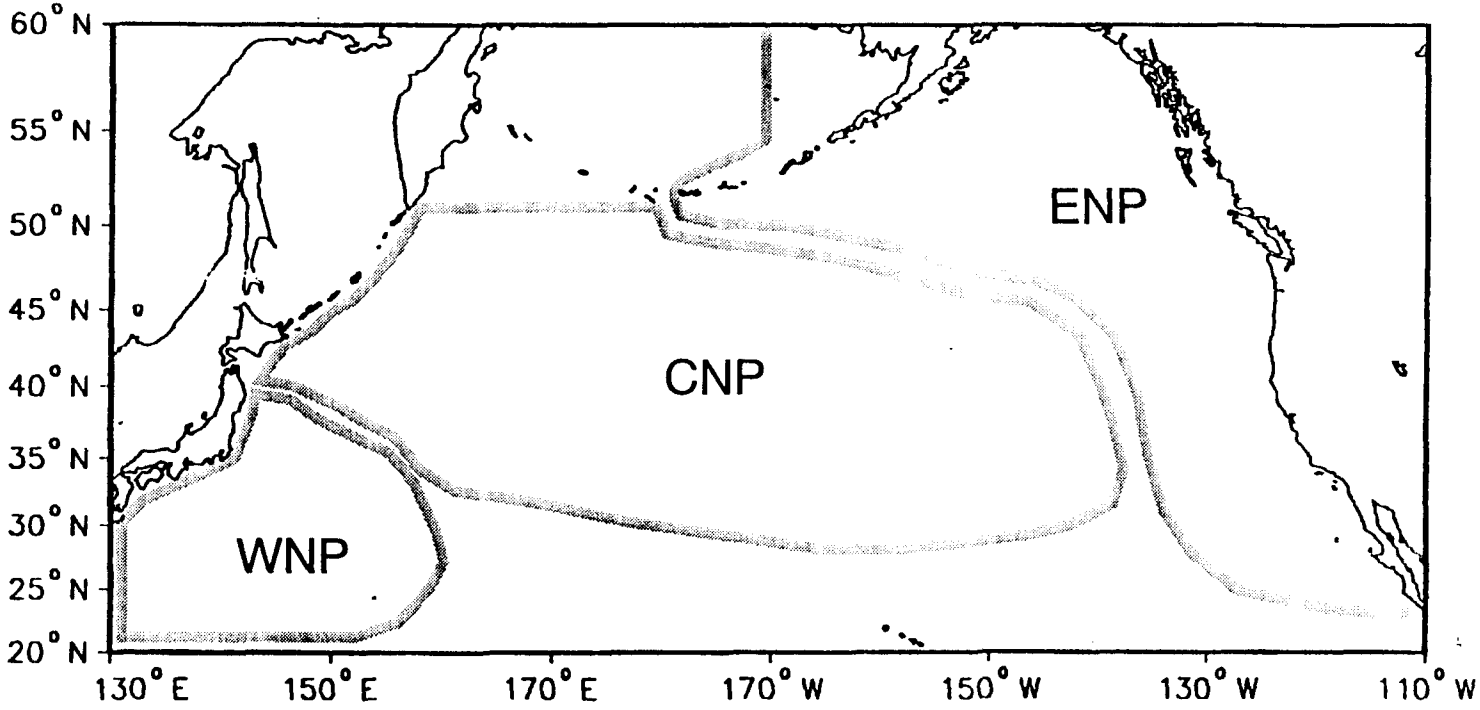

Figure 2.1 : Areas over which regional mean series of SST anomalies were computed.

	CNP	ENP	WNP
CNP	1.0	not signif.	0.86
ENP	--	1.0	not signif.
WNP	--	--	1.0

Table 2.1: Correlation matrix of regional SST series. Correlations are significant at the 99% level.

TAFs of nonseasonal SST EOFs	TAFs of nonseasonal wind stress curl EOFs: Mode 1	Mode 2	Mode 3	Mode 4
Mode 1	0.27	-0.27	-0.31	Not Signif.
Mode 2	Not Signif.	-0.18	0.18	Not Signif.
Mode 3	Not Signif.	0.17	Not Signif.	Not Signif.
Mode 4	0.14	-0.18	0.21	0.23

Table 2.2: Correlations among TAFs of nonseasonal SST and wind stress curl EOFs. Correlations are significant at the 99% level.

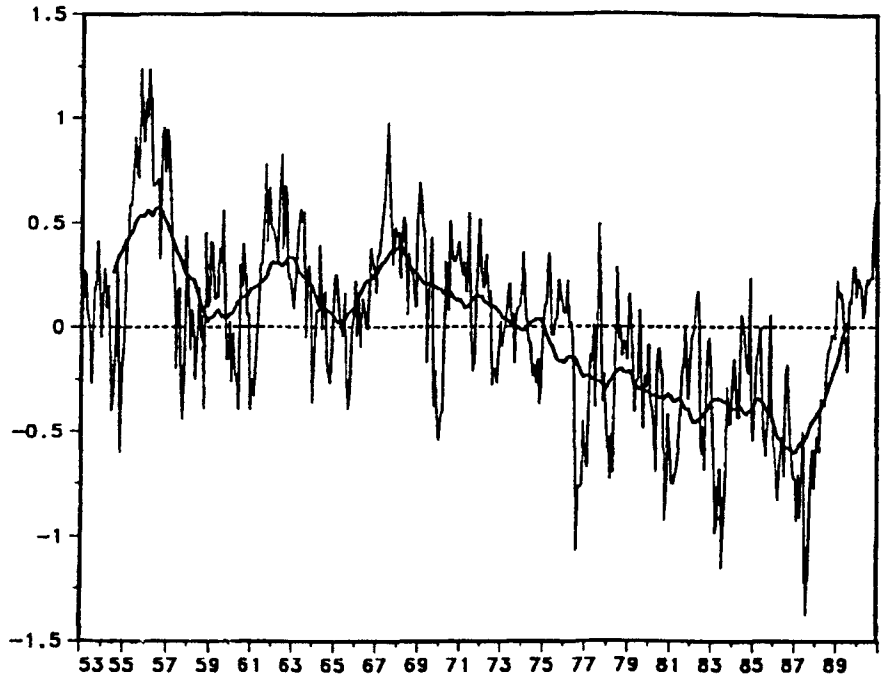

a)

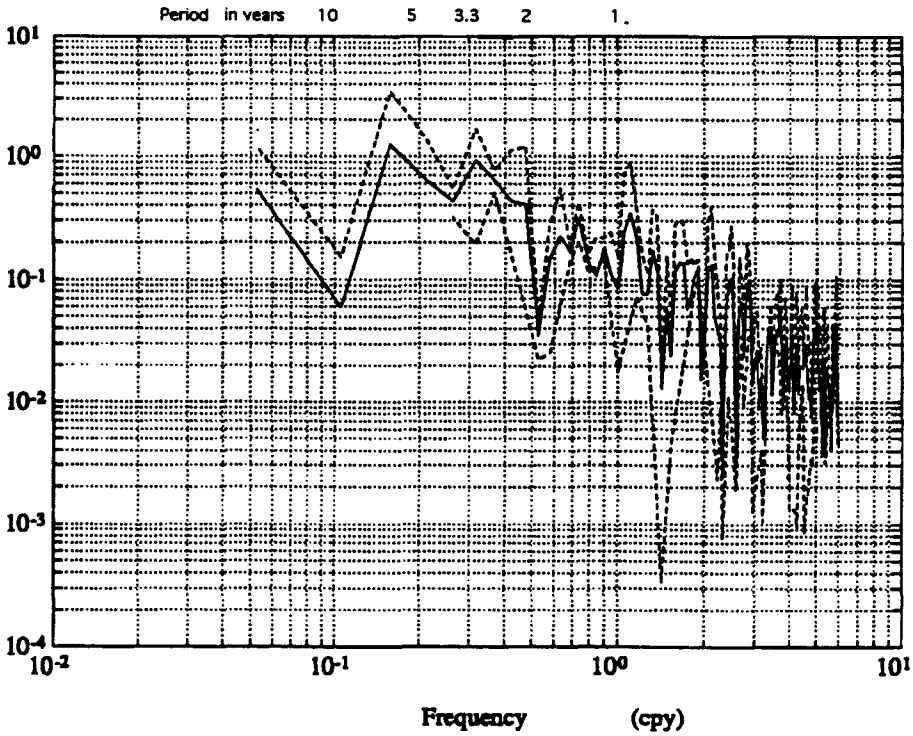

b)

Figure 2.2: a) Time series of CNP SST anomalies. Units are °C.
b) Power spectral density of CNP series.

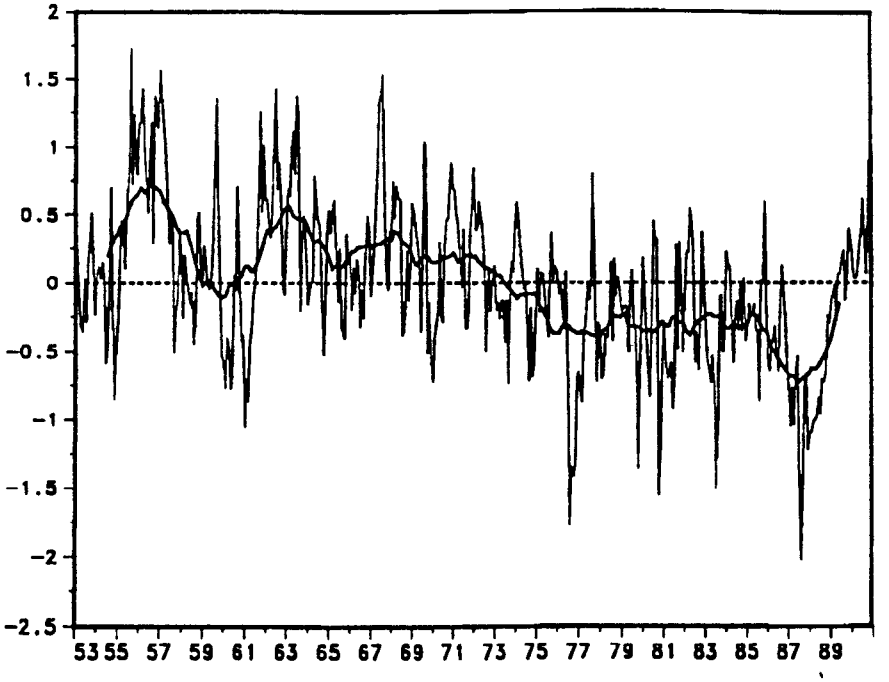

a)

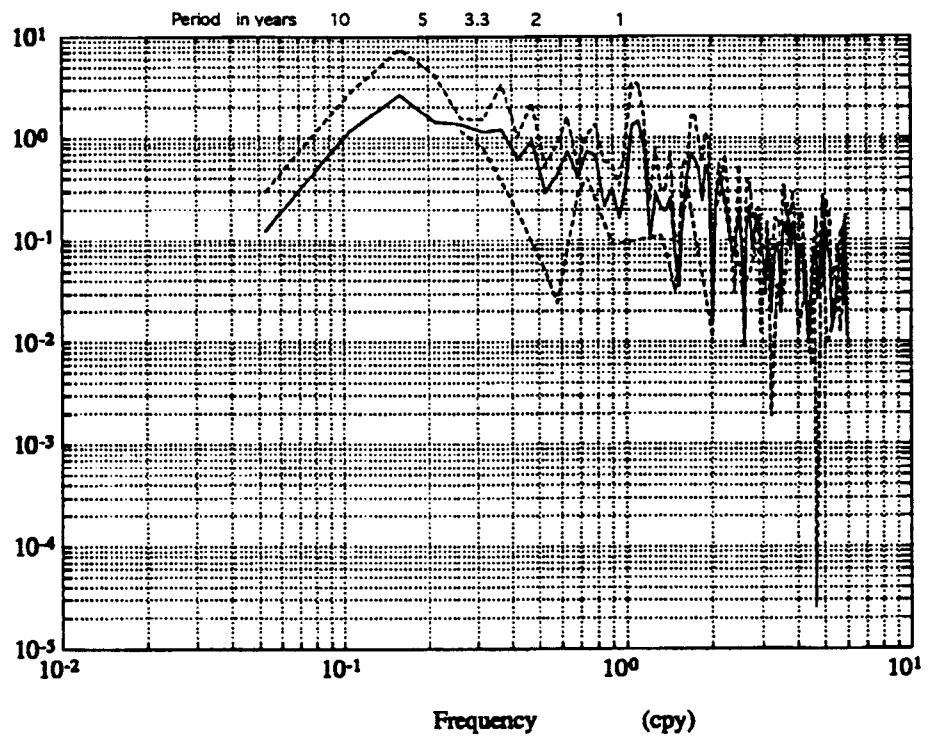

b)

Figure 2.3: a) Time series of WNP SST anomalies. Units are °C.
b) Power spectral density of WNP series.

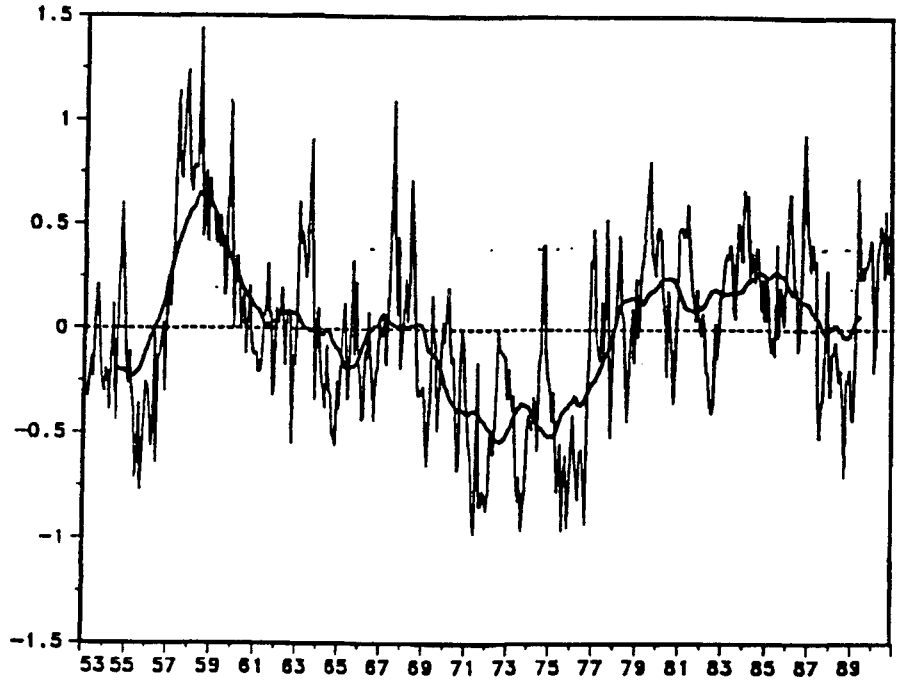

a)

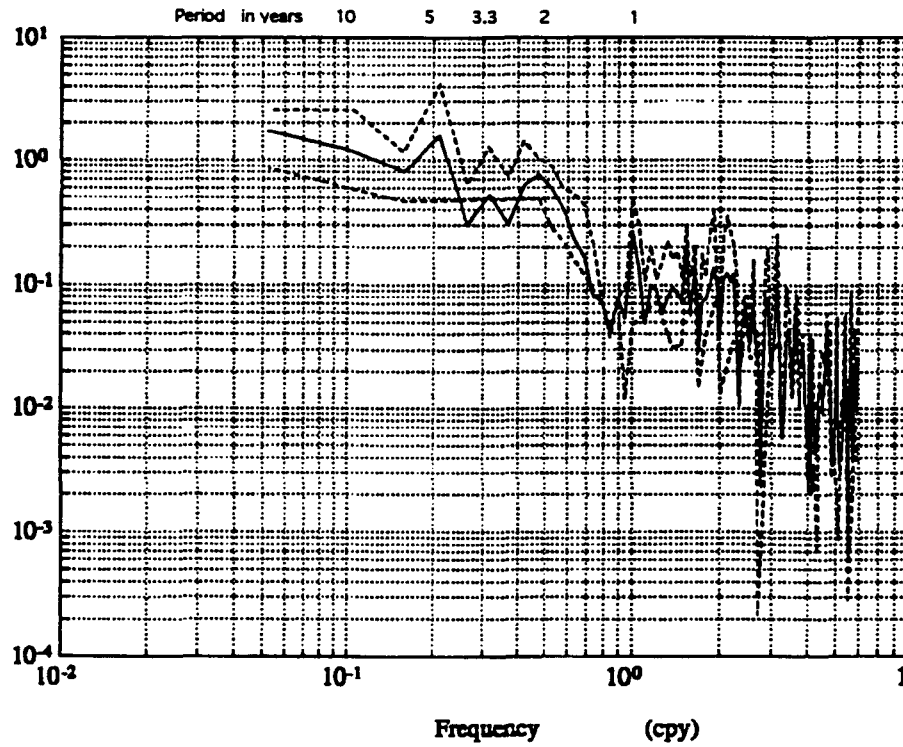

b)

Figure 2.4: a) Time series of ENP SST anomalies. Units are °C.
b) Power spectral density of ENP series.

(i.e. periods greater than 1.5 years) peaks at periods of 2.5 to 3 years and 6 to 7 years (figure 2.2b). The running mean of the WNP series shows the same pattern as the CNP except for the negative anomalies between 1959 and 1961 (figure 2.3a). There are no significant low frequency peaks in the power spectrum of the WNP series (figure 2.3b). The ENP series exhibits more oscillatory behavior than the CNP and WNP series in the sense that the sign of the running mean anomalies changes sign more often in the ENP series (figure 2.4a). Anomalously low ENP SST occurs from 1969 through 1977 and anomalously warm ENP SST occurs between 1979 and 1987. There are significant peaks in the ENP power spectrum at periods of 2 to 2.5 years and about 5 years (figure 2.4b).

EOF Analysis of North Pacific SST

The EOF method used for the analysis was described in chapter 1. The seasonal cycle was removed from the SST data in order to concentrate on interannual variability. The first four modes account for 49% of the nonseasonal variance of the SST field. EOF 1 explains 19% of the nonseasonal SST variability. The first eigenvector (figure 2.5a) shows that the Bering Sea, Gulf of Alaska, and and the eastern North Pacific east of about 135°W fluctuate in phase with each other and out of phase with most of the central and western North Pacific. Multiplication of the components of the TAF and the amplitudes of the eigenvector shows that the western and central North Pacific were anomalously warm from 1961 through 1975, and anomalously cold from 1977 through 1988, while the

anomalies were of opposite sign in the Bering Sea Gulf of Alaska and eastern North Pacific during these times. There are significant low frequency peaks in the power spectrum of the mode 1 TAF at periods of 3 years and 6 to 7 years (figure 2.5b). The mode 1 TAF (figure 2.5c) strongly resembles the time series of CNP SST and qualitatively suggests that they are related. Correlation coefficients between the mode 1 TAF and the CNP and ENP regions were found to be 0.90 and -0.51 respectively. These correlations occur at zero lag and explain 81% and 26% of the variance in the CNP and ENP regions respectively. These correlations further confirm the out of phase relationship between the CNP and ENP regions that is seen in the mode 1 eigenvector, and demonstrate that mode 1 fluctuations characterize variability in the CNP to a much greater extent than in the ENP region.

The first eigenvector shows the spatial pattern of SST variation that is characteristic of El Niño events [Weare et al., 1976, Iwasaka et al., 1987], although Wallace et al.[1990] note that the relationship between tropical and extratropical SST in this mode is not particularly strong. Therefore, while the first mode of nonseasonal SST variability is influenced by tropical Pacific variations, it appears that most of the variability occurring in this mode is determined by forcing that occurs outside of the tropical Pacific.

EOF 2 accounts for 12% of the nonseasonal variance. The mode 2 eigenvector shows the central North Pacific between about 25°N to 35°N and 160°E to 150°W to be out of phase with most of the rest of the extratropical North Pacific (figure 2.6a). This mode appears to represent a

largely meridional standing wave pattern. The highest amplitudes of this mode occur in the Gulf of Alaska and from 20°N to 25°N between 130°W and 110°W. The only significant low frequency peak in the power spectrum of the mode 2 TAF occurs at the 2 year period although there is energy concentrated near the 5 year period (figure 2.6b). The mode 2 TAF (figure 2.6c) qualitatively resembles the time series of ENP SST variability. This occurs because the entire ENP region is contained within the eastern region of the mode 2 eigenvector. Correlation coefficients between the mode 2 TAF and the CNP and ENP regions are 0.30 and 0.82 respectively, and are significant at the 95% and 99% levels respectively. Therefore mode 2 is representative of SST variations occurring in the ENP region and across the entire Pacific basin north of 40°N.

EOF 3 explains 10% of the nonseasonal variance. The mode 3 eigenvector represents zonal oscillations in the SST field (figure 2.7a). The spatial scales in the meridional direction span the basin between 20°N and 55°N. Maximum amplitudes of this mode occur off Japan between 40°N and 45°N, and in the central Pacific between 40°N and 45°N and 150°W to 160°W. The spatial maxima occur in regions of strong ocean-atmosphere heat fluxes as described by Terada and Hanzawa [1984] and Gyakum et al. [1989]. There is significant energy in the 2.5 to 3 year period band in the power spectrum of the mode 3 TAF, and there is energy concentrated near the 10 year period although it is not significant at the 95% confidence level (figure 2.7b).

EOF 4 explains 8% of the nonseasonal variance. Maximum amplitudes of the mode 4 eigenvector occur at about 35°N 175°E and 30°N

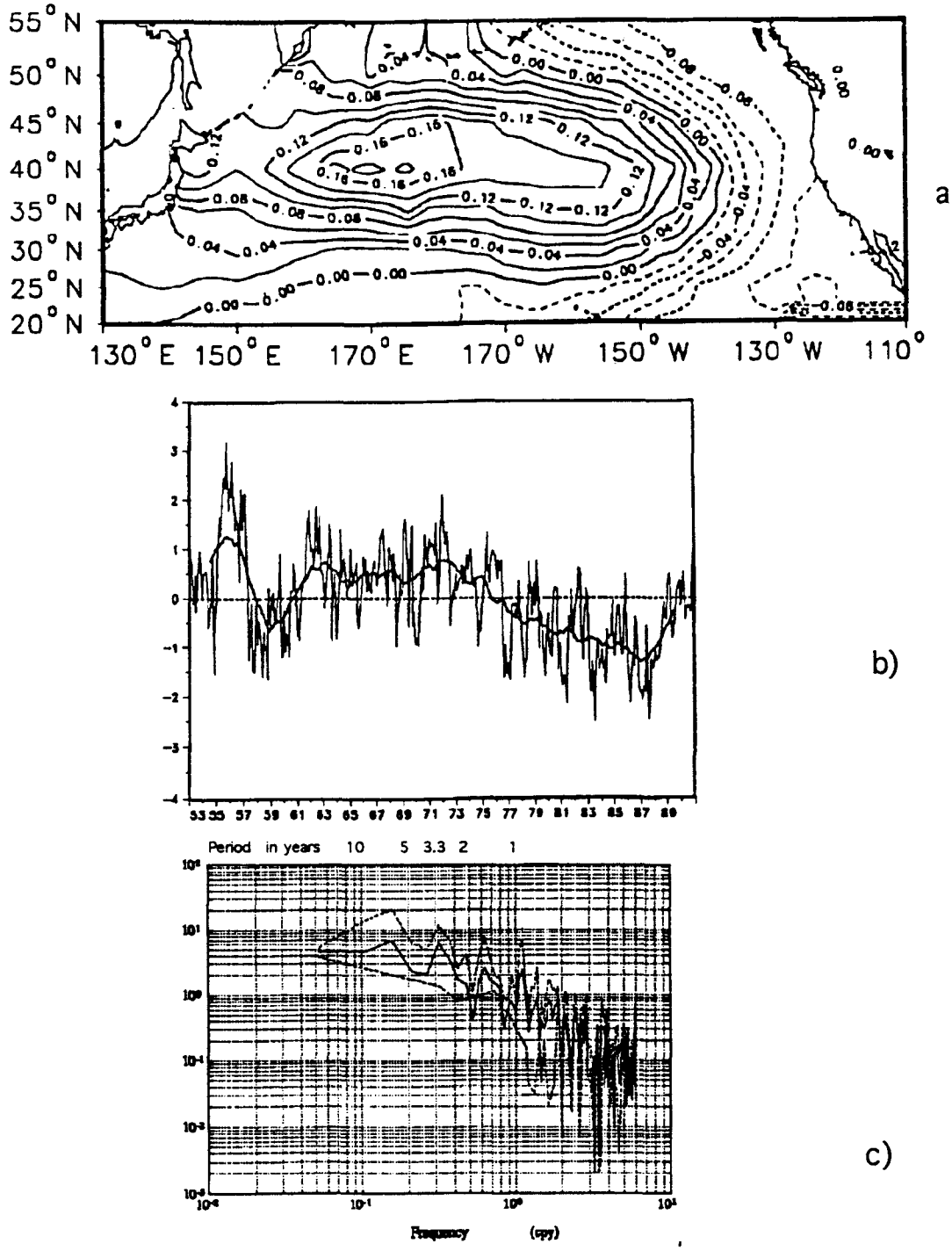

Figure 2.5: a) Mode 1 eigenvector of nonseasonal SST Units are dimensionless. b) Mode 1 TAF. Units are °C. c) Power spectrum of mode 1 TAF.

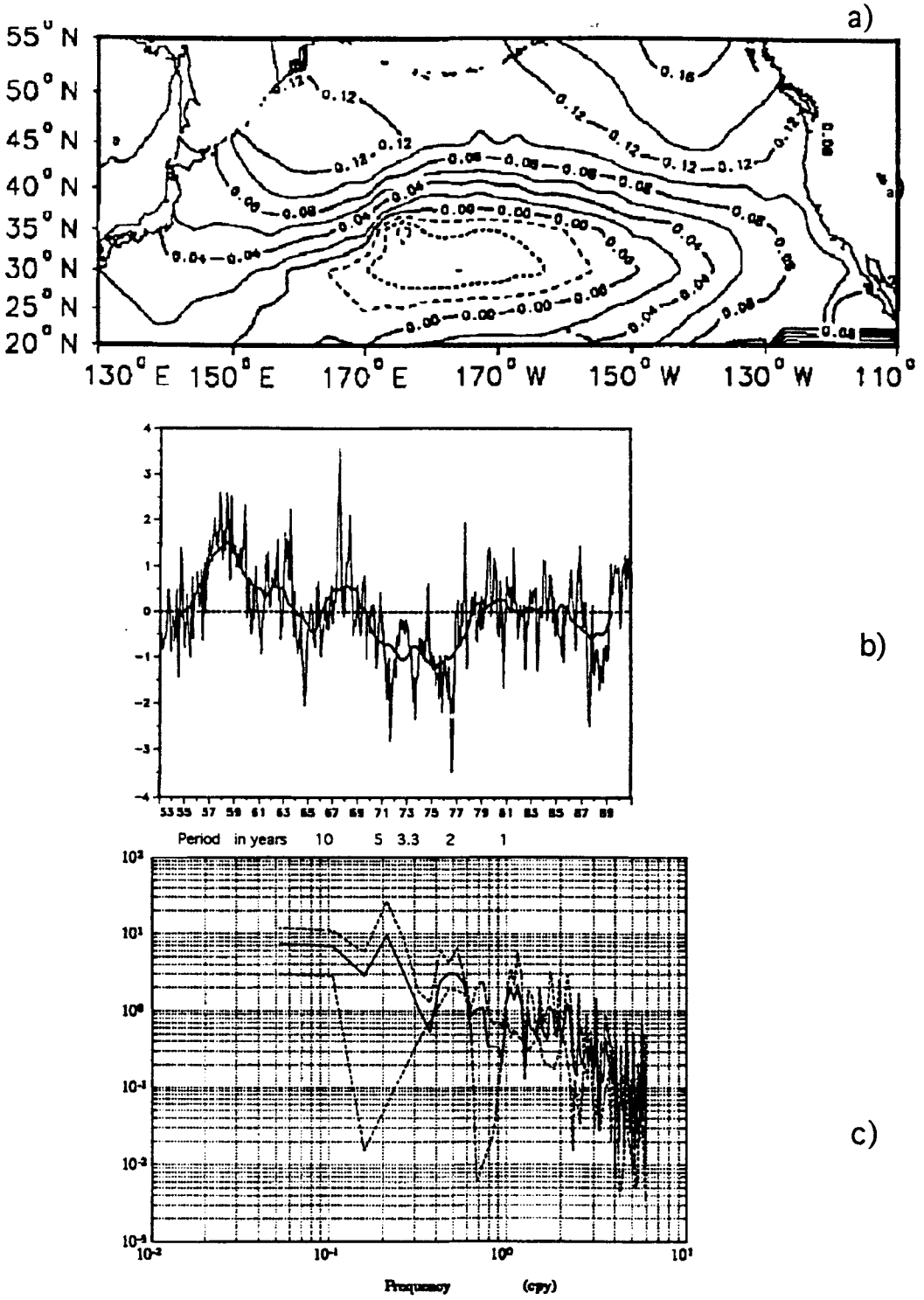

Figure 2.6: a) Mode 2 eigenvector of nonseasonal SST. CI =.02 dimensionless units. b) Mode 1 TAF. Units are °C. c) Power spectrum of mode 1 TAF.

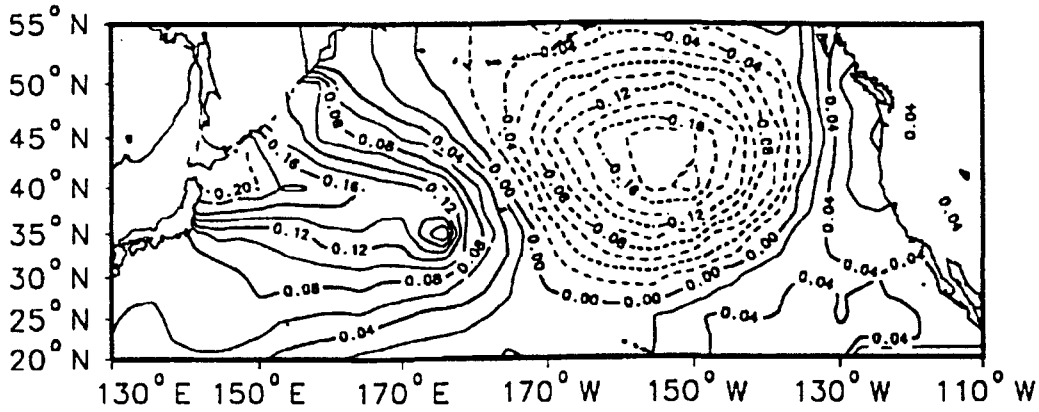

a)

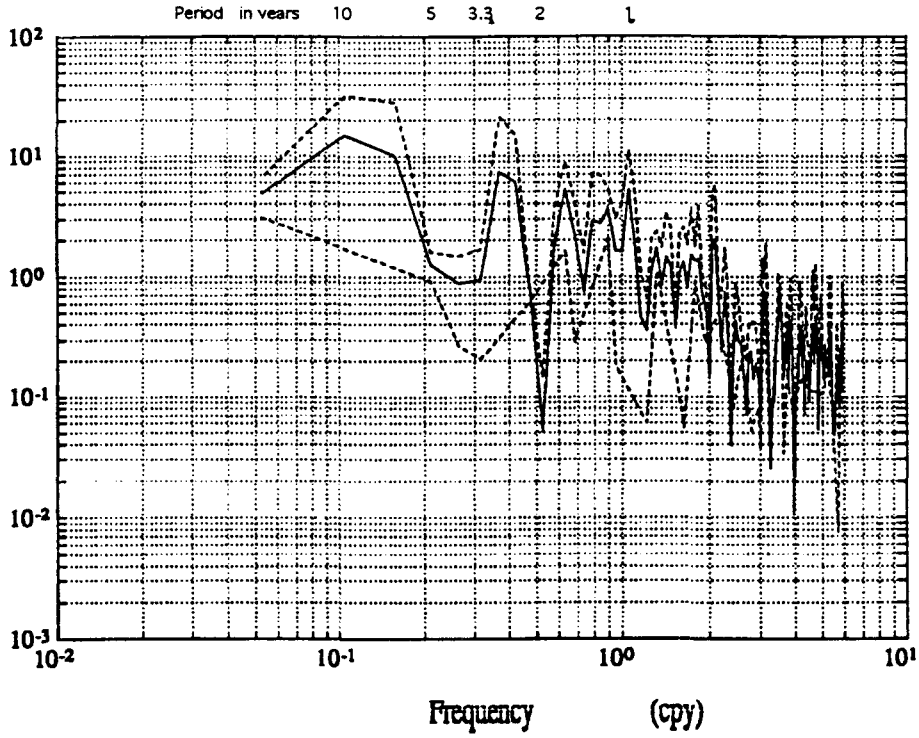

b)

Figure 2.7: a) Mode 3 eigenvector of SST. CI=0.02 dimensionless units. b) Power spectral density of the mode 3 TAF.

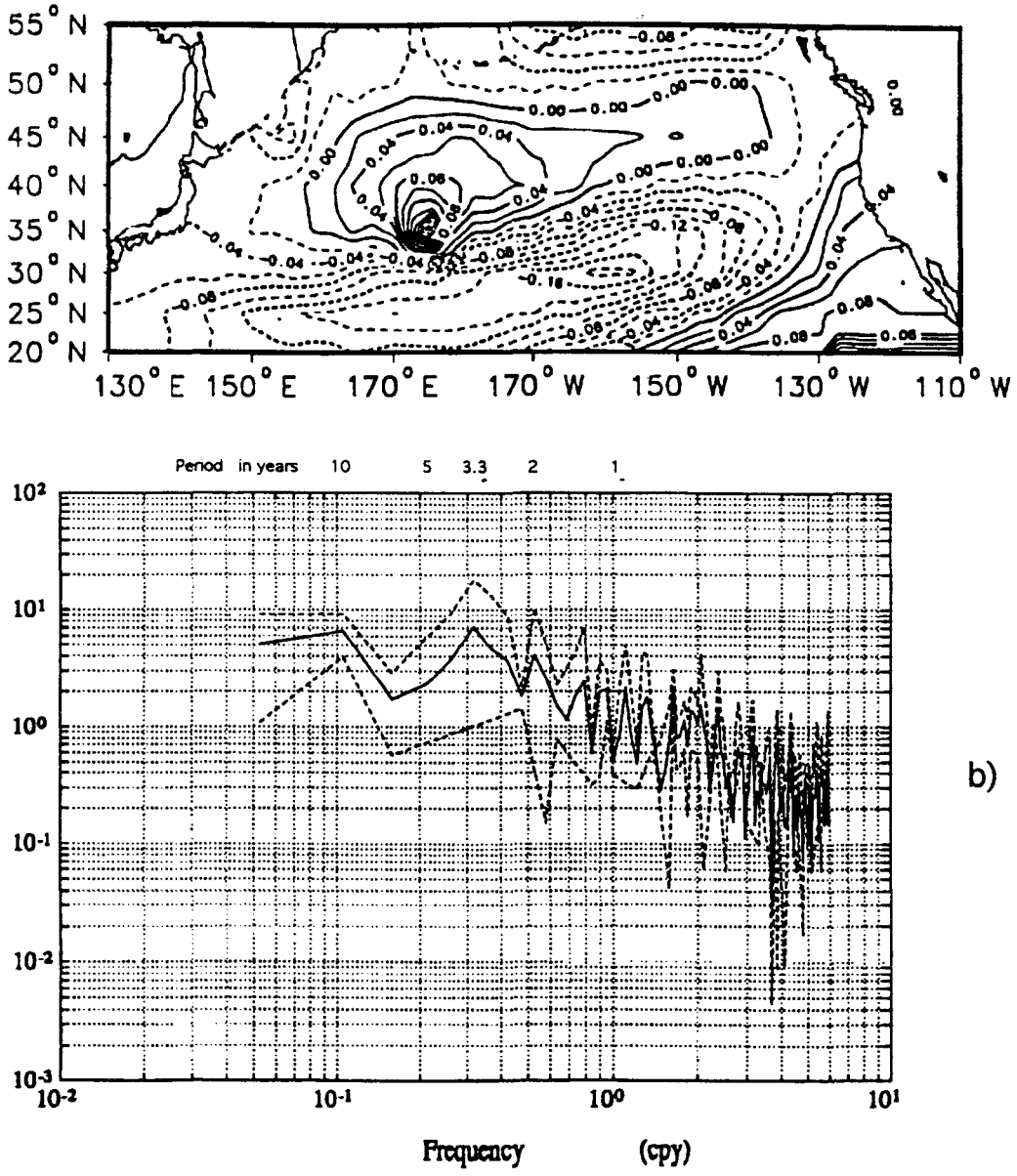

Figure 2.8: a) Mode 4 eigenvector of SST. CI=0.02 dimensionless units. b) Power spectral density of the mode 4 TAF.

160°W (figure 2.8a). The power spectrum of the mode 4 TAF shows a significant peak near the three year period (figure 2.8b).

The spatial patterns of EOFs 1 through 4 are qualitatively similar to those computed by Davis [1976], while only the first nonseasonal eigenvector of Weare et al. [1976] bears any strong resemblance to the eigenvectors computed in this study. Attention will be focused on nonseasonal modes 1 and 2 in this study since they represent variations with very large spatial scales, they account for the greatest amount of variance, and because they represent temporal variations corresponding to those in the CNP and ENP regions respectively.

Interrelationships between North Pacific Climate Variables

Relationships between the Large Scale Fields of Wind Stress Curl and SST

Running mean SST anomalies were strictly negative in the CNP region during 1976 through 1987. This is the same period during which running mean wind stress curl anomalies were strictly positive in the Aleutian Low region. Running mean SST anomalies in the ENP region were strictly positive during 1978-87. Similarly the smoothed curves show that negative curl anomalies within the weakened Aleutian Low from about 1960-1974 tend to coincide with strictly positive CNP and WNP SST running mean anomalies. Running mean SST anomalies in the ENP are often negative during this period, although the relationship is less evident than those between WNP and CNP SST and Aleutian Low wind stress

curl. The above relationships qualitatively suggest that Aleutian Low wind stress curl and North Pacific SST are strongly coupled, particularly on decadal time scales.

Temporal relationships between the large scale fields of SST and wind stress curl were determined using the regional time series of nonseasonal SST and curl anomalies and the TAFs of the dominant EOF modes of nonseasonal SST and wind stress curl variability. The cross correlation matrix of the TAFs (table 2.2) shows that fluctuations in wind stress curl consistently lead SST variations by one month. Figure 2.9 is characteristic of the plots with which lead-lag relationships were determined. Significant correlations with curl leading SST by one month occur in all four nonseasonal SST modes. The magnitudes of the correlation coefficients are generally small (but statistically significant) and in all cases account for less than 10% of the between field variance. Similarly, lagged cross correlations between regional wind stress curl and SST TAFs consistently indicate that variations in wind stress curl lead SST fluctuations by one month. Again the correlation coefficients are small and explain less than 15% of the variance between the respective fields (table 2.3).

The strongest correlations between regional North Pacific wind stress curl and SST occur between the curl of the Aleutian Low region and the WNP respectively. Correlation coefficients between WNP and CNP SST and Aleutian Low wind stress curl are larger than the correlation between ENP SST and Aleutian Low curl by a factor of more than two. These correlations suggest that the WNP and CNP regions are more

closely coupled to wind stress curl variability than is the ENP region. Eastern boundary effects such as coastal currents and trapped wave motions probably act to decrease the correlations between the regional SST and wind stress curl fields.

The low correlations between the fields of wind stress curl and SST are somewhat surprising in light of the fact that North Pacific SLP variations and geopotential height fluctuations at 500 mb and 700 mb tend to be strongly correlated to variations in the SST field (e.g. Douglas et al., 1982, Kawamura, 1984, Iwasaka et al, 1987, Namias et al, 1988, Wallace et al., 1990). Also, the smoothed curves of central and western Pacific SST, eastern Pacific SST, and Aleutian Low wind stress curl qualitatively suggested that the relationships between fluctuations in SST and curl are significant on longer time scales. In order to characterize and quantify the relationships that occur between curl and SST on time scales of years, the data were low pass filtered with a sixth order Butterworth filter with a cutoff period of 25 months. Hereafter, "low pass filtered" will be taken to mean that the data in question were filtered with the same filter as described above. The relationship between the low pass filtered Aleutian Low wind stress curl and SST in the CNP and WNP regions is much stronger than that obtained from the unsmoothed anomaly fields (table 2.4). The correlations now explain 43% and 49% of the between field variance between curl and CNP and WNP SST respectively, as compared to only 13% and 14% with the unfiltered data. The relationship between the low pass filtered Aleutian Low curl and ENP SST, as well as that between ENP SST and wind stress curl over the same region as the ENP,

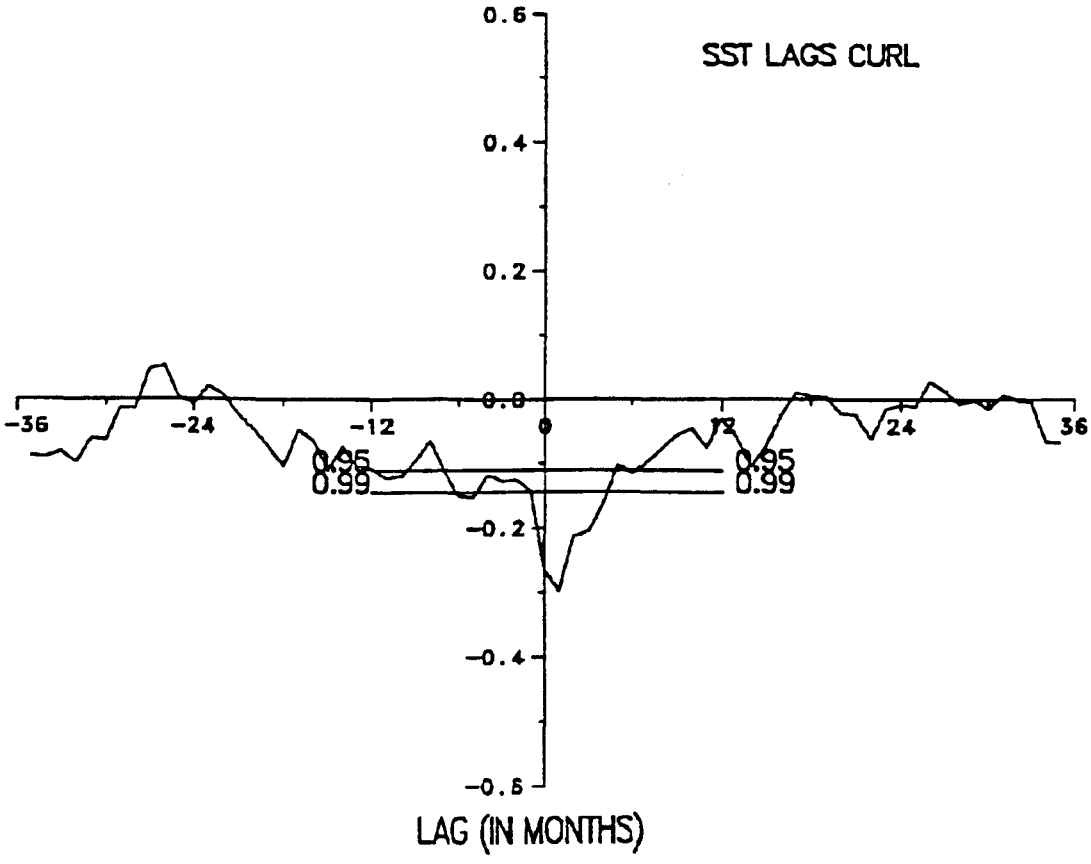

Figure 2.9: Correlation between wind stress curl and SST. This chart illustrates the lead-lag relationship found between both regional and TAF series of curl and SST.

	Aleutian Low curl	GOA curl	Bering curl	East Pacific High curl	Western Pacific curl
Mode 1	-0.32	Not Signif.	-0.20	Not Signif.	Not Signif.
Mode 2	-0.15	-0.16	Not Signif.	0.26	Not Signif.
Mode 3	0.19	0.25	Not Signif.	-0.12	0.14
Mode 4	0.20	Not Signif.	Not Signif.	0.32	Not Signif.

Table 2.3: Correlations among series of regional wind stress curl and nonseasonal SST EOF modes. Correlations are significant at the 99% confidence level.

	Aleutian Low Curl
WNP	-0.70
CNP	-0.66
ENP	0.25

Table 2.4: Correlations between lowpass filtered regional SST and Aleutian Lowwind stress curl. Correlations are significant at the 99% level.

	ENP SST	SST 25 N 125 W	SST 55 N 150 W
ENP SST	1.0	--	--
SST 25N 125W	0.72	1.0	--
SST 55N 150W	0.88	0.53	1.0

Table 2.5: Correlation matrix of lowpass filtered ENP SST series and representative points in ENP region.

remain nearly as weak as that obtained from the unfiltered fields. Each of these correlations accounts for only about 5% of the between field variance.

The high negative correlations between the low pass filtered WNP SST, CNP SST, and Aleutian Low wind stress curl quantitatively show that these fields are strongly coupled on time scales of years. The tendency for wind stress curl variations to lead changes in SST, coupled with the fact that the correlations account for nearly 50% of the variance on long time scales, suggests that for CNP and WNP SST variability, the atmospheric variability in the Aleutian Low region largely drives changes in the SST field. Therefore on time scales of years, the direct and indirect effects of wind stress curl forcing in the Aleutian Low region play a significant role, and possibly the most important role, in accounting for SST variability across much of the central and western North Pacific. In particular the diminished Aleutian Low of 1961-68 and 1970-75, and the intensified Aleutian Low that occurred during 1976-87 are partly responsible for the production of positive and negative SST anomalies respectively in the CNP and WNP regions during these periods.

ENP SST variability appears to be less strongly coupled to wind stress curl, although during the period 1977-88 wind stress curl and ENP SST tend to fluctuate in concert. The low correlations between ENP SST and regional wind stress curl suggest that processes associated with the eastern boundary region of the North Pacific might be important in modulating ENP SST variability.

Mechanisms of Interaction between SST and Wind Stress Curl

There are several possible mechanisms through which positive curl anomalies in an intensified Aleutian Low might force negative SST anomalies in the central and western North Pacific. The strongest relationships occur on time scales of years and represent the integrated long term effects of the forcing mechanisms. Therefore it is not possible to determine which of these effects are most important in forcing SST variations, probably a number of them contribute to the observed variability. Negative SST anomalies could be directly forced by vertical and horizontal advective effects in the ocean. Increased mid-ocean Ekman upwelling (Ekman suction) of cold thermocline waters in response to increased cyclone activity is a feasible mechanism for the vertical advection and maintenance of negative SST anomalies, as is the mechanism of increased mixing due to increased cyclone activity as noted by White et al. [1980]. Similarly negative anomalies would be horizontally advected due to increased southward transport in the boundary currents of the western subarctic Pacific in response to intensified cyclonic atmospheric circulation over the Bering Sea. Atmospheric mechanisms that could generate negative CNP and WNP SST anomalies in response to positive curl anomalies include the effects of increased ocean-atmosphere heat fluxes in relation to increased cyclone activity and increased surface cooling due to enhanced northerly winds associated with increased storm activity. The latter mechanism is cited by Trenberth [1990] as an important factor in causing decadal scale negative SST anomalies in the

central and western North Pacific. Ultimately all of the above mechanisms of SST variation are forced via an atmospheric link, in particular wind stress curl variability associated with changes in the strength and position of the Aleutian Low.

Negative curl anomalies associated with a weakened Aleutian Low are also consistent with the above mechanisms of SST variability. On decadal time scales, negative wind stress curl anomalies would suppress or reverse mid-ocean Ekman upwelling which would decrease the flux of relatively cold thermocline waters into the surface ocean. The long term effects of decreased storm activity would result in decreased ocean-atmosphere heat fluxes and decreased surface mixing, allowing for more heat to be stored in the surface ocean, resulting in positive SST anomalies. Negative curl anomalies would also decrease surface cooling as the winds weaken and cease to have a strong northerly component. A decrease in the Sverdrup transport in the western subarctic boundary current would also occur as a result of decreased poleward transports in the interior subarctic circulation. Therefore these proposed mechanisms of interaction between SST and wind stress curl are consistent with the interpretation of Aleutian Low wind stress curl variability as a primary factor in determining decadal scale SST variations in the CNP and WNP regions. However, the mechanisms cited above do not appear to be as applicable to SST variations in the ENP region, where an alternate explanation of long term SST variability appears to be warranted.

Implications of Decadal Scale Wind Stress Curl and SST Variability

Royer [1989] shows that SST variations in the northeastern North Pacific are characterized by low frequency fluctuations with a period of 20 to 30 years, and states that this low frequency fluctuation is not evident at latitudes south of 55°N. Royer believes that the rise in SST in the Northeast Pacific that occurred during the late 1970's and into the late 1980's is a part of this long period oscillation. Royer [1989] predicts that below normal water temperatures should occur in the northeastern North Pacific during the next 5 to 15 years (i.e. after 1989).

The first mode eigenvector of nonseasonal SST (figure 2.5a), and time series of SST anomalies and running means at individual gridpoints in the ENP region qualitatively suggest that the fluctuations described by Royer [1989] might be part of a more general and larger scale pattern of variability that occurs in the ENP between 20°N and 55°N and might extend into the eastern tropical South Pacific as far as 20°S (cf. fig. 7 in Weare et al., 1976). The low frequency pattern of temporal SST variation at 55°N and north of 55°N observed by Royer [1989] is very similar to the running mean patterns that occur between 20°N and 30°N in the ENP (figure 2.10). The patterns of variation of running mean ENP SST between 35°N and 50°N are similar to those observed at higher and lower latitudes except that the amplitudes are smaller between 35°N-50°N than they are at 55°N and from 20°N to 30°N. Correlations between low pass filtered ENP SST and individual gridpoints in the ENP from 20°N to 55°N show that the ENP time series is representative of the SST series for the ENP region

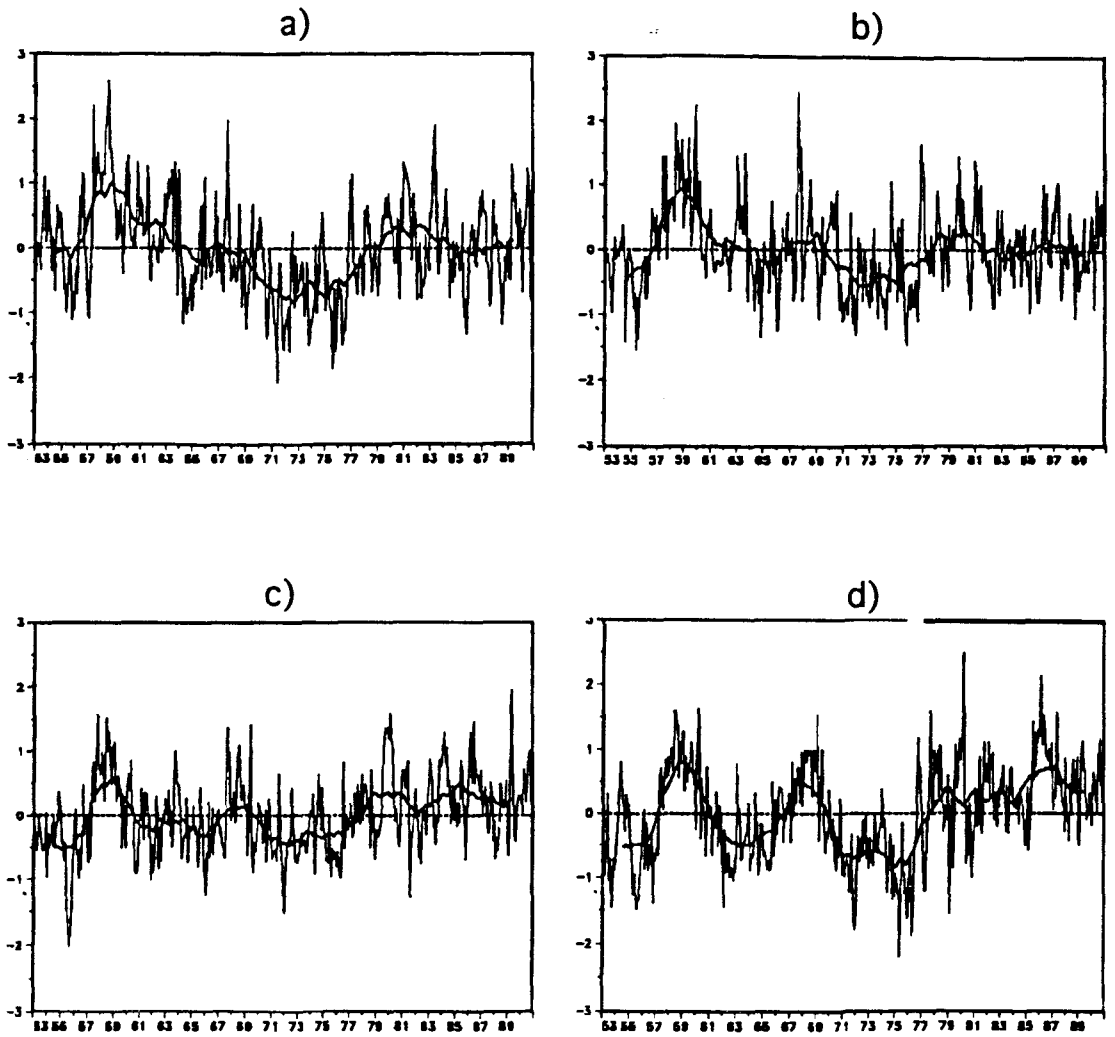

Figure 2.10: Anomalies of SST at representative points in the ENP region.
a) 50°N 130°W b) 40°N 130°W c) 30°N 130°W d) 20°N 130°W.
Units are °C.

(table 2.5). It appears that the SST fluctuations described by Royer are at least in part related to more general temporal variations in the ENP region.

The hypothesized large scale low frequency variation of SST in the ENP region provide a partial explanation for the low correlations between regional wind stress curl and ENP SST. It appears that long term ENP SST variability occurs at least in part on very large spatial scales that may extend from the subtropical South Pacific to the high latitude North Pacific. Therefore the anomalously warm ENP SST observed during 1978-87, while occurring in conjunction with an intensified Aleutian Low, was partly forced by atmospheric or oceanic conditions occurring external to the region influenced by the Aleutian Low.

In chapter 1 it was suggested that the change in sign of the Aleutian Low running mean wind stress curl anomaly from positive to negative during 1988 signaled the end of the intense Aleutian Low that had persisted from 1976 through 1987. During 1987 a trend toward negative anomalies began in the running mean that continued through the end of the record. During 1987 the cooling trend observed in central North Pacific SST since 1969 reversed, and running mean SST anomalies began and continued to rise through the end of the record. This reversal of the CNP SST trend appears to be the result of the concurrent weakening of the Aleutian Low. Finally, ENP SST fluctuations tend to be out of phase with variations in CNP SST, especially on long time scales. In particular, strictly positive running mean ENP SST anomalies occurred concurrently with strictly negative CNP SST anomalies during 1976-87. Therefore the

apparent warming trend in CNP SST and the weakening of the Aleutian Low that began during 1987 are likely to occur concurrently with a cooling trend in ENP SST on time scales of years. Therefore the results of this study suggest that Royer is correct in predicting a cooling in northeastern North Pacific SST over the next 5 to 15 years. It is also suggested that the cooling will not be restricted to the high latitude North Pacific, but will occur over much of the ENP region. It is also suggested that on time scales of years the cooling in the ENP region will occur concurrently with a weakening of the Aleutian Low and a warming of SST in the CNP and WNP regions.

Interannual Variability of Wind Stress Curl, SST and Subarctic Air Temperatures

Intensified cyclone activity in the Aleutian Low during 1976-88 occurs in conjunction with large scale changes in regional SST. It is of interest to determine the relationships between winds, SST and air temperatures on time scales of years. Running mean air temperature anomalies at Sitka (57°N 135°W) in the northeastern Gulf of Alaska and at St. Paul (55°N 170°W) in the eastern Bering Sea were strictly positive during 1976-89 and 1978-89 respectively, and strictly negative during 1964-75 and 1969-77 respectively (figure 2.11). The period of anomalously warm air temperatures is coincident with the time period of the intensified Aleutian Low and with positive low frequency ENP SST anomalies, while anomalously low air temperatures correspond closely to periods of a

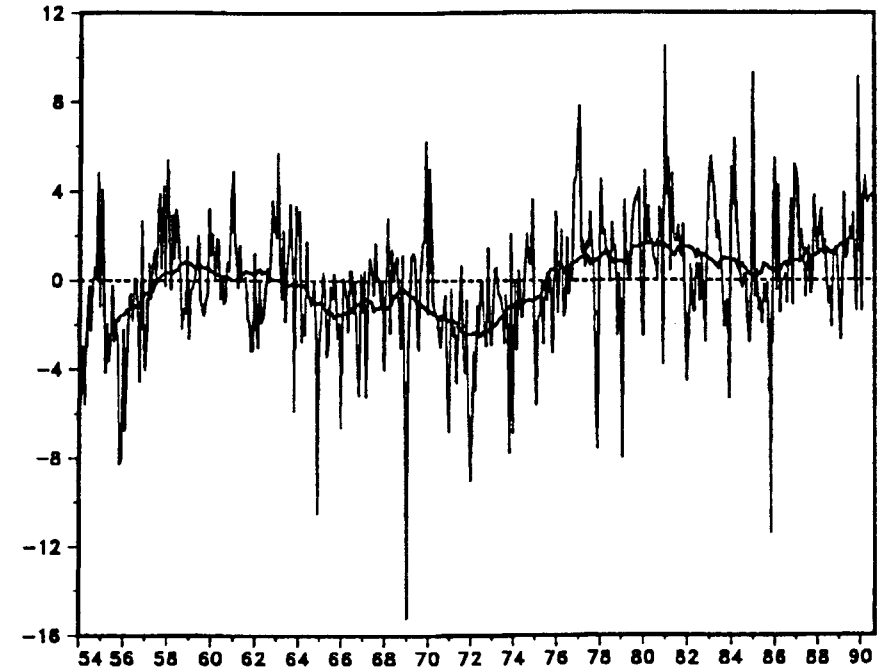

a)

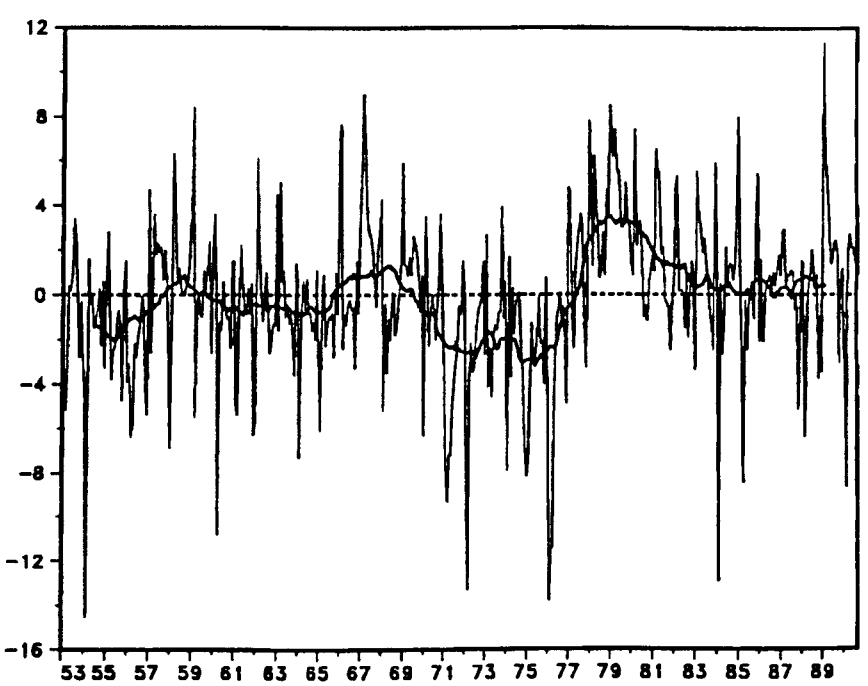

b)

Figure 2.11: a) Anomalies of Sitka air temperature.
b) Anomalies of St. Paul air temperature. Units are °C.

weakened Aleutian Low and anomalously low ENP SST. These observations qualitatively suggest that wind stress curl, SST, and air temperatures are closely coupled on long time scales.

Air temperature variations at Sitka and St. Paul are positively correlated with each other and show that there is a weak tendency for changes in air temperature at St. Paul to lead those at Sitka by about one month. This might be an effect of the generally eastward passage of cyclones through these regions. Air temperature anomalies at Sitka and St. Paul are positively correlated with SST variations in the ENP region and with regional wind stress curl (table 2.6). Changes in air temperature and SST occur at zero lag in the Gulf of Alaska, while air temperature variations lead changes in SST by about one month in the eastern Bering Sea. These correlations explain 12% and 17% of the between field variances in the Bering Sea and Gulf of Alaska respectively. Maximum correlations between air temperature and wind stress curl occur at zero lag in the Bering Sea and Gulf of Alaska, and explain 14% and 18% of the variance respectively.

The correlations between the low pass filtered data sets are stronger than those between the unfiltered data and quantitatively demonstrate that wind stress curl, SST, and air temperatures in the Aleutian Low region are closely coupled on time scales of years (table 2.7). Fluctuations in Sitka and St. Paul temperatures are correlated to each other 25% of the time on time scales of years. The correlations between air temperature and SST explain 38% and 39% of the variance between these fields in the Bering Sea and Gulf of Alaska respectively. Correlations between air temperature

	Sitka Air Temp.	St. Paul Air Temp.	ENP SST	Aleut. Low Curl
Sitka Air Temp.	1.0	--	--	--
St. Paul Air Temp.	0.18	1.0	--	--
ENP SST	0.42	0.36	1.0	--
Aleut. Low Curl	0.43	Not Signif.	Not Signif.	1.0

Table 2.6: Correlation matrix of subarctic air temperatures, ENP SST and Aleutian Low wind stress curl. Correlations are significant at the 99% confidence level.

	Sitka Air Temp.	St. Paul Air Temp.	ENP SST	Aleut. Low Curl
Sitka Air Temp.	1.0	--	--	--
St. Paul Air Temp.	0.50	1.0	--	--
ENP SST	0.63	0.62	1.0	--
Aleut. Low Curl	0.61	0.35	0.25	1.0

Table 2.7: Correlation matrix of lowpass filtered subarctic air temperatures, ENP SST and Aleutian Low wind stress curl. Correlations are significant at the 99% confidence level.

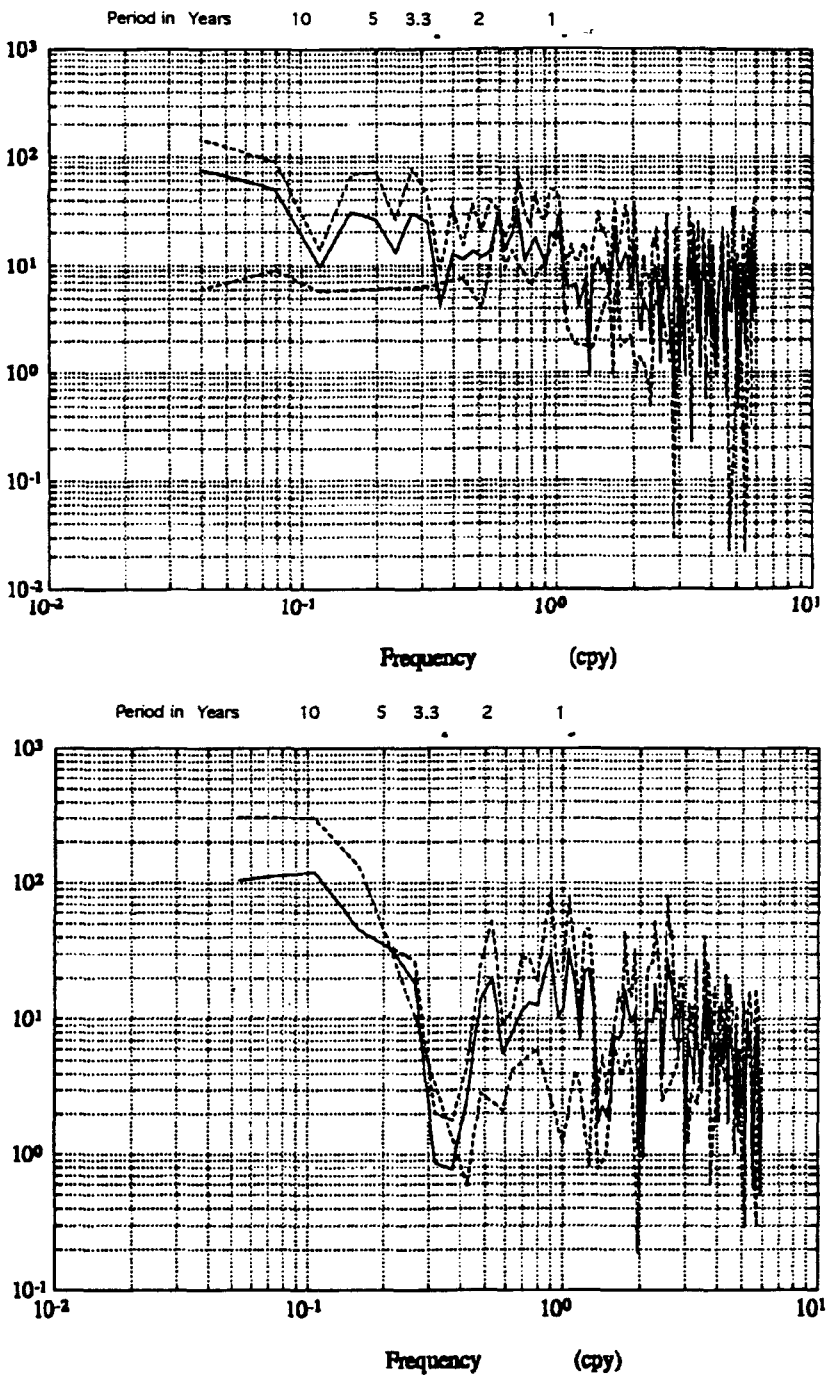

Figure 2.12: a) Power spectral density of Sitka air temperature.
b) Power spectral density of St. Paul air temperature.

and regional wind stress curl explain 38% and 37% of the variance in the Bering Sea and Gulf of Alaska respectively. Significant peaks appear in the power spectrum of Sitka air temperatures at periods of about 3.5 and 6 to 7 years (figure 2.12a). These time scales are very close to those observed in the power spectrum of Gulf of Alaska wind stress curl. The only significant peak in the spectrum of St. Paul air temperatures occurs at the 1.6 to 2 year period (figure 2.12b). A peak at the 2 year period also occurs in the Bering Sea wind stress curl power spectrum (figure 1.27b). The overlap of the air temperature spectral peaks with those of the regional wind stress curl and the strong correlations between these fields on time scales of years shows that anomalously warm air temperatures in the Gulf of Alaska and Bering Sea are associated with long period increases in storm activity, while negative air temperature anomalies correspond to periods of weakened circulation in the Aleutian Low.

Relationships Between Wind Stress Curl and Sea Ice Cover

Running mean anomalies of Bering Sea ice cover were strictly negative from 1978 through 1986, and strictly positive from during 1971-77 (figure 2.13a). Since the periods of negative and positive anomalies correspond closely to periods of strengthened and diminished circulation in the Aleutian Low, this qualitatively suggests that variations in Bering Sea ice cover are closely related to the strength of the Aleutian Low on time scales of years. Wind stress curl anomalies over the Bering Sea are negatively correlated with fluctuations in the sea ice cover. Fluctuations

in wind stress curl lead those in ice cover by about one month (figure 2.14). Positive curl anomalies over the Bering Sea are associated with intensified cyclone activity, warm south winds, and positive air temperature anomalies which force the Bering Sea ice cover to decrease, particularly during 1977-88. Negative wind stress curl anomalies are associated with anticyclones, cold northeast winds, and low air temperature anomalies that promote the southward advance of the ice cover. These conditions occurred during the mid 1950's, early 1960's and from about 1969-77. The coupling between wind stress curl, air temperature, and ice cover is stronger during 1977-88 than it is during the 1953-77 period.

Correlations between the low pass filtered series of Bering Sea ice cover and regional wind stress curl explain 28% of the between field variance. Also, significant low frequency peaks appear in the power spectrum of Bering Sea ice cover at periods of about 2, 4, and 10 years (figure 2.13b). Peaks with periods very close to those in the spectrum of Bering Sea ice cover also occur in the spectrum of Bering Sea wind stress curl, suggesting the importance of the strength of the Aleutian Low in forcing interannual variations in ice cover. Finally, 58% of the variance can be explained between the low pass filtered ice cover series and that of eastern Bering Sea air temperatures. This again suggests that on long time scales the integrated effects of intensified or diminished cyclone activity in the Bering Sea play an important role in governing long term variations in the ice cover of this region. The results concerning Aleutian Low wind stress curl and Bering Sea ice cover are consistent with those of Overland and Pease [1982] who show that south winds associated with the

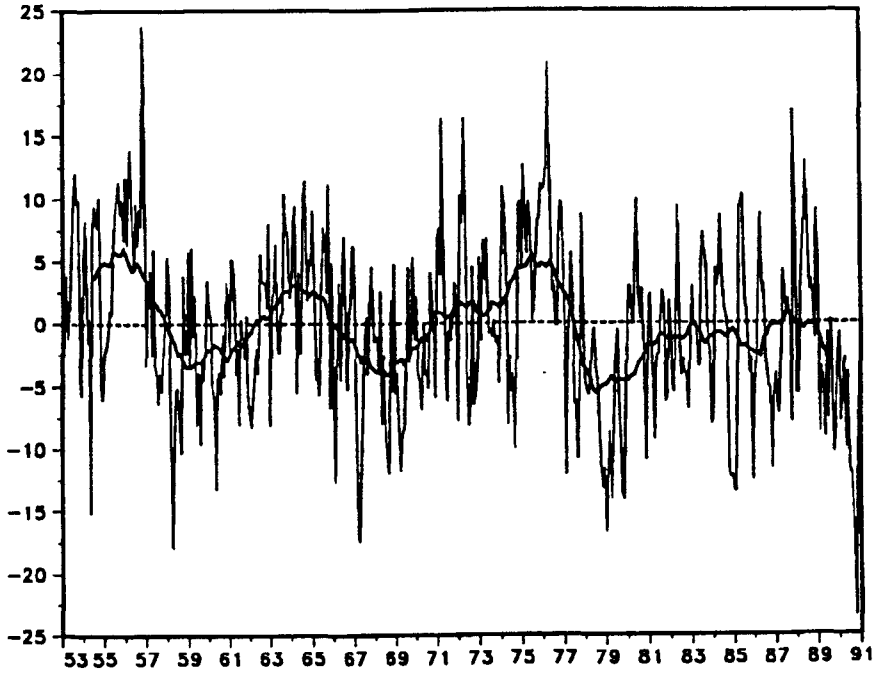

a)

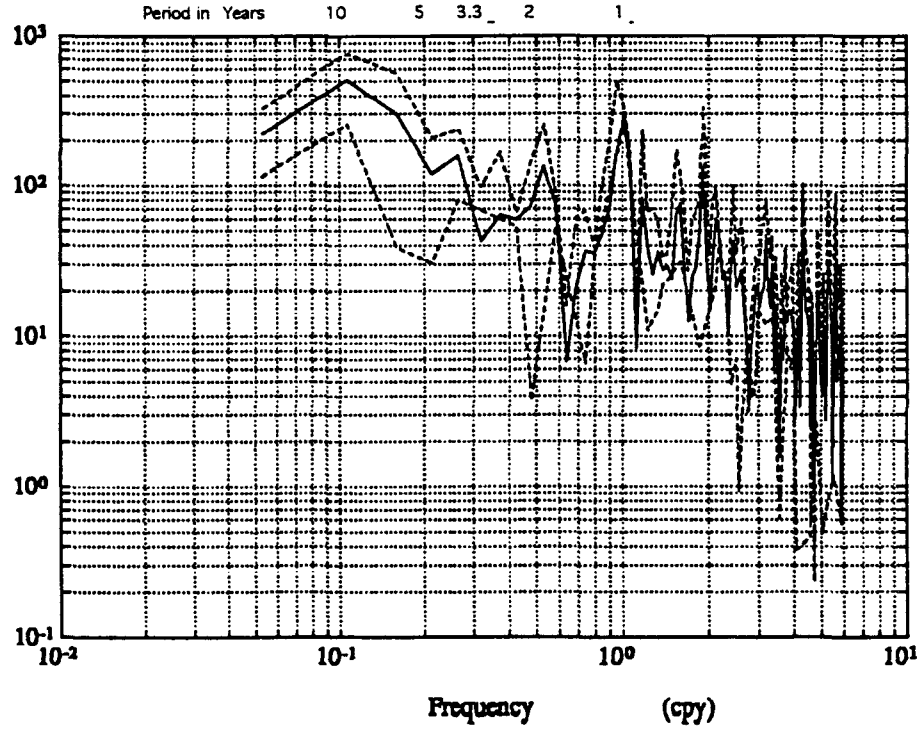

b)

Figure 2.13: a) Time series of Bering Sea ice cover anomalies. Units are dimensionless. b) Power spectrum of Bering Ice series.

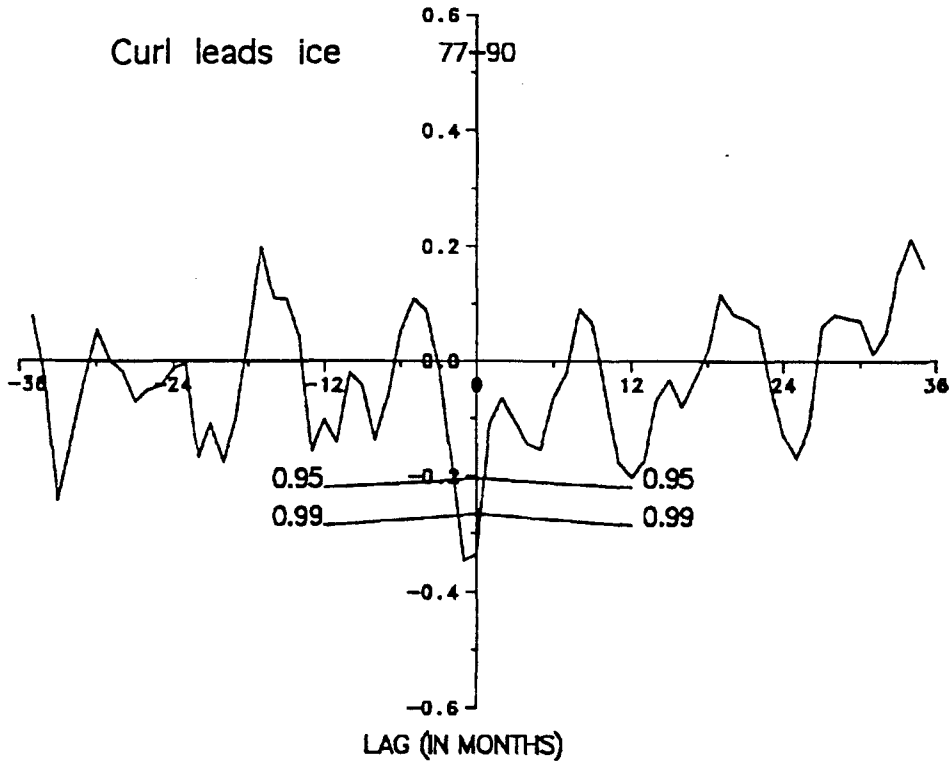

Figure 2.14: Correlation between Bering Sea ice cover and wind stress curl. This chart illustrates the lead-lag relationship found between both regional and TAF series of curl and SST.

westward displacement of cyclone tracks over the Bering Sea tend to inhibit ice advance in the eastern Bering, while northeast winds associated with eastward shifted cyclone tracks promote the advance of the ice cover.

Interannual Variability in the Tropical Pacific Atmosphere: the Southern Oscillation Index and Pacific North American Index

The term El Niño-Southern Oscillation (ENSO) event is often used to refer to large scale changes in the oceanic and atmospheric environments of primarily the tropical and extratropical Pacific regions, however the effects of ENSO events on the climate system are global in nature. In this paper the term "El Niño event " will be used to refer to changes in the temperature and flow regimes of the tropical Pacific *Ocean* in response to large scale changes in the tropical Pacific atmosphere such as a weakened trade wind system and shifts in convective regions and associated changes in the Walker and Hadley circulations. These changes often occur concurrently with changes in the atmosphere represented by variations in the Southern Oscillation Index (SOI). The occurrence of El Niño events is highly correlated with the SOI, which is a measure of the intensities of the South Pacific subtropical high and the Indonesian low pressure systems. These systems fluctuate in concert with each other and are intricately linked to the trades and to convective activity. Positive anomalies of the SOI indicate that both systems are intense, while negative anomalies indicate that both are weak [Wyrtki,

1982]. El Niño events often occur when the SOI drops precipitously (negative swings in the SOI), indicating amongst other things, a weakening of the easterly trade wind system. El Niño events during the past sixty years, however, have also occurred both prior to and subsequent to negative swings in the SOI, indicating that El Niño and the Southern Oscillation are more loosely coupled than has been suggested by other studies [Deser and Wallace, 1987]. It appears that the relationship between El Niño events and the SOI is an imperfect one.

There are a number of characteristic changes that occur in the large scale atmospheric circulation over the extratropical North and South Pacific in relation to the occurrence of ENSO events in the tropical Pacific. In the South Pacific, the surface ocean trough in the westerlies between 15°S and 45°S is anomalously strong during the mature phase of an El Niño event [Van Loon and Shea, 1985]. Namias [1976] noted that during El Niño periods the North Pacific mid-latitude westerlies strengthen while the subtropical easterlies weaken. Pan and Oort [1983] reported that the Ferrel easterlies appear to be intensified at 200 mb and at the surface during warm periods. Hanson and Long [1985] find that there is a tendency for ENSO years to coincide with storm formation frequency maxima in the Kuroshio region. Namias also noted that SLP falls between 50°N and 60°N while it rises at 20°N. In other words the Aleutian Low, East Pacific High, and the Siberian High intensify during the occurrence of El Niño events. The Aleutian Low has been observed not only to deepen, but also to shift to the southeast during ENSO events

[Bjerknes, 1969, 1972, Niebauer, 1988], however this does not occur in the case of every ENSO event.

The Pacific North American (PNA) index is defined as a linear combination of 500 mb atmospheric geopotential height anomalies at four centers of action located at 20°N 160°W, 45°N 165°W, 55°N 115°W, and 30°N 85°W [Wallace and Gutzler, 1981]. The structure of the PNA pattern in the 500 mb geopotential height field is linked to tropical variations, and on interseasonal to interannual time scales is mainly associated with ENSO events [Mo and Livezey, 1986], although the PNA pattern is not always directly associated with tropical forcing [Douglas et al, 1982, Niebauer and Day, 1989]. There is evidence that the source region of the PNA pattern lies in the tropical western Pacific near 10°N 155°E [Livezey and Mo, 1987]. In the SLP field over the North Pacific, the positive phase of the PNA pattern manifests itself as an intense Aleutian Low [Wallace and Gutzler, 1981], and is characterized by strong ridging in the pressure field over western Canada and Alaska [Wallace and Gutzler, 1981, Niebauer, 1988]. The negative phase of the PNA is associated with an anomalously weak Aleutian Low [Wallace and Gutzler, 1981]. The surface signature of the PNA pattern is confined mostly to the North Pacific in the region between 25°N-75°N and 145°E-125°W [Trenberth, 1990]. A trend toward stronger PNA patterns, particularly during winter in the 1980's has been noted by Namias et al. [1988] and Nitta and Yamada [1989]. Although the SOI and PNA appear to be manifestations of variability in the tropical Pacific, it appears that the effects of variations in these parameters extend from the tropics to the high latitude North Pacific.

Running mean anomalies of the SOI were negative during the period 1977-88 (figure 2.15a). This is the longest period in the record (since 1950) for which a persistently negative SOI occurs. The period 1976-88 is characterized by the occurrence of several ENSO events but no strong La Niña events, resulting in a persistently negative SOI, as noted by Trenberth [1990]. This period of strong negative anomalies coincides with the period of occurrence of strong and persistent anomalies of subarctic wind stress curl and air temperatures, as well as extratropical SST. Therefore, the occurrence of strong and persistent anomalies in the ocean and atmosphere from the tropical to high latitude Pacific suggests that the climate anomalies that occurred during 1976-88 are coherent over very large spatial scales. An intense La Niña, as manifested by large positive SOI anomalies, occurred in 1989 and appears to represent a relaxation or termination of the climate regime that occurred during 1976-88 in the tropical Pacific.

Running mean anomalies of the PNA index were strictly positive during 1976-87 and strictly negative during 1948-56 (figure 2.15b). The behavior of the low frequency anomalies is oscillatory during 1956-75. Positive anomalies of the PNA from 1976-88 are consistent with the observations of an intensified Aleutian Low, indicating that this well known teleconnection between the tropical and midlatitude Pacific was particularly strong during this period. Both the SOI and the PNA exhibit persistently anomalous behavior during 1976-88. The occurrence of anomalies of similar duration and strength in the extratropics, and the existence of teleconnections between the tropics and extratropics suggests

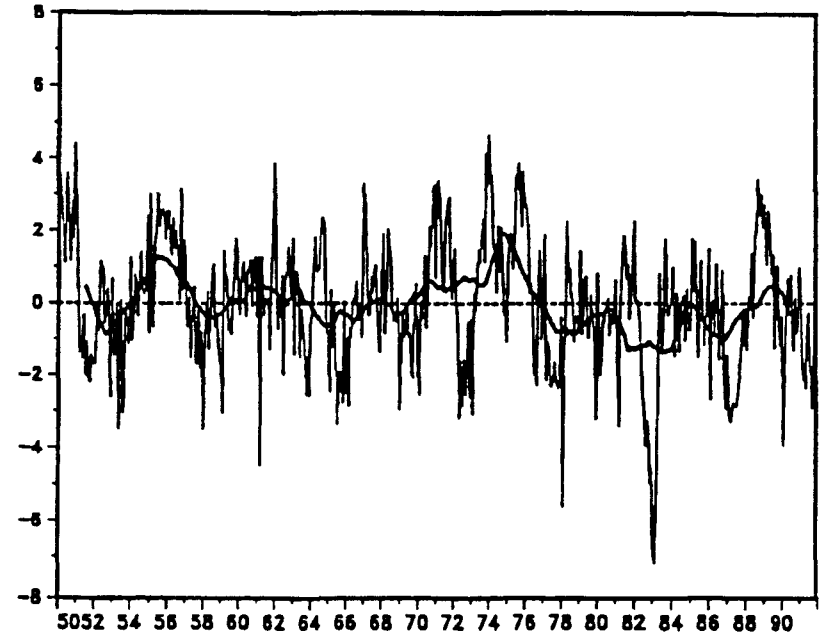

a)

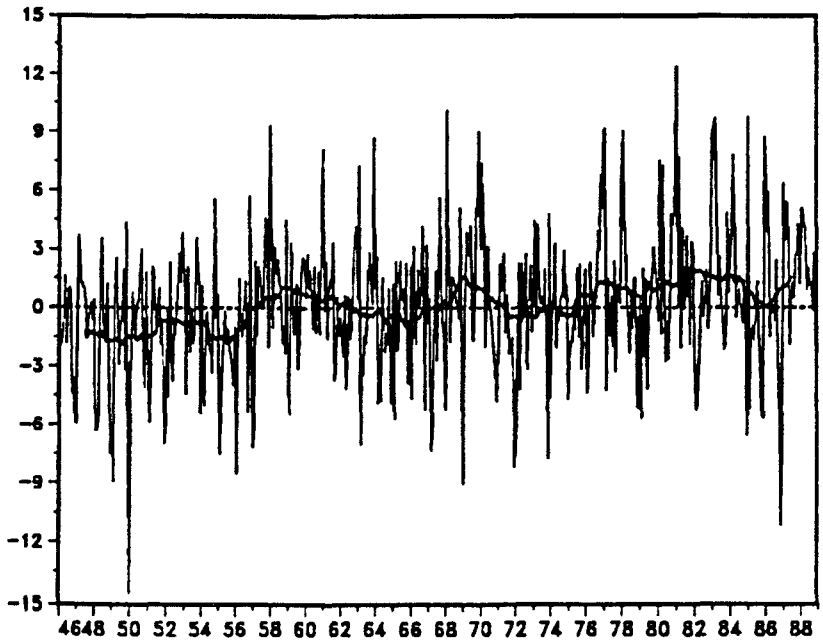

b)

Figure 2.15: a) Southern Oscillation Index.
b) Pacific North American Index.

that the physical links between these regions were amplified during 1976-88, and the spatial scales of this climate anomaly extend from the tropics to the high latitude North Pacific.

Relationships between Tropical Variables, Extratropical SST and Wind Stress Curl

Relationships between large scale fluctuations in extratropical North Pacific SST and tropical Pacific forcing were examined by correlating the TAFs of the first 4 nonseasonal SST EOF modes with the SOI and SST in the Niño 1+2 region (table 2.8). The mode 1 TAF is the only SST mode that is significantly correlated to both of the tropical variables. The mode 2 SST TAF is not significantly correlated at the 99% level with either of the tropical variables. Changes in the mode 1 SST TAF lag fluctuations in the tropical variables by 1 to 8 months (figure 2.16). Since the mode 1 TAF is largely representative of SST variability in the CNP region, it appears that changes in CNP SST might occur as a response to tropical forcing. However, the correlations between the mode 1 SST TAF and the tropical indices explain only 15% to 20% of the between field variance. Therefore while tropical variations manifest themselves most strongly in mode 1 of extratropical North Pacific SST, most of the SST variability occurring within mode 1 is not directly associated with events forced in the tropical Pacific region. This is consistent with the results of Wallace et al. [1990] who show that tropical Pacific SST fluctuations can explain about 29% of the variance of the TAF of Weare's [1976] leading nonseasonal SST EOF.

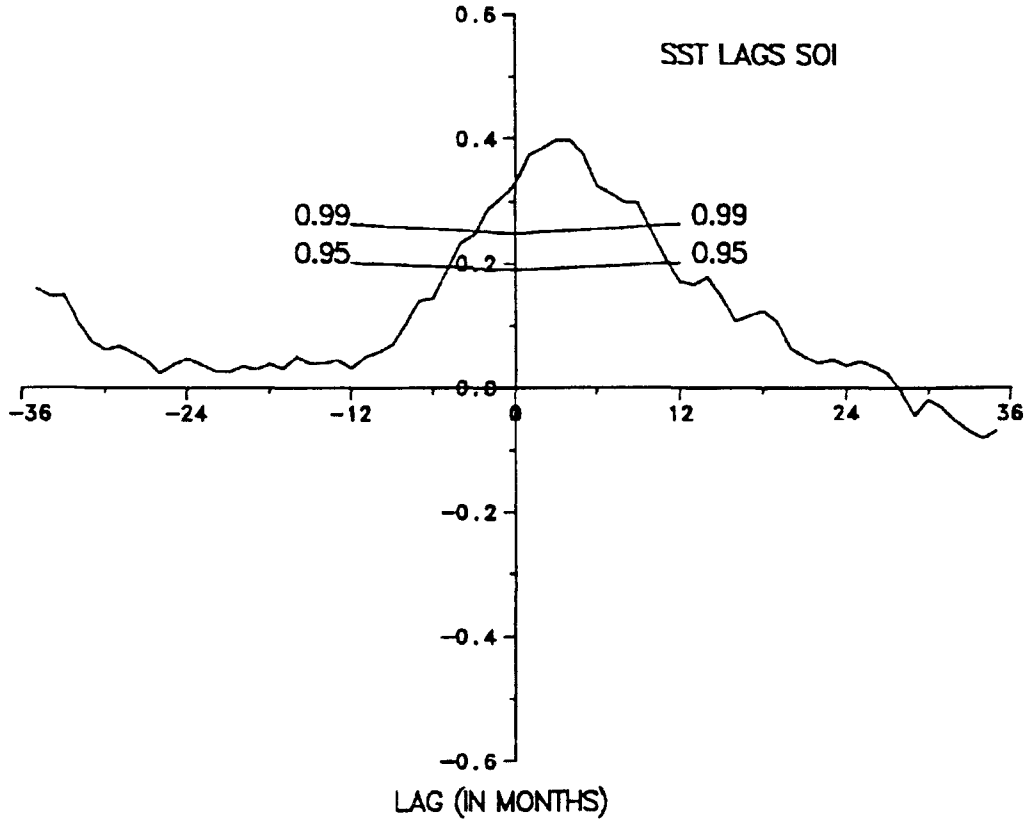

Figure 2.16: Correlation between the SOI and extratropical SST. This chart illustrates the lead-lag relationship that is typical of those between the SOI and each regional SST series.

	SOI	Niño 1+2
Mode 1	0.40	-0.44
Mode 2	-0.18	Not Signif.
Mode 3	0.23	Not Signif.
Mode 4	-0.30	0.39

Table 2.8: Correlations among nonseasonal SST EOF modes and tropical variables.

Also, Iwasaka et al. [1987] note that the dominant mode of nonseasonal SST variability is not always coherent with fluctuations in the equatorial Pacific Ocean.

Correlations between the SOI, Niño 1+2 SST and the regional extratropical SST series suggest that SST variability in the CNP and WNP regions is significantly influenced by tropical forcing, while SST in the ENP region is less clearly related to variations occurring in the tropical Pacific (table 2.9). Ten percent to 23% of the variance can be explained by the correlations in the CNP and WNP regions, while only 7% to 8% of ENP variability is explained. The CNP and WNP regions are inversely correlated to Niño 1+2 SST and positively correlated to the SOI, while the correlation coefficients in the ENP are of opposite to those in the WNP and CNP. SST variations in all three of the extratropical regions lag changes in the tropical variables by 1 to 6 months, and therefore appear to be responses to tropical forcing. Low pass filtering the data increases the amount of variance explained by the correlations to 21% in the WNP, 30% to 42% in the CNP and 7% to 16% in the ENP. Tropical effects appear to be particularly important in modulating extratropical SST on long time scales.

The PNA is significantly correlated with two of the first four nonseasonal SST EOF modes (table 2.10). The PNA is negatively correlated with WNP and CNP SST and positively correlated with ENP SST (table 2.11). The correlations between SST and PNA occur with PNA fluctuations leading changes in SST by 1 month, and explain from about 5% to 20% of the variance. This is consistent with the results of Lanzante

[1984] and Iwasaka et al. [1987] who show that atmospheric fluctuations, in particular the PNA, tend to lead variations in extratropical SST by about 1 month. Correlations between low pass filtered regional SST and the PNA demonstrate that these fields are coupled to each other on time scales of years (table 2.12). The correlation between ENP SST and the PNA is much weaker than those between the PNA and WNP and CNP SST, as was the case with regional SST and wind stress curl. This is consistent with the PNA being an indicator of the strength of the Aleutian Low.

None of the first four EOF modes of nonseasonal wind stress curl are significantly correlated to SST in the Niño 1+2 region (table 2.13). Three of these 4 modes are significantly correlated to the SOI, although each of the correlations explains less than 5% of the between field variance. The maximum correlations occur near zero lag, with the SOI leading by at most 1 month. Negative swings of the SOI tend to be associated with intensified wind stress curl in the Aleutian Low and in the subtropical anticyclone, while positive values of the SOI are associated with diminished wind stress curl in both of these regions. The correlation between the low pass filtered series of the SOI and Aleutian Low wind stress curl explains 24% of the between field variance, while the correlation between the low pass filtered SOI and East Pacific High curl explains 13% of the variance. Again the correlations between extratropical and tropical variables improve as the time scales of variation increase. It is also apparent that much of the interannual variability in wind stress curl in the Aleutian Low is associated with tropical forcing related to El Niño and the SOI.

	SOI	Niño 1+2
WNP SST	0.32	-0.46
CNP SST	0.39	-0.49
ENP SST	-0.26	0.28

Table 2.9: Correlations among tropical variables and regional SST series.

	PNA
SST 1	-0.45
SST 2	Not Signif.
SST 3	0.23
SST 4	Not Signif.

Table 2.10: Correlations between the PNA and TAFs of nonseasonal SST. Correlations are significant at the 99% level.

		PNA
SST	WNP	-0.36
	CNP	-0.40
	ENP	0.21

Table 2.11: Correlations between regional extratropical SST and the PNA.

		PNA
SST	WNP	-0.57
	CNP	-0.58
	ENP	-0.36

Table 2.12: Correlations between lowpass filtered extratropical SST and the PNA.

	SOI	Niño 1+2
Curl 1	0.15	Not Signif.
Curl 2	-0.19	Not Signif.
Curl 3	-0.15	Not Signif.
Curl 4	nsc	Not Signif.

Table 2.13: Correlation matrix of nonseasonal wind stress curl EOF modes and tropical variables.

TAFs of Wind Stress Curl	PNA
Mode 1	-0.32
Mode 2	0.54
Mode 3	0.47
Mode 4	Not Signif.

Table 2.14: Correlations between the PNA and TAFs of nonseasonal wind stress curl. Correlations are significant at the 99% level.

	Aleutian Low curl	GOA curl	Bering curl	East Pacific High curl	Western Pacific curl
PNA	0.52	0.26	0.25	Not Signif.	Not Signif.

Table 2.15: Correlations between the PNA and regional wind stress curl. Correlations are significant at the 99% confidence level.

The PNA is significantly correlated to three of the first four nonseasonal EOF modes of wind stress curl (table 2.14). Correlations between curl and the PNA occur at zero lag and explain 10% to 29% of the variance. The correlation coefficients between the PNA and regional wind stress curl are small except in the Aleutian Low region where the correlation is positive and explains 28% of the variance (table 2.15). Correlations between the low pass filtered PNA and wind stress curl EOF modes explain 30% to 42% of the between field variance. The correlation between the PNA and Aleutian Low wind stress curl explains 40% of the variance between the low pass filtered series, while the correlations between the PNA and regional wind stress curl in the subtropical region remain small and account for less than 2% of the variance. Based on the results of cross correlation analyses it appears that Aleutian Low wind stress curl variability is more strongly related to PNA fluctuations on time scales of years than on time scales of months.

Summary and Discussion

Nonseasonal wind stress curl variations in the Aleutian Low are inversely correlated to changes in SST in the WNP and CNP between 20°N and 50°N. Wind stress curl variations tend to lead changes in SST by 1 month in these regions. Aleutian Low wind stress curl variability is positively correlated with and leads SST variability by 1 month in the ENP. On time scales of years, greater than 40% of the between field variances

are explained by the correlations between Aleutian Low wind stress curl and CNP and WNP SST, while the correlation between ENP SST and Aleutian Low wind stress curl explains only 5% of the between field variance. Decadal scale wind stress curl variation in the Aleutian Low is suggested to be an important factor in long term central and western North Pacific SST variability. In particular negative SST anomalies in the central and western North Pacific during 1976-87 can be largely explained in terms of the effects of an intensified Aleutian Low as manifested by positive anomalies of Aleutian Low wind stress curl. Also, positive central and western North Pacific SST anomalies during 1961-68 occur in conjunction with negative wind stress curl anomalies in the Aleutian Low. The role of wind stress curl is weaker with respect to eastern North Pacific SST variations over the length of the entire record, although eastern North Pacific SST variability during 1976-87 appears to be closely related to changes in Aleutian Low wind stress curl during this period.

Air temperature fluctuations in the Gulf of Alaska and Bering Sea are positively correlated to regional wind stress curl and SST variability. Maximum correlations between air temperature anomalies and wind stress curl occur at zero lag while changes in SST tend to lag changes in air temperature by 1 month. On time scales of years, 35% to 40% of the variance between these parameters can be explained by the correlations between them. Bering Sea and Gulf of Alaska air temperatures fluctuate in concert with Aleutian Low wind stress curl on decadal time scales, particularly during 1960-74 and 1976-88.

Wind stress curl variations over the Bering Sea are negatively correlated with anomalies of eastern Bering Sea ice cover. On long time scales the direct and indirect effects of changes in Aleutian Low wind stress curl appear to be important factors in governing interannual variability in Bering Sea ice cover. In particular Bering Sea wind stress curl variations are closely related to air temperature anomalies. The air temperature anomalies, in turn, explain over 50% of the variance of Bering Sea ice cover. The coupling between ice cover and wind stress curl anomalies is particularly strong during the period 1977-88.

North Pacific SST variability is significantly correlated with atmospheric and oceanic fluctuations in the tropical Pacific. Variations in regional North Pacific SST lag changes in the tropical indices by 1 to 8 months. SST variability in the central and western North Pacific appears to be more clearly related to tropical variations than does SST variability in the ENP region. Correlations between low pass filtered regional SST and tropical variability show that the CNP and WNP are closely related to tropical Pacific variability on long time scales, while ENP variations are only weakly related to tropical fluctuations on these longer time scales.

North Pacific wind stress curl variability is influenced by variations in the tropical atmosphere but is not significantly correlated with changes in tropical Pacific SST. Correlations between low pass filtered wind stress curl and the SOI show that Aleutian Low wind stress curl is more strongly influenced by changes in the SOI than is wind stress curl in the subtropical anticyclone. Anomalies of the SOI and subarctic Pacific wind

stress curl are most strongly related to each other during the period 1976-88.

Wind stress curl variations in the Aleutian Low and the subtropical anticyclone are related to fluctuations in the PNA index. The strongest correlations occur between the PNA and Aleutian Low wind stress curl. This correlation is positive and occurs at zero lag. On long time scales, 40% of the between field variance is explained by the correlation of low pass filtered Aleutian Low wind stress curl and the PNA. Correlations between low pass filtered wind stress curl in the subtropical anticyclone and the PNA remain as weak as the correlations between the unfiltered data.

It has been demonstrated in this study that decadal scale North Pacific wind stress curl variability occurs concurrently and consistently with long term variations in a number of Pacific region climate parameters and therefore represents real changes that have occurred in the climate system of the North Pacific region during the past forty five years. These relationships are especially apparent during the period of intensified Aleutian Low wind stress curl that occurred during 1976-88 and during the period of weakened circulation in the Aleutian Low occurring form 1960-68 and from 1971-75. The observed relationships between Aleutian Low wind stress curl and North Pacific SST suggest that long term cooling in the CNP and WNP regions during 1969 to 1987 ended in conjunction with a reversal of the intensification of the Aleutian Low that occurred during 1976-88. It is also suggested on the basis of the out of phase relationship between CNP and ENP SST, and on the basis of the

relationships between Aleutian Low curl and CNP SST cited above that the warming observed in ENP SST during 1978-88 will also reverse and ENP SST will begin to cool as CNP SST begins to warm and Aleutian Low wind stress curl weakens.

Chapter Three

Interannual Variability of North Pacific Blocking Activity and its Relation to Climate Change

Introduction

The northeastward passage of subtropical depressions along the Aleutian storm track is sometimes interrupted by the presence of large scale anticyclones over the northcentral North Pacific. This results in the storm systems being deflected away from the Gulf of Alaska, either northward into the Bering Sea or to the southeast toward Oregon and Washington [Wilson and Overland, 1986]. This type of anticyclone is known as a blocking ridge or blocking high [White and Clark, 1975, Treidl et al., 1981]. The occurrence of blocking ridges over the central North Pacific Ocean significantly alters the most important paths of storm systems propagating across the ocean and thereby also alters storm tracks further downstream [White and Clark, 1975]. The occurrence of blocking features is thought to be a significant factor in causing interannual shifts in the positions of the main storm tracks into the Bering Sea [Overland and Pease, 1982], and the Gulf of Alaska [Wilson and Overland, 1986].

Physical aspects that characterize blocking ridges are distinct from those of anticyclonic systems that are normally known as cold high

pressure systems or ridges. Blocking ridges tend to intensify in situ, migrate slowly and often retrogress, whereas other anticyclonic systems usually originate in the Arctic, intensify as they migrate to the southeast, and move at speeds of atmospheric short waves [Treidl et al., 1981]. Blocking ridges tend to persist for longer periods than cold high pressure systems and therefore affect specific regions for a relatively long time period [Treidl et al., 1981].

Blocking ridges occur over the North Pacific most frequently during fall and winter [White and Clark, 1975, Lejenas and Okland, 1983]. White and Clark [1975] find that interannual variability in North Pacific blocking activity is inversely correlated with the strength of the mean fall and winter mid-latitude westerlies. Over the North Pacific blocking ridges occur as high latitude phenomena in the sense that they are often generated between 52°N and 60°N with maximum generation occurring between 56°N-58°N [Treidl et al., 1981]. Blocking ridges are often centered near 170°W [White and Clark, 1975, Treidl et al., 1981] and have wavelengths of up to 7000 km that span the Pacific basin, also suggesting that they are of marine origin [White and Clark, 1975]. Fall and winter block development is closely coupled to local ocean-atmosphere sensible heat transfers, and blocking ridge activity and the strength of the mid-latitude westerlies fluctuate in concert with the Southern Oscillation during the period 1950-1970 [White and Clark, 1975]. White and Clark [1975] also find that ridging activity is strongly inversely correlated with variations in eastern tropical Pacific SST.

This study examines blocking activity over the North Pacific during fall and winter for the period 1946-1990. It is shown that blocking tends to occur during winters one year prior to the occurrence of ENSO events, while there is a lack of blocking activity during the mature phase of ENSO events. Blocking activity during winter is shown to be closely correlated to negative extrema of the PNA index, indicating that winter blocking activity is a manifestation of very weak circulation in the Aleutian Low. Decadal scale changes in fall and winter blocking activity support the hypothesis that during the period 1976-1988 a unique climate regime existed over the North Pacific.

Data

The occurrence of ridging features over the North Pacific and Bering Sea was investigated using contour maps of monthly mean SLP. The analysis is for the months of September through March for the period 1946 through 1990. This data set contains as a subset the pressure grid used to compute wind stress curl over the North Pacific and was described in chapter one.

Definition and Characteristics of Marine Ridges

There are three patterns in the SLP field that are characteristic of the phenomena that will be discussed in this paper, two blocking patterns and one nonblocking pattern (figure 3.1). The SLP pattern characterizing

the nonblocking situation (figure 3.1a) occurs most frequently and depicts the Aleutian Low as a single intense cyclonic structure over the northern North Pacific. The atmospheric motions associated with this pattern are generally zonal across the central North Pacific, and are largely represented by the northeastward passage of subtropical depressions through the region of the midlatitude westerlies. The most frequently occurring blocking pattern (figure 3.1b, henceforth the type 1 block) consists of troughs over the northwestern North Pacific or Sea of Okhotsk and the Gulf of Alaska separated by a ridge over the northcentral North Pacific. The central pressure in each of the troughs is generally higher than the central low pressure in the nonblocking situation by about 10 mb. The other blocking pattern (figure 3.1c, henceforth the type 2 block) is characterized by a single cell of weakened low pressure in the northwestern North Pacific juxtaposed against high pressure in the northeastern North Pacific, particularly over the Gulf of Alaska. Again, the central pressure within the blocked low is higher than in the nonblocking situation, so that blocked flow in the high latitude SLP field might be interpreted as a characteristic feature of weakened circulation within the Aleutian Low. The type 1 and type 2 blocks are different, in that the geostrophic flow field associated with type 1 blocking patterns advects cold Arctic air toward the south into the eastern Bering Sea and northern North Pacific regions during winter, while type 2 blocks advect warm subtropical air poleward into these regions. White and Clark [1975] distinguish between blocking ridges over the central North Pacific Ocean and those over the western part of North America (and therefore did not

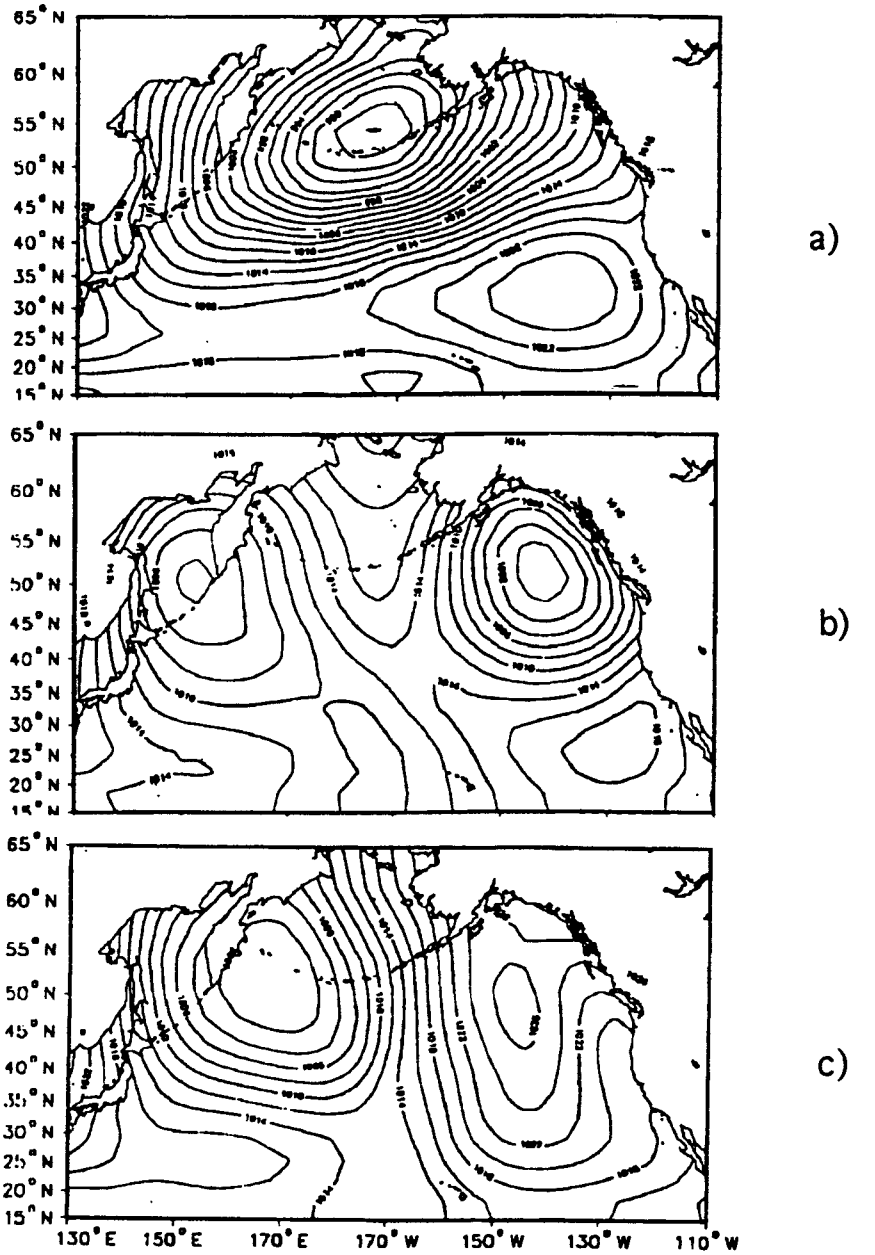

Figure 3.1: Characteristic North Pacific sea level pressure fields.

a) no blocking b) type 1 blocking c) type 2 blocking

CI= 2 mb.

include the latter in their study) since these features appear to have distinct origins, the first marine and the other continental. This distinction will also be made in the present study for comparative purposes.

The definition of blocking ridge that will be used in this study is based on that given by White and Clark [1975] which is modified from the definition given by Rex [1951]. White and Clark use 700 mb height maps and SLP maps to catalog blocking activity over the central North Pacific for the period 1950-1970. The definition is somewhat subjective, however in most cases there is no doubt as to the characterization of the SLP pattern as a blocking or nonblocking pattern. The only ambiguity that might have arisen was in deciding whether an anticyclone was simply a ridge or whether it was a blocking ridge, but again in most cases this was a straightforward operation. In the present study, the distinction between blocking ridges and ridges is less important than the difference between ridging and nonridging SLP patterns. Also since the FNOC SLP data set begins in 1946, the SLP fields for 1950-1970 are analyzed and compared with the results of White and Clark. This allows for a consistent evaluation of the pressure fields so that a direct comparison of blocking activity can be made between the data used in this study and the pressure fields used by White and Clark [1975].

The working definition of blocking ridge used in this study derives from the archetypal ridging patterns exemplified by figures 3.1b and 3.1c. A blocking ridge will be taken to exist when either the Aleutian Low is split into two cells both of which have higher pressure than the mean

single celled low structure or when high pressure over the entire northeastern North Pacific is juxtaposed against a weak Aleutian Low cell that has been distorted to the extent that storms are deflected meridionally over the open ocean. A nonblocking ridge will be taken to be a feature that has the same general spatial pattern as a blocking ridge, but the circulation is not weakened to the extent that it is when a blocking ridge is present. The pressure in the nonblocking situation is usually 4-8 mb lower than in the blocking situation, that is, the nonblocking pattern represents a stronger circulation than the blocking ridge. The terms "marine ridges" or "ridging features" will be used to refer to both blocking ridges and nonblocking ridges that occur over the open ocean regions of the Bering Sea and northern North Pacific.

As noted by White and Clark [1975], due to the use of monthly mean maps we cannot discern information concerning the time scales of growth (which appear to be on the order of weeks, [White and Clark, 1975]) and decay of the ridging features, but can only note that they occur for long enough to dominate the monthly mean SLP fields during those months when they are present. We will therefore be concerned with the persistent occurrence of ridges and their effects on the large scale atmospheric circulation, and not with more ephemeral ridging episodes and their short term effects.

Analysis

Comparison with White and Clark [1975]

The occurrence of ridging activity determined from monthly mean SLP and 700 mb height maps by White and Clark [1975] for 1950-1970 is compared with the results of this study. In 137 of 147 cases (93%), features identified as blocking or nonblocking ridges by White and Clark were also identified as ridging features in this study. In 8 of 147 cases (5%), features regarded as ridges in one study were not identified as such in the other study. These differences probably occur as a result of the use of only SLP charts in the present study, while White and Clark used both SLP and 700 mb maps. Overall the results of this study and that of White and Clark are in exact agreement 88% of the time and in agreement as to the identification of ridging or nonridging features 93% of the time.

Marine Ridging Activity 1946-1990

The distribution of the occurrence of blocking and nonblocking ridges over the central North Pacific Ocean during October through March for the period 1946 to 1990 is shown in table 3.1. The distribution of the frequency of occurrence of open ocean blocking ridges has changed during fall and winter for the period 1971-1990, relative to 1950-1970. The most prominent differences occur during the months of January, February, and October. The January frequency has decreased from 1971-

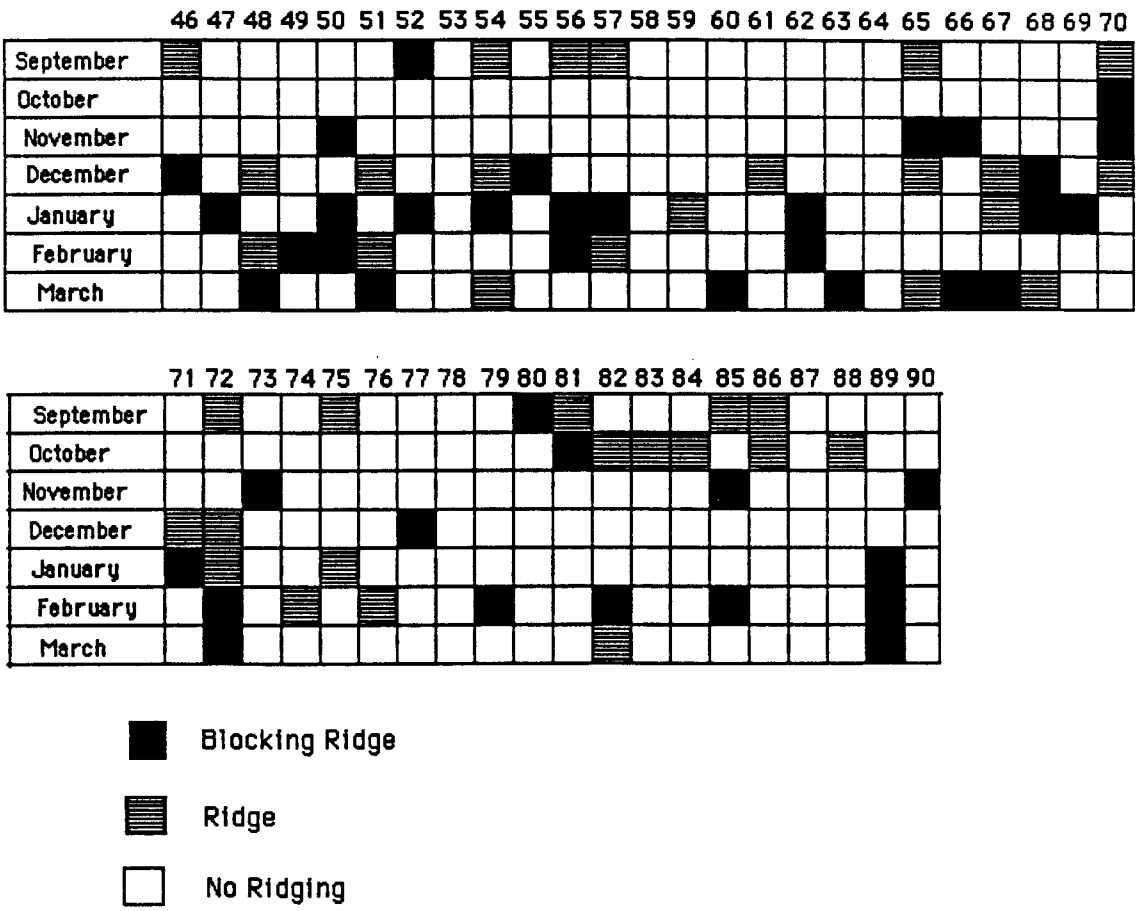

Table 3.1: Frequency of occurrence of marine ridges during fall and winter.

90 relative to 1950-70, while the February frequency has increased during the same periods respectively. In October only one ridging feature occurred during the period 1950-1970 while six occurred during 1971-1990. All of the October ridging features present during the latter period occurred between 1981 and 1988. October ridging during 1981-88 appears to represent a significant departure from the October climatology in the sense that only 1 ridge appeared during the 35 year period prior to 1981; after which ridges were present during 6 of the subsequent 8 years. Previous studies of central North Pacific blocking by White and Clark [1975] for the period 1950-1970 and Lejenas and Okland [1983] for the period 1950-1979 show that a pronounced winter (and annual) maximum in North Pacific blocking activity occurs during January, while the fall maximum is in November. Apparently since 1970 there has been a shift in the months of maximum open ocean blocking ridge activity from January to February during winter, and from November to October during fall.

Marine Ridging Activity as a Precursor to El Niño -Southern Oscillation Events

In chapter two it was noted that a number of large scale tropical and extratropical atmospheric phenomena occur as a result of ENSO events in the tropical Pacific. There also appear to be a number of phenomena that occur as precursors to ENSO events. In the South Pacific, the trough in the westerlies over the ocean surface between 15°S

and 45°S is anomalously weak during southern fall and winter before the occurrence of ENSO events [van Loon and Shea, 1985]. Namias [1976] noted that the East Pacific High over the eastern third of the North Pacific was weaker during winters preceding El Niño events. Emery and Hamilton [1985] use three month (December, January, February) composite charts for the period 1947 through 1982 to show that El Niño events often follow winters with weak Northeast Pacific, i. e. Aleutian Low, SLP patterns, although they note that the relationship between the strength of Northeast Pacific pressure patterns and ENSO events is far from being perfect and regular.

There is a tendency for marine ridging to occur during winters prior to the occurrence of ENSO or Southern Oscillation events (table 3.2). Marine ridging activity usually does not occur during winters that coincide with the mature phase of ENSO events. These observations qualitatively suggest a relationship between marine ridging activity and the SOI. Time sequences of the frequency of North Pacific marine ridging activity during January, February, and March (JFM) and the derivative of the mean SOI were cross correlated for those years when the SOI decreased from values greater than 1 positive dimensionless unit to negative values. An exception is 1986 when the mean SOI went from slightly negative to strongly negative values. In all but 1 of these cases (1989) an El Niño event ensued during that year. The correlation coefficient for this relationship was found to be 0.69 which is significant at the 99.9% confidence level, and accounts for 48% of the variance between the two sequences. Therefore, there is a tendency for ridges to appear over

El Niño	Ridging activity during previous winter (J,F,M)	Ridging activity during subsequent winter (J,F,M)
1951-52	Feb., Mar., 51	Jan., Mar, 52
1953-54	None	Jan., Mar, 54
1957-58	Jan., Feb., 57	None 58
1963-64	Mar. 63	None 64
1965-66	Mar. 65	Mar. 66
1969-70	Jan. 69	None 70
1972-73	Jan.,Feb.,Mar.72	None 73
1976-78	Feb. 76	None 77, 78
1982-83	Feb., Mar., 82	None 83
1987	None 86	None 87
1989-90	Jan.,Feb.,Mar.89	None 90

Table 3.2: Relationship between frequency of occurrence of marine ridging and ENSO events during January, February and March (J, F, M).

the northern North Pacific and Bering Sea during the periods when the mean SOI begins to decrease rapidly from positive to negative values. During 9 of the 11 times (82%) since 1951 that the mean SOI has decreased at least 1 unit from positive to negative values, marine ridging has occurred over the northern North Pacific in conjunction with the onset of the drop. The two cases where marine ridging did not occur when the SOI decreased were during 1953 and 1986. These years are similar in that prior to these two ENSO events the SOI went from near zero to negative and from slightly negative to strongly negative respectively as opposed to the positive to negative swings that occurred in the other nine cases. Therefore it appears that large scale changes in the tropical atmosphere (changes in the SOI) have a tendency to follow changes in the Aleutian Low region from between nine months to one year before the occurrence of the mature phase of El Niño events. This result is consistent with that of Emery and Hamilton [1985] concerning the appearance of weak SLP patterns prior to ENSO events. This result also extends that of Emery and Hamilton [1985] since the relationship between marine ridging and the SOI has been somewhat quantified, and shows that the observed relation between ENSO events and ridging prior to ENSO events occurs quite consistently (i.e. 82% of the time).

The 9 month running mean SOI tends to decrease during years prior to the occurrence of the mature phases of ENSO events while years when the 9 month mean SOI rises are characterized by the occurrence of the mature phases of ENSO events. The correlation coefficient between sequences of the first derivative of the 9 month mean SOI for the period

1950-90 and the occurrence of marine ridges during JFM of each year is -0.49. This is significant at the 95% confidence level and accounts for 25% of the variance between the two parameters. The correlation suggests that there is a tendency for ridging to occur over the northern North Pacific during the year prior to the occurrence of the mature phase of ENSO events, while marine ridging activity tends to be suppressed during years when the mature phase occurs.

Marine ridging activity is also significantly correlated to fall and winter SST variations in the Niño 1+2 region of the eastern tropical South Pacific. During 1970-90 marine ridging activity was inversely related to variations in Niño 1+2 SST with a correlation coefficient of -0.53. This is consistent with the results of White and Clark [1975] who show that North Pacific blocking activity is correlated to fall and winter SST variations at Canton Island in the South Pacific with a correlation coefficient of -0.69 for the period 1950-70. The differences in the magnitude of the correlation coefficient are probably due to the fact that White and Clark use data that is representative of the central and eastern tropical Pacific, while the Niño 1+2 data are more representative of regional variations in the eastern tropical Pacific. It has been shown that there is an imperfect relationship between ENSO events in the tropical Pacific and ridging activity over the North Pacific during the winter (JFM) preceding the occurrence of El Niño events. Ridging activity over the extratropical North Pacific may be a precursor to (or at least an indicator of) the onset of ENSO events in the sense that the ridges appear from 9 months to one year before the mean

SOI reaches its local negative extremum and tropical Pacific SST reaches a local maximum.

The original data set used for this study covered the period 1946 through 1988 and the analysis of blocking activity and the observations of ridging features occurring concurrent with the onset of ENSO events were made for this data set. The data were later updated through April, 1991 in order to test the validity of some of the ideas developed concerning marine ridging activity and various atmospheric circulation parameters. The "predictions" made for the 1989-1991 period are based on the relationships ascertained from the earlier data and provided a test of the validity of these hypotheses. In 1989 marine ridges were present over the northern North Pacific consecutively during January, February and March. Based on the work described previously a sharp drop in the SOI would be anticipated, possibly coupled with the onset and occurrence of an ENSO event during late 1989 and early 1990. During 1989 the mean SOI underwent a sharp drop and swung from positive to negative as is characteristic of ENSO events. Apparently there was not an El Niño event associated with the decrease in the SOI so that this event is considered a Southern Oscillation event (SST increased in the eastern tropical Pacific, but the amplitude of the rise was small enough to not be considered an El Niño event). The persistent presence of ridges in the North Pacific pressure field therefore appears to be more strongly correlated to precipitous drops in the SOI than to the occurrence of ENSO events. This suggests that the link between tropical Pacific fluctuations and North Pacific blocking frequency is an atmospheric one. This is consistent with the results of White and Clark

[1975] who show that ridging activity and the strength of the mid-latitude westerlies and the SOI fluctuate in concert during the period 1950-70. Furthermore the persistent presence of ridging features over the northern North Pacific serves to indicate the onset of events that occur within the ENSO cycle. These events often occur as precursors to El Niño, although they are more indicative of changes occurring in the tropical atmosphere in relation to the SOI than they are of the onset of El Niño events.

No ridging activity occurred during JFM of 1990. Based on this observation, an ENSO event would not be predicted to occur in 1991. However, during 1991 a moderate ENSO event did take place. This demonstrates once again that the relationship between marine ridging and the SOI is imperfect. However, during 1990-1991 the mean SOI changed in manner that is quite similar to that in which it changed during the other 2 occasions in which no ridging activity was observed during winter prior to the occurrence of an ENSO event. While the physical mechanism is not clear, it appears that when the SOI does not reach large positive values prior to the occurrence of an ENSO event, marine ridging activity does not occur prior to the mature phase of the event. Therefore the relationship between ridging and ENSO events holds in 9 of 12 cases. In the 3 cases where the relationship does not hold, it appears to fail for the same reason in each case.

Numerical models of the coupled tropical ocean-atmosphere system have been successful in predicting the occurrence of ENSO events three to nine months in advance [Barnett et al., 1988] and also indicate that El Niño may be predictable one to two years before it occurs [Cane et al.,

1986]. The results contained in this study demonstrate that atmospheric conditions over the extratropical North Pacific might be used in conjunction with tropical ENSO models to indicate the possible occurrence of large decreases in the SOI that usually result in the onset and occurrence of an El Niño event during the subsequent year.

Relationships between Marine Ridging and the Pacific North American Teleconnection

The fields of SLP and wind stress curl provide direct information concerning the strength of the Aleutian Low. Another indicator of the strength of the circulation within the Aleutian Low is the PNA teleconnection. The spatial structure of what is often referred to in the literature as the "PNA pattern" is most often associated with positive values of the PNA index., This pattern is most strongly developed during periods that coincide with maximum positive values in the PNA index. It has been noted that strong ridging along the west coast of North America is associated with "PNA events" [e.g. Niebauer, 1988], which again are associated with positive extrema in the PNA index. Wallace and Gutzler [1981] also note that strong ridging over western Canada coincides with positive values in the PNA index. This west coast ridging associated with positive extrema in the PNA index appears to be characterized by amplified mountain waves of continental origin [White and Clark, 1975]. Wallace and Gutzler [1981] also show that the spatial pattern at 500 mb of

composite PNA negative extremes is distinct from the pattern that occurs in association with positive PNA extrema.

A qualitative analysis of the spatial structure of North Pacific SLP fields during the occurrences of large negative values of the PNA index suggested a relationship between marine ridging activity and the negative extrema of the PNA index. On annual time scales, the negative extrema of the PNA tend to occur during fall and winter. Time sequences of the frequency of fall and winter ridging activity were correlated with the fall and winter negative extrema of the PNA index. The correlation coefficient for this relationship was found to be -.60, explaining 36% of the variance between the sequences. The correlation is significant at the 99.9% confidence level according to the nonparametric Spearman Rank Correlation Test. Therefore marine ridging activity is associated with the negative extrema of the PNA index in the sense that ridges are frequently present over the central North Pacific within one month of the occurrence of fall and winter negative extreme values in the PNA index. The correspondence between negative PNA extrema and marine ridging is further demonstrated by the general absence of marine ridging activity associated with positive maxima of the PNA. Positive maxima of the PNA during October through December and January through March for the period 1946-88 were compared to marine ridging sequences during the same period. It was found that in only 5 of 73 cases (7%), that PNA positive extrema occurred in conjunction with marine ridging patterns in the SLP field.

There is also a strong relationship between the largest negative extrema of the PNA index and the occurrence of marine ridges. Of 31 negative values of the PNA index with a magnitude of greater than 50 normalized units that have occurred between 1950 and 1985, 27 (87%) of them are attributable to marine ridging activity. In 19 of those 27 cases marine ridges were present during the same month when the extreme value occurred, while marine ridges were present within one month of the extrema in the other 8 cases. Therefore when the Aleutian Low is very weak as evidenced by negative extrema of the PNA index, the spatial pattern of the associated SLP field is often characterized by a marine ridging pattern. The strong correspondence between marine ridging and negative PNA extrema, along with the lack of marine ridging activity associated with positive PNA maxima also shows that marine ridging over the central North Pacific is characteristically distinct from ridging that occurs over the west coast of North America, since ridging over the west coast of North America occurs most often in conjunction with positive values and positive extrema of the PNA index. This is consistent with the results of White and Clark [1975] who note that marine ridging is of oceanic origin, while ridging along the west coast of North America appears to be forced by continental effects.

Namias et al. [1988] and Nitta and Yamada [1989] note that the PNA pattern has become a dominant pattern over the North Pacific during winter seasons in the 1980's. In other words values of the PNA index have often been positive during winter seasons in recent years. It was also shown in chapter 2 that long term mean anomalies of the PNA were

strictly positive during 1976-1988. This recent shift to positive values provides a partial explanation for the observed decrease in winter season marine ridging activity during recent years. Marine ridging activity does not occur in association with positive PNA extrema, therefore the observed shift of the PNA during recent years to more positive winter values has resulted in a decrease in the occurrence of winter marine ridging activity during this period.

Decadal Scale Variability in Marine Ridging Activity

Anomalies of long term mean Bering Sea wind stress curl can be directly related to the occurrence of marine ridging activity in this region. The time series of mean wind stress curl over the Bering Sea for the period 1946-1988 was divided into six time periods based on the sign of the mean curl anomaly over the time interval. The total number of ridges occurring during each of these time periods strongly indicates that during periods of negative curl anomalies there is a tendency for marine ridges to be present frequently, while during periods of positive anomalies the frequency of occurrence of marine ridges decreases significantly (table 3.3). When strictly negative mean wind stress curl anomalies occur, correlation coefficients for the sequences of wind stress curl anomalies versus ridging activity account for 20% to 46% of the variance during periods of negative curl anomalies. When positive curl anomalies are present less than 4% of the variance is explained. Therefore, periods of frequent marine ridging activity are highly correlated with negative wind stress curl anomalies over the Bering Sea, which are associated with a

weakened Aleutian Low. Also, marine ridging tends to occur less frequently during periods of intensified synoptic storm activity associated with positive curl anomalies related to an intensified Aleutian Low.

The number of marine ridges occurring during each ten year period from 1950-59 through 1980-89 is nearly the same, varying in each case by one from the mean of eighteen (table 3.4). However when marine ridging activity during fall and winter is considered separately for each ten year period some large and obvious differences become apparent. The period 1980 through 1989 is characterized by less frequent marine ridging activity during winter (November through February) than any of the previous three decades by a factor of two (table 3.4). This same time period is also characterized by maximum ridging activity during fall (September and October). Fall ridging activity during 1980-89 also exceeds fall activity during the previous three decades by a factor of 2.5 to 10. During the decade 1960-69 winter marine ridging activity was at a maximum relative to the other three decades, while fall ridging activity was at a minimum. It appears that fall and winter marine ridging minima and maxima are out of phase on decadal time scales.

The periods of maximum and minimum winter ridging activity correspond closely to periods of weakened and intensified circulation in the Aleutian Low respectively as determined from the low pass filtered time series of Aleutian Low wind stress curl. These periods of weakened and intensified circulation also occur in conjunction with anomalously warm and anomalously low central North Pacific SST respectively. Correlations between marine ridging and the PNA showed that marine

a)

Years	Sign of Anom.	Freq.
1953-57	-	10
1962-67	-	12
1968-70	+	5
1971-75	-	10
1976-80	+	4
1983-88	+	3

b)

	Sign of Anomaly	r	r squared
1953-57	-	-0.68	0.46
1962-67	-	-0.45	0.20
1968-70	+	-0.19	<0.04
1971-75	-	-0.51	0.26
1976-80	+	-0.16	<0.04
1983-88	+	-0.13	<0.04

Table 3.3: a) Frequency of occurrence of marine ridges in relation to sign of Bering Sea curl anomalies. b) Correlations between frequency of occurrence of marine ridging and sign of Bering Sea wind stress curl anomalies.

	1950-59	1960-69	1970-79	1980-89
September October	4	1	4	10
November December January February March	16	17	14	8

Table 3.4: Decadal frequency of occurrence of marine ridges during fall and winter 1950-1989.

ridging conditions are characterized by weakened circulation in the Aleutian Low, while marine ridging tends not to occur during periods of strengthened circulation as manifested by positive anomalies of the PNA. Therefore, strong circulation in the Aleutian Low corresponds to conditions that are unfavorable for the development of marine ridges, while weak circulation in the Aleutian Low is associated with conditions that are favorable for block development. This is consistent with the results of White and Clark [1975] who show that marine ridging frequency is inversely correlated to the strength of the midlatitude westerlies. In particular blocking ridge development appears to be precluded during years of intense midlatitude westerlies [White and Clark, 1975]. Also White and Clark [1975] show that marine ridging occurs more frequently during periods of anomalously low ocean-atmosphere sensible heat transfer. Therefore the strong ocean-atmosphere heat fluxes in the central North Pacific associated with the intensified Aleutian Low during 1976-87, and manifested as anomalously low SST would also result in conditions that were not conducive to the development and maintenance of marine ridges. Similarly, positive CNP SST anomalies during 1960-69 are a manifestation of anomalously low ocean-atmosphere heat fluxes, conditions that are conducive to the development of marine ridges. Therefore the decrease in winter ridging activity during 1980-89 relative to the previous 30 years appears to be attributable in part to oceanic and atmospheric effects in the strengthened Aleutian Low that occurred during winter from 1976 through 1987. The winter marine ridging maximum that occurred during 1960-69 appears to be a result of the

oceanic and atmospheric effects associated with the weakened Aleutian Low that occurred during this period.

Intensified circulation in the Aleutian Low during winter provides a consistent explanation for the long term decrease in winter ridging activity for this period, however it does not explain why fall marine ridging activity occurred more frequently during 1980-89 than during any decade of the previous thirty years. Since marine ridges are associated with weakened circulation in the Aleutian Low, the increase in fall ridging activity during 1980-89 suggests that circulation during fall in the Aleutian Low might have been anomalously weak during this period. Wind stress curl anomalies over the Bering Sea and Gulf of Alaska during October from 1976-88 show that fall circulation was anomalously weak during 1981 through 1988. During October from 1976-88 wind stress curl anomalies were negative over the Bering Sea and Gulf of Alaska only when marine ridges were present, otherwise the anomalies were both positive or of opposite sign (figure 3.2). Similarly only during periods when ridges are present are the curl anomalies negative in both regions. That is, during October from 1976-88, there is a one to one correspondence between the occurrence of marine ridges and the sign of curl anomalies over the Bering Sea and Gulf of Alaska both being negative. This one to one correspondence does not occur in the earlier parts of the record, however for 1976-88 it strongly suggests that the decadal maximum in fall ridging activity is largely attributable to weakened fall conditions in the Aleutian Low. Also SLP averaged over the Aleutian Low region shows distinct trends toward lower pressures during the winter months, while

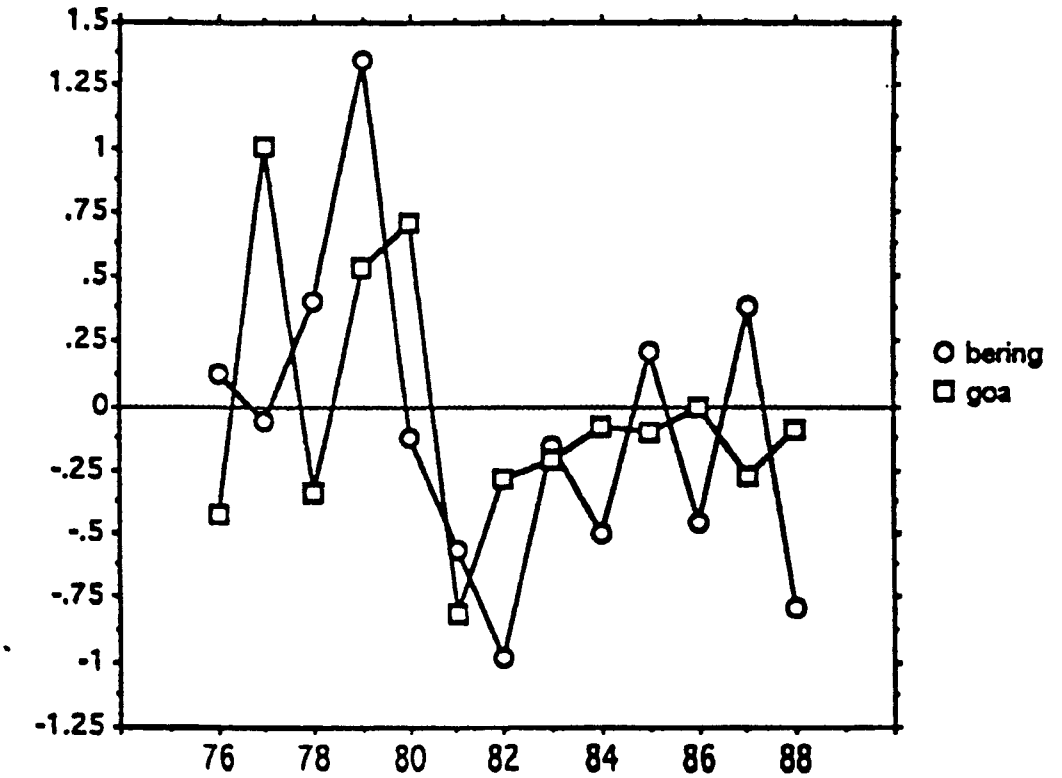

Figure 3.2: October wind stress curl over Bering Sea and Gulf of Alaska (goa) 1976-1988. Units are 10^{-7} N/m^3.

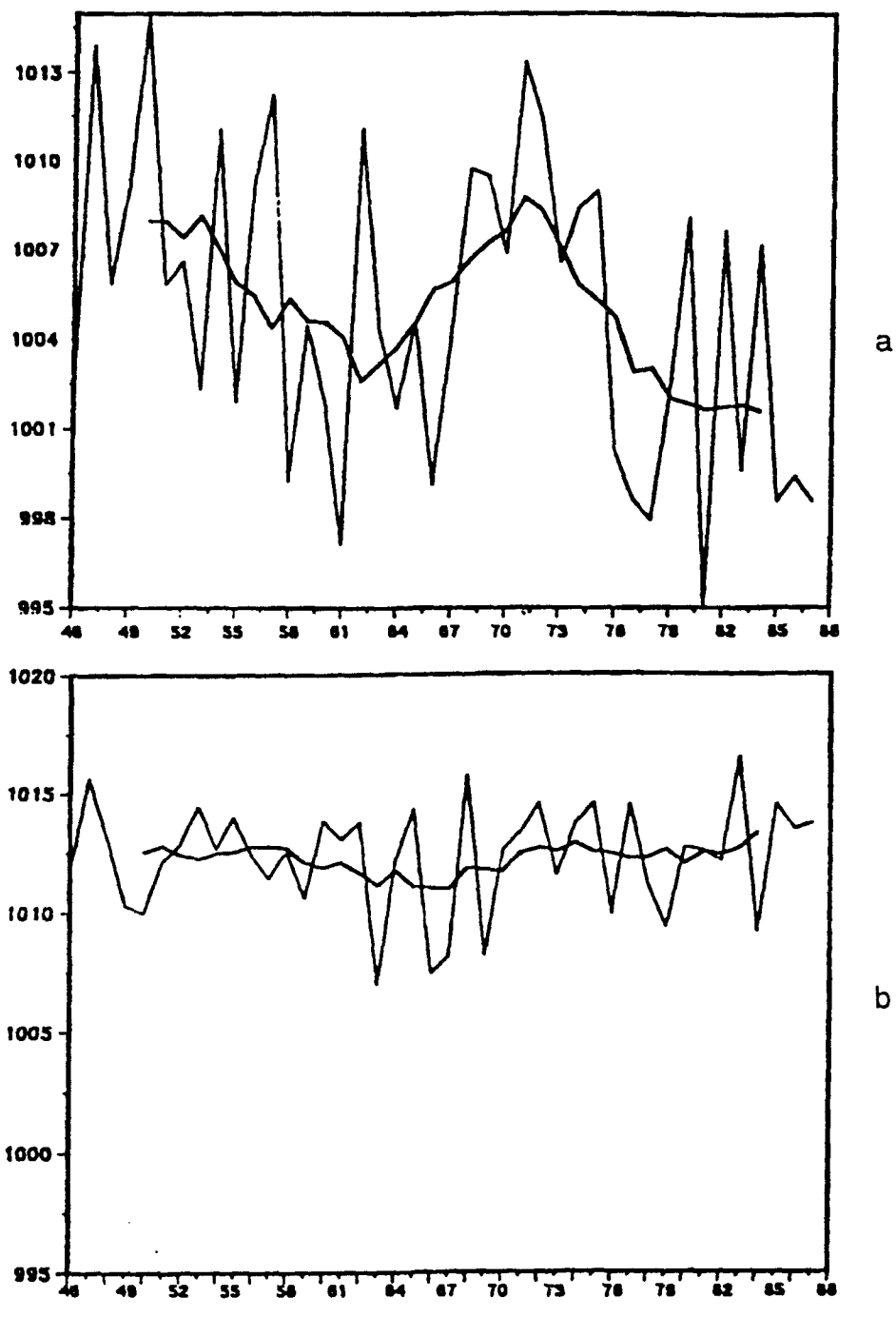

Figure 3.3 : Sea level pressure in the Aleutian Low representative of winter and fall conditions. a) January b)September. Units are mb.

SLP variations show no such trend during fall (figure 3.3). Therefore it appears that the Aleutian Low was anomalously strong during most winters from 1980-89, and was anomalously weak during most falls from 1980-89. Marine ridging occurred frequently during fall from 1980-89 which is consistent with marine ridging as a manifestation of a weak Aleutian Low. Marine ridging occurred infrequently during winter during 1980-89 due to the intense Aleutian Low. The ridging events that did occur during this period occurred in conjunction with ENSO events in the tropical Pacific and represent temporary weakening in the winter circulation of the Aleutian Low. These results are consistent with those of Trenberth [1990] who reports that North Pacific SLP during 1976-88 shows decreasing trends during each month from November through March, while no such decreasing trends are evident during any other months of the year.

Summary and Discussion

Winter and fall marine ridging activity in the SLP field over the North Pacific Ocean has been documented for the period 1946-1990 and compared with blocking activity during 1950-1970 as determined by White and Clark [1975]. There has been a decrease in the occurrence of blocking events during January and an increase during February and October during 1971-1990 relative to the earlier period. This represents a shift in the month of maximum blocking activity from January to February in winter and November to October during fall. The occurrence of ridging

features during October for six of the eight years between 1981 and 1988 represents a significant departure from the fall climatology since only 1 ridging event occurred during October in the 35 year period previous to 1981.

Interannual variability in the occurrence of marine ridges has been shown to be consistent with observed long term changes in Aleutian Low wind stress curl and central North Pacific SST. Marine ridging has been shown to occur more frequently during periods of weakened circulation within the Aleutian Low than during periods of strengthened circulation. In particular the intensification of the Aleutian Low that occurred in winter during 1976-87 is characterized by a lack of winter marine ridging activity. Similarly the weakened Aleutian Low that occurred in winter during 1960-69 is characterized by frequent winter ridging activity. Decadal scale maxima and minima in fall marine ridging activity are out of phase with the winter maxima and minima of 1976-87 and 1960-69 respectively. The intensification of the Aleutian Low observed during winter months in wind stress curl and SLP is usually not apparent during fall. This partially explains the occurrence of the fall ridging maximum during the same decade as the winter ridging minimum occurs.

The spatial structure in the pressure field associated with the PNA exhibits at least two patterns, one associated with positive values of the PNA index, the other with negative values. The spatial structures of these patterns are quite different although they are both characterized by ridging patterns in the pressure field. Marine ridging is closely associated with negative PNA extrema, while continental ridging along

the west coast of North America is associated with the positive phase and positive extrema of the PNA. The positive maxima of the PNA index are associated with periods where no marine ridging occurs in the SLP field. The processes responsible for driving marine ridging over the North Pacific and ridging along the west coast of North America are different. Ridging activity over the ocean is forced by anomalous heat fluxes in the marine environment while ridging along the west coast of North America is of continental origin and is topographically forced.

Long term variability in marine ridging activity appears to be related to decadal scale variations in the PNA, in particular the recent observed trend toward more positive values of the PNA during winter is consistent with the observed decrease in winter ridging activity during 1980-89 relative to the previous three decades.

Circulation within the Aleutian Low has a tendency to weaken during winters (January through March) preceding ENSO events, but more specifically, these same winters are often characterized by the persistent presence of ridges over the northcentral North Pacific Ocean. During winters preceding ENSO events there is a tendency for ridging activity to occur from one to three months consecutively, while the winters during which the mature phase of the ENSO event occurs are characterized by a lack of marine ridging. This is consistent with the observations of a weakened winter circulation within the Aleutian Low preceding ENSO events, a strengthened Aleutian Low in response to ENSO events, and the interpretation that open ocean blocking ridges are manifestations of a weakened Aleutian Low.

Chapter Four

Conclusions

Surface wind stress curl anomalies and the frequency of occurrence of blocking anticyclones indicate that the atmospheric circulation of the subarctic North Pacific was intensified during 1976-88. On interannual time scales, changes in the atmospheric circulation appear to have occurred over a larger region than the Pacific subarctic. For example, westerly winds at 700 mb in the subtropical Pacific (cf. fig. 15 of Namias et al., 1988) intensified after 1976, and the running mean anomalies remained positive through the end of the record (1984). Therefore from 1976 to 1988 the high latitude North Pacific wind field fluctuated in phase with the midlatitude westerlies on the decadal time scale. Persistent negative anomalies of the long term mean SOI during 1976-88 are associated with the occurrence of several El Niño events but no strong La Niña events. This indirectly suggests that a weakening of the trade winds occurred during this period in the tropical Pacific. Inoue and O'Brien [1987] show that the Pacific trade wind field weakened throughout the period 1974-81. Figures 4 and 5 of Cooper et al. [1989] are characterized by the reversal, after 1976, of a trend toward intensification of the Pacific trade wind field that began in 1950. The weakening of the trade winds continued after 1976. Therefore on time scales of years the Pacific trade wind field was out of phase with the midlatitude westerlies and the high

latitude wind field (i.e. Aleutian Low). This out of phase relationship was most strongly manifested during the period 1976 to 1988.

During much of the period 1950-75 atmospheric conditions in the Pacific were often opposite to those observed during 1976-88. The trade winds were intense [Cooper et al., 1989], midlatitude westerlies were weak [cf. fig. 15, Namias et al, 1988], and wind stress curl anomalies in the subarctic show that the Aleutian Low was anomalously weak. Therefore on interannual to decadal time scales, an intensified Pacific trade wind field occurs in conjunction with weakened circulation in the midlatitude westerlies and in the subarctic North Pacific. On time scales of years to a decade, the high latitude (45°N-60°N) North Pacific atmospheric circulation fluctuates in phase with the strength of the midlatitude westerlies. Furthermore, the westerlies and the subarctic wind field fluctuate out of phase with the strength of the trade winds on decadal time scales in the Pacific.

Relationships between Interannual Variations in the Pacific and Atlantic

Van Loon and Rogers [1978], Wallace and Gutzler [1981], and Shabbar et al. [1990] show that there is a strong tendency for the strength of the high latitude winter atmospheric circulation over the oceans to be out of phase. That is, the intensities of the Aleutian Low of the North Pacific and the Icelandic Low of the North Atlantic are out of phase. This suggests that Aleutian Low wind stress curl anomalies might be used as a proxy indicator of the strength of the Icelandic Low on interannual time

scales. Using this proxy, it is suggested that the Icelandic Low was intensified during 1960-75, and weak during 1976-88.

The western Atlantic trade winds were anomalously weak from the 1960's to mid 1970's, and anomalously strong after 1975. This can be inferred from the data of Servain and Seva [1987, their figure 1]. This is in contrast to the situation in the Pacific where the trade winds were intensified during the 1960's and mid 1970's and weakened after 1975. Newell and Kidson [1984] suggest that the trade winds and the southwesterlies fluctuate out of phase in the Atlantic. Therefore on interannual time scales the Atlantic is analogous to the Pacific in that the trade winds fluctuate out of phase with the midlatitude westerlies and the high latitude wind field. Furthermore, on these same time scales the Pacific and Atlantic trades are out of phase with each other, as are the midlatitude westerlies and the high latitude wind fields.

The out of phase relationships between the wind fields of the Pacific and Atlantic suggest that interannual to interdecadal scale climate variability in the Atlantic might be related to variability on these scales in the Pacific. Two examples are given that suggest that the long term variability observed in the Pacific occurred in conjunction with changes on these time scales in the Atlantic.

In the Pacific La Niña conditions are characterized by strong trade winds, strong convection in the western tropical Pacific atmosphere, low SST in the eastern equatorial region and dry conditions in the eastern tropical Pacific atmosphere and adjacent continental region. During El Niño conditions, the trades weaken, SST rises and upwelling is

suppressed in the eastern tropical Pacific, and large scales convective zones shift eastward bringing rains to the arid regions of western South America. The situation in the tropical Atlantic is quite similar. Strong Atlantic trade winds occur in conjunction with low SST in the eastern tropical region and low precipitation in the adjacent continental desert regions [Servain and Seva, 1987, Philander, 1990]. Weak trades correspond to El Niño type events and occur in conjunction with higher SST and decreased upwelling in the eastern tropics and enhanced precipitation in the desert regions, in particular the Sahel of West Africa. Intensified wind stress after 1975 (cf. fig. 1b of Servain and Seva, 1987) in the tropical Atlantic occurs in conjunction with persistent negative rainfall anomalies in the Sahel region as can be inferred from the data of Folland et al. [1986, their figure 1a], and Servain and Seva [1987 their figure 3a]. Therefore it appears that while El Niño type conditions prevailed in the tropical Pacific during 1976-88, La Niña conditions were dominant in the tropical Atlantic. Therefore on time scales longer than those of ENSO, climate variations in the tropical Pacific and Atlantic are related to each other and occur out of phase. This suggests that the strong climate anomalies observed in the Pacific during 1976-88 occurred as part climate event with a spatial scale larger than the Pacific.

Over the North Atlantic, a strong Icelandic Low results in strong cold advection from the north over the Greenland region [Wallace and Gutzler, 1981]. It would be expected that increased southward flow of cold air in the Icelandic Low would result in more ice cover over the Greenland Sea region, while a weaker Icelandic Low would be associated with

decreased cold advection and decreased Greenland Sea ice cover. Long term mean sea ice cover anomalies in the Greenland Sea region were positive from 1962-72 and negative from 1973 through the end of the record (1984) (cf. fig. 19 in Mysak and Manak, 1989). The periods of positive and negative sea ice cover anomalies correspond to periods of weakened and intensified circulation in the Aleutian Low respectively, and by inference the positive and negative ice anomalies correspond to periods of strengthened and weakened circulation in the Icelandic Low. Further evidence that the Icelandic Low was weak after 1976 is that there was a virtual shutdown of deep convection in the Greenland Sea during the late 1970's and 1980's as observed by Schlosser et al. [1991]. Therefore, it is suggested that the sea ice cover anomalies observed in the Greenland Sea are closely related to the strength of the Icelandic Low on interannual time scales. In particular long term positive Greenland Sea ice cover anomalies during 1961-72 correspond to an intensified Icelandic Low while negative ice anomalies during 1973-84 are associated with a weakened Icelandic Low. After 1976 ice cover anomalies in the Bering Sea and Greenland Sea were in phase as a result of the strong out of phase relationship between the strength of the Aleutian and Icelandic Lows. The strong climatic feedbacks observed in the ocean-ice-atmosphere system of the Pacific during 1976-88 appear to also be manifested in the North Atlantic. This example also demonstrates that the strong interactions and feedbacks observed in the Pacific during 1976-88 occurred as part of a climate regime with spatial scales that are larger than the Pacific. On the basis of the above observations and the large scale physical

links that exist between the Atlantic and Pacific, that the climate anomalies observed in the Pacific and Atlantic after 1975 occurred as part of a hemispheric or global scale climate regime that is characterized by both its strength and persistence.

Based on the FNOC data, it was found in this dissertation that the wind stress curl forcing was anomalously strong in the subarctic North Pacific during 1976-88. This is in contrast to the period 1954-75 when negative wind stress curl anomalies in the Aleutian Low during winter show that the subarctic atmospheric circulation was weak. Atmospheric circulation was also anomalous in the western subtropical anticyclone region of the North Pacific during the period 1976-88. Negative curl anomalies in this region after 1976 are consistent with the interpretation that the midlatitude westerlies intensified (inferred from Namias et al., 1988, their figure 15) while the northeast trade winds weakened (inferred from figures 4 and 5 of Cooper et al., 1989,). It is concluded that on interannual to decadal time scales in the Pacific, the subarctic (45°N-60°N) atmospheric circulation fluctuates in phase with the strength of the midlatitude westerlies. Furthermore, both the westerlies and the subarctic wind field fluctuate out of phase with the strength of the trade winds on decadal time scales in the Pacific.

Changes in the frequency of blocking anticyclone activity over the North Pacific occurred during fall and winter from 1976-88 relative to the previous three decades. The trend toward more positive values of the PNA during 1976-88 provides an explanation for the decrease in winter blocking

activity. This is because marine blocking activity is often associated with negative extrema of the PNA. The decrease in the winter occurrence of these features during this period is consistent with the intensification of the atmospheric circulation observed in the subarctic region. The occurrence of these blocking features during winter after 1976 is more strongly tied to fluctuations in the SOI than during the previous three decades.

Oceanic transport variations in the eastern and western subarctic North Pacific occur in conjunction with fluctuations of regional wind stress curl forcing on time scales of years. Transports in the Gulf of Alaska vary primarily on time scales of 2.5 to 3 years and 5 to 7 years during 1946-66 and 1966-88 respectively. Transport variations in the Oyashio region of the western subarctic have decadal time scales. In particular the circulation was weak during 1960-75 and intensified during 1976-85. These periods of weakened and intensified oceanic circulation occurred in conjunction with negative and positive low frequency Bering Sea wind stress curl anomalies respectively. Therefore on interannual to decadal time scales, ocean transport variations in the subarctic North Pacific are strongly linked to changes in regional wind stress curl forcing. Interannual oceanic transport fluctuations in the eastern and western subarctic of the North Pacific occur on the dominant time scales of changes in wind stress curl over the Gulf of Alaska and Bering Sea respectively.

North Pacific SST, subarctic air temperatures, Bering Sea ice cover, the PNA, SOI, and eastern tropical Pacific SST are all characterized by low frequency anomalies that did not change sign during the period 1976-88. This suggests that the spatial scale of this climate regime extended at least from the subtropical South Pacific to the high latitude North Pacific, and occurred in both the ocean and atmosphere. The strongly phase locked behavior that occurred between these parameters during 1976-88 did not occur in the earlier three decades of the record. These strong phase relationships appear to be a result of the anomalous strength and duration of the forcing mechanisms. The amplitude and persistence of the anomalous forcing appears to have caused the feedbacks between atmosphere, ocean and ice to be more strongly manifested during 1976-88 than during previous periods.

Changes in the long term mean anomalies of North Pacific wind stress curl in the subarctic and subtropics, central North Pacific SST, and the SOI after 1988 suggest that the decadal scale climate regime observed after 1976 relaxed or ended after 1988. The Aleutian Low began to weaken after 1988, while a 20 year cooling trend of central North Pacific SST ended after 1987. Also the occurrence of a strong La Niña during 1989 (the first strong La Niña to occur since 1976) may have signaled a reversal of the previously observed regime in the tropical Pacific. However, the occurrence of El Niño during 1991-92 suggests that the observed reversals may only have indicated a relaxation of the 1976-88 regime. The next few years should be important in determining whether the climate regime

observed during 1976-88 occurred as an amplified quasi-periodic phenomenon, or whether these changes occurred as the beginning of a long term trend that might support a global warming hypothesis.

Anomalies of tropical Atlantic wind stress, Sahel (northwest Africa) rainfall, and Greenland Sea ice cover are characterized by strong and persistent anomalies after 1975. On the basis of these observations and plausible physical links between the climate systems of the Pacific and Atlantic, it is suggested that the climate anomalies observed in the North Pacific during 1976-88 occurred as part of a global scale climate regime. Again, the next few years will be important in determining whether the large scale links observed between the Pacific and Atlantic will continue as part of a climate regime characterized by strongly phase locked behavior, or whether the relationships will not be as clearly manifested as the strength observed climate regime ends in conjunction with changes in the strength and persistence of the climatic forcing.

It is not clear what the ultimate causal mechanisms for these large scale persistent changes are. It is suggested that the climate regime that occurred during 1976-88 has its origins in the tropics. Consideration of the period 1976-88 as an ENSO like event with a decadal time scale leads to a consistent explanation of the observed variations documented in this study. If the negative anomalies of the SOI during 1976-88 are viewed as an extended ENSO event, then the persistent anomalies that occurred in the oceanic and atmospheric parameters considered in this study can be explained in terms of changes in the tropics. For example, during the

mature phase of ENSO events the Aleutian Low intensifies [Bjerknes, 1969, 1972, Namias, 1976]. If we view 1976-88 as an extended ENSO like event (at least in the Pacific region), then we would expect the Aleutian Low to be more intense during this period, which it was, as manifested in positive wind stress curl anomalies during 1976-88. If the Aleutian Low and Icelandic Low are linked through some planetary wave scale dynamical mechanism, then a prolonged ENSO event could also explain the weakening of the Icelandic Low during 1976-88 and the subsequent shutdown of Greenland Sea deep convection. Similarly ENP SST warms and CNP SST cools during an ENSO event. Therefore if 1976-88 is considered to be an ENSO like event of extended duration, the observed SST fluctuations in the CNP and ENP region can be viewed as the response to this protracted ENSO event. In the subarctic, air temperature anomalies tend to be positive during ENSO events while Bering Sea ice cover anomalies are negative. Therefore changes in these parameters after 1976 can also be consistently rationalized within the framework of an extended ENSO event. This analogy also extends to tropical and extratropical cyclogenesis. Atkinson [1977] suggests tropical cyclone frequencies tend to be high during ENSO years, while Hanson and Long [1985] show that years of maximum extratropical cyclogenesis in the Kuroshio region tend to coincide with ENSO years. It can be inferred from the data of Chan [1985], that the frequency of occurrence of tropical cyclones increased after 1976 relative to the previous three decades. It can also be inferred from the data of Chen et al. [1991] that East Asian extratropical cyclogenesis increased markedly after 1976 in a manner that is consistent with the

observations of climatic shifts in the other variables that have been considered in this study. Therefore it appears reasonable to suggest that the hemispheric or global scale climate regime observed during 1976-88 existed as an ENSO like event of particularly long duration. An ENSO like event of decadal scale duration is proposed to have occurred during the period 1937-46 (e.g. Barnett, 1984a, Folland et al., 1984, Oort et al, 1987, Cooper et al., 1989). The ENSO like event of 1937-46 is characterized by variations that are similar to those observed during 1976-88. Therefore the climate regime of 1976-88 appears to have had its origins in the equatorial region, most likely the equatorial Pacific Ocean (or possibly the Indian Ocean since this is where the propagating component of the SOI originates as suggested by Barnett [1984b]). However, changes in the atmosphere (i.e. changes in planetary waves) and ocean (changes in deep convection in the Atlantic) at high latitudes might also have played an important role in affecting the global scale transfers of heat, moisture and momentum. It seems likely that the ultimate causal mechanism is part of a very complicated feedback system with important components both at high and low latitudes within the coupled ocean atmosphere system.

References

Anderson, D. and R. Corry, Ocean response to low frequency wind forcing with application to the seasonal variation in the Florida Straits-Gulf Stream transport, Progress in Oceanography, 14, 7-40, 1985.

Angell, J. and J. Korshover, Comparison of year-average latitude, longitude, and pressure of the four centers of action with air and sea temperature, Mon. Wea. Rev., 110, 300-303, 1982.

Atkinson, G., Proposed system for near real time monitoring of global tropical circulation and weather patterns, 11th Tech. Conf. on Hurricanes and Tropical Meteorology, American Meteorological Society, 645-652, 1977.

Bakun, A., Coastal upwelling indices, west coast of North America, 1946-71, U.S. Dept. of Commerce, NOAA, Tech. Rep. NMFS SSRF-671, 1973.

Bang, I., Numerical modeling study of the circulation in the Gulf of Alaska, Ph.D. Thesis, University of Alaska, 1991.

Barnett, T., Long term trends in surface temperature over the oceans, Mon. Wea. Rev., 112, 303-312, 1984a.

Barnett, T., Interaction of the monsoon and Pacific trade wind system at interannual time scales Part II: The tropical band, Mon. Wea. Rev., 112, 2380-2387, 1984b.

Barnett, T., N. Graham, M. Cane, S. Zebiak, S. Dolan, J. O'Brien and D. Legler, On the prediction of the El Niño of 1986-1987, Science, 241, 192-196, 1988.

Barnier, B., Investigation of seasonal variability of the wind stress curl over the North Atlantic Ocean by means of empirical orthogonal function analysis, J. Geophys. Res, 91, 863-868, 1986.

Bjerknes, J., Atmospheric teleconnections from the equatorial Pacific, Mon. Wea. Rev., 97, 162-172, 1969.

Bjerknes, J., Large scale atmospheric response to the 1964-65 Pacific equatorial warming, J. Phys. Oceanogr., 2, 212-217, 1972.

Breidenbach, J., EOFs of pseudo-stress over the Indian Ocean (1977-1985), Bull. of Amer. Met. Soc., 71, 1448-1454, 1990.

Bunker, A., Computation of surface energy flux and annual air-sea interaction cycles of the North Atlantic Ocean, Mon. Wea. Rev., 104, 1122-1139, 1976.

Cane, M., S. Zebiak and S. Dolan, Experimental forecasts of El Niño, Nature, 321, 827-832, 1986.

Chan, J., Tropical cyclone activity in the Northwest Pacific in relation to the El Niño/Southern Oscillation Phenomenon, Mon. Wea. Rev., 113, 599-606, 1985.

Chao, S., Coastal jets in the lower atmosphere, J. Phys. Oceanogr., 15, 361-371, 1985.

Chen, L. and E. Rieter, Sea surface temperature anomalies in the Kuroshio region and temperature anomalies over North America, Meteorol. Atmos. Physics, 35, 1-9, 1986.

Chen S., Y. Kuo, P. Zhang and Q. Bai, Synoptic climatology of cyclogenesis over East Asia 1958-1987, Mon. Wea. Rev., 119, 1407-1421, 1991.

Cooper, N., K. Whysall and G. Bigg, Recent decadal climate variations in the tropical Pacific, International Journal of Climatology, 9, 221-242, 1989.

Cummins, P., A quasi-geostrophic circulation model of the northeast Pacific. Part II: Effects of topography and seasonal forcing, J. Phys. Oceanogr., 19,1649-1668, 1989.

Cummins, P., L. Mysak and K. Hamilton, Generation of annual Rossby waves in the North Pacific by the wind stress curl, J. Phys. Oceanogr., 16, 1179-1189, 1986.

Davis, R., Predictability of sea surface temperature and sea level pressure anomalies over the North Pacific Ocean, J. Phys. Oceanogr., 6, 249-266, 1976.

Deser, C. and J. Wallace, El Niño events and their relation to the Southern Oscillation:1925-1986, J. Geophys. Res., 92, 14189-14196, 1987.

Dickson, R., W. Gould, P. Gurbutt and P. Killworth, A seasonal signal in ocean currents to abyssal depths, Nature, 295, 193-198, 1982.

Douglas, A., D. Cayan and J. Namias, Large scale changes in North Pacific and North American weather patterns in recent decades, Mon. Wea. Rev., 110, 1851-1862, 1982.

Ehret , L. and J. O'Brien, Scales of North Atlantic wind stress curl determined from COADS, J. Geophys. Res., 94, 831-841, 1989.

Emery W. and K. Hamilton, Atmospheric forcing of interannual variability in the northeast Pacific Ocean: connections with El Nino, J. Geophys. Res., 90, 857-868, 1985.

Folland, C., K. Parker and F. Kates, Worldwide marine temperature fluctuations 1856-1981, Nature, 310, 670-673, 1984.

Folland, C., T. Palmer and D. Parker, Sahel rainfall and worldwide sea surface temperatures 1901-1985, Nature, 320, 602-607, 1986.

Frankignoul, C. and P. Muller, Quasi-geostrophic response of an infinite beta-plane ocean to stochastic forcing by the atmosphere, J. Phys. Oceanogr., 9, 104-127, 1979.

Gill, A., *Atmosphere-Ocean Dynamics,* Academic Press, 1982.

Gyakum, J., J. Anderson, R. Grumm and E. Gruner, North Pacific cold-season surface cyclone activity: 1975-1983, Mon. Wea. Rev., 117, 1141-1155, 1989.

Hanawa, K., Long term variations of the atmospheric circulation over the North Pacific and the Oyashio, Bull. Hokkaido Natl. Fish. Res. Inst., 55, 125-139, 1991.

Hanson, H. and B. Long, Climatology of cyclogenesis over the East China Sea, Mon. Wea. Rev., 697-707, 1985.

Harrison, D., On climatological monthly mean wind stress and wind stress curl fields over the world ocean, J. Climate, 2, 57-70, 1989.

Hastenrath, S. and P. Lamb, Climatic atlas of the tropical Atlantic and eastern Pacific Oceans, Univ. of Wisconsin, 1977.

Hellerman, S., An updated view of the wind stress on the world ocean, Mon. Wea. Rev., 95, 607-626, 1967.

Hellerman, S. and M. Rosenstein, Normal monthly wind stress over the world ocean with error estimates, J. Phys. Oceanogr.,13, 1093-1104, 1983.

Hickey, B., The California current system- hypotheses and facts, Progress in Oceanography, 8, 191-279, 1979.

Hidaka, K., Computation of the wind stresses over the oceans, Rec. Oceanogr. Works Japan, 4, 77-123, 1958.

Inoue, M. and J. O'Brien, Trends in sea level in the western and central equatorial Pacific during 1974-75 to 1981, J. Geophys. Res., 92, 5045-5051, 1987.

Iwasaka, N., K. Hanawa and Y. Toba, Analysis of SST anomalies in the North Pacific and their relation to 500 mb height anomalies over the Northern Hemisphere during 1969-1979, J. Meteorological Soc. Japan, 65, 103-113, 1987.

Iwasaka, N., K. Hanawa and Y. Toba, Partition of the North Pacific Ocean based on similarity in temporal variations of the SST anomaly, J. Meteorological Soc. Japan, 66, 433-443, 1988.

Jonsson, S., Seasonal and interannual variability of wind stress curl over the Nordic Seas, J. Geophys. Res., 96, 2649-2660, 1991.

Kawamura, R., Relation between atmospheric circulation and dominant SST anomaly patterns in the North Pacific during winter, J. Meteorological Soc. Japan, 62, 910-916, 1984.

Kutsuwada, K., New computations of the wind stress over the North Pacific Ocean, J. Oceanogr. Soc. Jpn., 38, 159-171, 1982.

Kutsuwada, K., Spatial characteristics of interannual variability in wind stress over the western North Pacific, J. Climate, 1, 333-347, 1988.

Lanzante, J., A rotated eigenanalysis of the correlation between 700 mb heights and sea surface temperatures in the Pacific and Atlantic, Mon. Wea. Rev., 112, 2270-2280, 1984.

Lau, N. and M. Nath, A general circulation model study of the atmospheric response to extratropical SST anomalies observed in 1950-79, J. Climate, 3, 965-989, 1990.

Lejenas, H. and H. Okland, Characteristics of northern hemisphere blocking as determined from a long time series of observational data, Tellus, 35, 350-362, 1983.

Livezey, R. and K. Mo, Tropical-extratropical teleconnections during the Northern Hemisphere winter: Part II: Relationships between monthly mean Northern Hemisphere circulation patterns and proxies for tropical convection, Mon. Wea. Rev., 115, 3115-3132, 1987.

Livingstone, D. and T. Royer, Observed surface winds at Middleton Island, Gulf of Alaska and their influence on the ocean circulation, J. Phys. Oceanogr., 10, 753-764, 1980.

Luick, J., T. Royer and W. Johnson, Coastal atmospheric forcing in the Northern Gulf of Alaska, J. Geophys. Res., 92, 3841-3848, 1987.

McCreary, J. and S. Chao, Three dimensional shelf circulation along an eastern ocean boundary, J. Mar. Res., 43, 13-36, 1985.

Mo, K. and R. Livezey, Tropical-extratropical geopotential height teleconnections during the Northern Hemisphere winter, Mon. Wea. Rev., 114, 2488-2515, 1986.

Muller, P. and C. Frankignoul, Direct atmospheric forcing of geostrophic eddies, J. Phys. Oceanogr., 11, 287-308, 1981.

Munk, W., On the wind driven circulation, Journal of Meteorology, 7, 79-93, 1950.

Mysak, L. and D. Manak, Arctic sea ice extent and anomalies 1953-1984, Atmosphere-Ocean, 27, 376-405, 1989.

Namias, J., Some statistical and synoptic characteristics associated with El Nino, J. Phys. Oceanogr., 6, 130-138, 1976.

Namias, J., X. Yuan and D. Cayan, Persistence of North Pacific sea surface temperature and atmospheric flow patterns, J. Climate, 1, 682-703, 1988.

Newell, R. and J. Kidson, African mean wind changes between Sahelian wet and dry periods, J. Climatology, 4, 27-33, 1984.

Niebauer, H., Effects of El Nino-Southern Oscillation and North Pacific weather patterns on interannual variability in the subarctic Bering Sea, J. Geophys. Res., 93, 5051-5068, 1988.

Niebauer, H. and R. Day, Causes of interannual variability in the sea ice cover of the eastern Bering Sea, GeoJournal,18, 45-59, 1989.

Nitta, T. and S. Yamada, Recent warming of tropical sea surface temperature and its relationship to the Northern Hemisphere circulation, J. Meteorological Soc. of Japan, 67, 375-383, 1989.

Okkonen, S., Circulation variability in the Gulf of Alaska and Bering Sea, Ph.D. Thesis, University of Alaska, 1992.

Oort, A., Y. Pan, R. Reynolds and C. Ropelowski, Historical trends in the surface temperature over the oceans based on the COADS, Climate Dynamics, 2, 29-38, 1987.

Overland, J. and C. Pease, Cyclone climatology of the Bering Sea and its relation to ice extent, Mon. Wea. Rev., 110, 5-13, 1982.

Pan, Y. and A. Oort, Global climate variations connected with SST anomalies in the eastern Pacific Ocean for the period 1958-1973, Mon. Wea. Rev., 111, 1244-1258, 1983.

Philander, S. G. H., *El Niño, La Niña, and the Southern Oscillation,* Academic Press, 1990.

Reason, C , L. Mysak and P. Cummins, Generation of annual period Rossby waves in the South Atlantic by the wind stress curl, J. Phys. Oceanogr., 17, 2030-2042, 1987.

Reid, R., The equatorial currents of the eastern Pacific as maintained by the stress of the wind, J. Mar. Res., 7, 74-99, 1948.

Reiter, E., Long term wind variability in the tropical Pacific, its possible causes and effects, Mon. Wea. Rev., 106, 324-330, 1978.

Rex, D., Blocking activity in the middle troposphere and its effect on regional climate, Tellus, 2, 275-301, 1951.

Rienecker, M. and L. Ehret, Wind stress curl variability over the North Pacific from COADS, J. Geophys. Res., 93, 5069-5077, 1988.

Royer, T., Upper ocean temperature variability in the northeast Pacific Ocean: Is it an indicator of global warming?, J. Geophys. Res., 94, 18175-18183, 1989.

Schlosser, P., G. Bonisch, M. Rhein and R. Bayer, Reduction of deepwater formation in the Greenland Sea during the 1980s: Evidence from tracer data, Science, 251, 1054-1056, 1991.

Sekine, Y., Anomalous southward intrusion of the Oyashio east of Japan, I, Influence of seasonal and interannual variations in the wind stress over the North Pacific, J. Geophys. Res., 93, 2247-2256, 1988.

Sekine, Y., Anomalous southward intrusion of the Oyashio east of Japan, in: *Long-term Variability of Pelagic Fish Populations and their Environment*, Pergamon Press, 1991.

Servain, J. and M. Seva, On relationships between tropical Atlantic SST, wind tress, and regional precipitation indices 1964-84, Ocean-Air Interactions, 1, 183-190, 1987.

Servain, J. and D. Legler, Empirical orthogonal function analyses of tropical Atlantic sea surface temperature and wind stress: 1964-1979, J. Geophys. Res., 91, 14,181-14191, 1986.

Shabbar, A., K. Higuchi and J. Knox, Regional analysis of 50kPa geopotential heights from 1946 to 1985, J. Climate, 3, 543-557, 1990.

Tabata, S., Long-term ocean variability at Ocean Station P in the northeast Pacific Ocean- An update to 1989, in: *Long-term Variability of Pelagic Fish Populations and their Environment*, Pergamon Press, 1991a.

Tabata, S., Annual and interannual variability of baroclinic transports across line P in the northeast Pacific Ocean, Deep Sea Res., 38, Suppl. 1, S221-S245, 1991b.

Talley, L., Ventilation of the subtropical North Pacific: the shallow salinity minimum, J. Phys. Oceanogr., 15, 633-649, 1985.

Talley, L., Potential vorticity distribution in the North Pacific, J. Phys. Oceanogr., 18, 89-106, 1988.

Terada, K. and M. Hanzawa, Climate of the North Pacific Ocean, in: *World Survey of Climatology*, Vol. 15, 431-478, Elsevier Sci., 1984.

Thompson, K., R. Marsden and D. Wright, Estimation of low frequency wind stress fluctuations over the open ocean, J. Phys. Oceanogr., 13, 1003-1011, 1983.

Treidl, R., E. Birch and P Sajecki, Blocking action in the Northern Hemisphere: a climatological study, Atmos.-Ocean, 19, 1-23, 1981.

Trenberth, K., Recent observed interdecadal climate changes in the Northern Hemisphere, Bull. American Meteorol. Soc., 71, 988-993, 1990.

Trenberth, K., J. Olson and W. Large, A global ocean wind stress climatology based on ECMWF analyses, NCAR Tech. Note NCAR/TN-338, 1989.

van Loon, H. and J. Rogers, The seesaw in winter temperatures between Greenland and Northern Europe, Part I: General description, Mon. Wea. Rev., 106, 296-310, 1978.

van Loon, H. and D. Shea, The Southern Oscillation. Part IV: The precursors south of 15S to the extremes of the oscillation, Mon. Wea. Rev., 113, 2063-2074, 1985.

Wallace, J. and D. Gutzler, Teleconnections in the geopotential height field during the Northern Hemisphere winter, Mon. Wea. Rev., 109, 784-812, 1981.

Wallace, J., C. Smith and Q. Jiang, Spatial patterns of atmosphere-ocean interaction in the northern winter, J. Climate, 3, 990-998, 1990.

Weare, B., A. Navato and R. Newell, Empirical orthogonal analysis of Pacific sea surface temperatures, J. Phys. Oceanogr., 6, 671-678, 1976.

White, W., The resonant response of interannual baroclinic Rossby waves to wind forcing in the eastern midlatitude North Pacific, J. Phys. Oceanogr., 15, 403-415, 1985.

White, W. and N. Clark, On the development of blocking ridge activity over the central North Pacific, J. Atmos. Sci., 32, 489-502, 1975.

White, W. and J. Saur, A source of annual baroclinic waves in the eastern subtropical North Pacific, J. Phys. Oceanogr., 11, 1452-1462, 1981.

White, W. and J. Saur, Sources of interannual baroclinic waves in the eastern subtropical North Pacific, J. Phys. Oceanogr., 13, 664-673, 1983.

White, W. and S. Tabata, Interannual westward-propagating baroclinic long-wave activity on Line P in the eastern midlatitude North Pacific, J. Phys. Oceanogr.,17, 385-396, 1987.

White W., R. Bernstein, G. McNally and S. Pazan, The thermocline response to transient atmospheric forcing in the interior midlatitude North Pacific 1976-1978, J. Phys. Oceanogr., 10, 372-384, 1980.

Willebrand, J., Temporal and spatial scales of the wind field over the North Pacific and North Atlantic, J. Phys. Oceanogr., 8, 1080-1094, 1978.

Wilson, J. and J. Overland, Meterology, In: The Gulf of Alaska Physical Environment and Biological Resources, 1986.

Wyrtki, K., The Southern Oscillation, ocean atmosphere interaction and El Niño, Mar. Technol. Soc. J., 16, 3-10, 1982.

Wyrtki, K. and G. Meyers, The trade wind field over the Pacific Ocean, J. Appl. Meteor, 15, 698-704, 1976.